Navigation Solution for Marine Applications using MEMS-based Sensors and GPS

by Bjørn Eskildsen

10th semester of IAS
Group 1052 (11gr1052@es.aau.dk)
Department of Electronic Systems
Aalborg University

February 2012

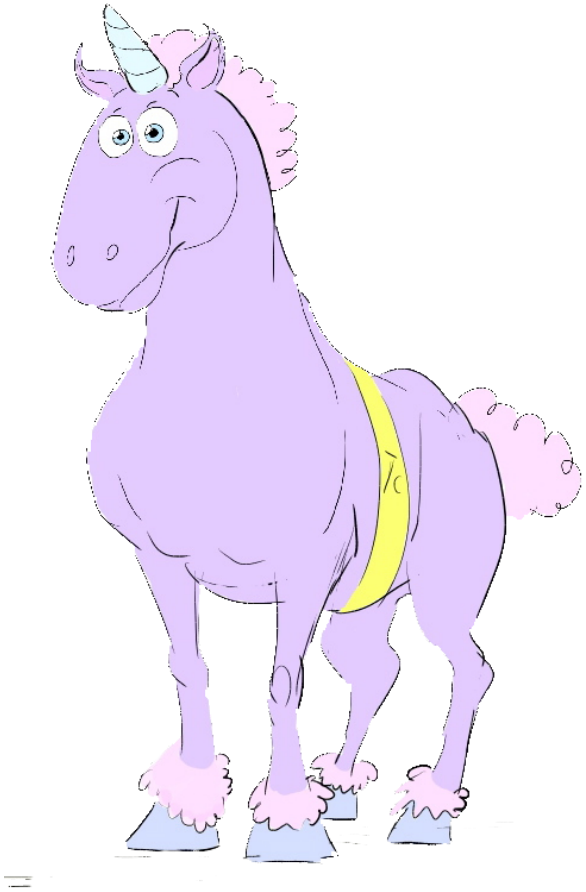

This page is intentionally left with a unicorn as this is considered more entertaining than a simple blank page

AALBORG UNIVERSITET

The Faculties of Engineering, Science and Medicine
Department of Electronic Systems
Section of Automation and Control
Frederik Bajers Vej 7
Phone: +45 96 35 86 00
http://es.aau.dk

Title:
Navigation Solution for Marine Applications using MEMS-based Sensors and GPS

Project period:
September 1st, 2011
- February 17th, 2012

Project group: 11gr1052

Group members:
Bjørn Eskildsen

Supervisor:
Anders La-cour Harbor
Morten Bisgaard

Number of copies: 4
Number of report pages: 89
Appended documents:
(1 appendix, 1 CD-ROM)
Total number of pages: 100
Finished: February 17th 2012

Abstract:

This thesis concerns the estimation of the position, velocity and attitude using inertial sensors, magnetometer and GPS.
The purpose is to apply a model based estimation filter to fuse these sensor inputs together to form estimations of the states of interest.
This thesis has been made in collaboration with the company: CDL - inertial engineering.

The main hardware platform is a MiniSense2 (MS2), produced by CDL. The sensors on the MS2 platform consist of a 3-axis gyroscope, a 3-axis accelerometer and a 3-axis magnetometer. These are all low-price MEMS based sensors.

In this thesis, it is chosen to base the design of the navigation solution on a loosely coupling between the sensors of the MiniSense2 and GPS. The estimation filter utilized in this is based on the structure of the extended Kalman filter.

Differential equations regarding motion on the rotating earth are derived together with models of the sensors, which includes the assumption of additive biases of the MS2 sensors. The thesis also concerns models of the gravitational field and magnetic field of the earth.
As the extended Kalman filter is chosen as basis for the filter design, a linear small state perturbation model is also addressed.

Two tests have been conducted for evaluation of the designed navigation solution.
The first test was based on a designed simulation environment, as this has the advantage of having the true values of the system states for reference. The simulation environment was based on a point mass which is affected by forces and momentums in such a way that it executes oscillations comparable to the ones of a ship at sea. To simulate the behavior of sensors, noise and biases were added to the state outputs.
The second test is based on real world data which originate from a boat trip at sea. Along with the data from a MS2 and a GPS, attitude estimates from a high-grade Attitude and Heading Determination System (AHDS) are available for reference.
In both tests, simulated GPS outages have been included to evaluate the handling of this scenario.

In the test on the simulated data, the navigation solution was able to correctly estimate all the sensor biases. The performance during GPS coverage and outage were both acceptable. This led to the conclusion that the basic concepts of the designed filter work.
In the test on the real world data, the designed navigation solution did not have an acceptable performance even though it was seemingly able to estimate the biases of the gyroscope. The estimates of the magnetometer bias indicated that a non-included effect were present in the magnetometer measurements. It was suggested that a non-included lever between the GPS and MS2 and a ”soft iron” magnetometer effect could be the causes of the bad test results.

Preface

This report describes the project developed by Group 1052 on the 10^{th} semester, Intelligent Autonomous Systems - Department of Control, Institute of Electronic Systems, Aalborg University. The target group for the report is primarily supervisors and students attending 10^{th} semester Control Engineering.

When using references in the text, equations are denoted "(*no.*)" and figures are denoted "Fig. *no.*". Units in calculations are given in square brackets, while units used in the body text are denoted in *italic*. Source references are given with square brackets and possibly page reference and nomenclature is defined on page v. All sources are listed in the Bibliography on page 99.

A composed DVD containing used data sheets, source code, MATLAB scripts, Simulink Models, and Internet sources, is subjoined.

Acknowledgements

The group would like to thank CDL for the collaboration in the project with special thanks to Rolf Christensen and Matthew Hellewell for answers of questions and data provision.

Author Signature

Bjørn Eskildsen

Table of Contents

Nomenclature

Acronyms

INS	Inertial Navigation System
SINS	Strapdown Inertial Navigation System
GNSS	Global Navigation Satellite System
GPS	Global Positioning System
DGPS	Differential GPS
MEMS	Micro Electro-Mechanical System
NRF	Navigation Reference Frame
ECI	Earth Centered Initial Reference Frame
ECEF	Earth Centered Earth Fixed Reference Frame
SRF	Sensor Reference Frame
HVRF	Host Vehicle Reference Frame
DOF	Degrees Of Freedom
MS2	MiniSense2
DCM	Direct Cosine Matrix
IMU	Initial Measurement Unit
IGRF	International Geomagnetic Reference Field

Notation

The following mathematical notations are used.
Vectors are written as:

$$\boldsymbol{v}$$

Matrices are written as:

$$\underline{\boldsymbol{M}}$$

A vector described in the reference frame "c" is indicated as

$$^{c}\boldsymbol{v}$$

A direct cosine matrix describing the rotation from the "a" frame to the "b" frame is defined as

$$^{s}\underline{\boldsymbol{C}}_{c} \tag{1}$$

The transpose is denoted

$$\boldsymbol{v}^{T}$$

The complex conjugate is denoted

$$\boldsymbol{q}^*$$

The inverse of a matrix is written as

$$\underline{\boldsymbol{M}}^{-1}$$

Unit vectors are typed as

$$\hat{\boldsymbol{u}}$$

Label assignment to variables and constants are written as a subscript as

$$\boldsymbol{q}_{label}$$

Time derivatives are denoted with a dot as

$$\dot{x}$$

The angular velocity of reference frame b wrt. reference frame c, described in reference frame a

$$^a\omega_{bc}$$

The skew-symmetric representation of the angular velocity of reference frame b wrt. reference frame c, described in reference frame a

$$^a\Omega_{bc}$$

Indication that the value of a is determined using an external model

$$\breve{a}$$

Indication that the value of a is a measurement

$$\widetilde{a}$$

Indication that the value of $\hat{a}$ is very close to the value of a

$$\hat{a}$$

The difference between $\hat{a}$ and a

$$\delta a = \hat{a} - a$$

Indication that the value of a is a *a prior* estimate

$$a_-$$

Indication that the value of a is a *posterior* estimate

$$a_+$$

Symbols

Symbol	Description	Unit
R_M	Earth radius at equator	$[m]$
R_m	Earth radius at poles	$[m]$
ω_{earth}	Rotation rate of the earth	$[^{rad}/_{s}]$
L	Longitude	$[^{\circ}]$
l	Latitude (geodetic/geographic)	$[^{\circ}]$
TS	Sample period	$[s]$

Chapter 1

Introduction

This thesis has been conducted in collaboration with the company CDL - inertial engineering, located in Aberdeen, Scotland. CDL designs and manufactures equipment for surface and sub sea use in the offshore and maritime industry. Typical applications for these systems include the Remotely Operated (sub sea) Vehicles (ROV) and oil survey ships.

A substantial product of the portfolio of CDL are the Attitude and Heading Reference Systems (AHRS) which, as the name indicates, estimate the 3 degrees-of-freedom (DOF) angles; roll, pitch and yaw.

This thesis concerns a desire at CDL to combine one of their low-cost hardware platform, with aid from GPS to realm a 6 DOF navigation system, estimating both attitude and position.

The scope of this thesis is to be basis for a commercial low-cost navigation product aimed for use on oil survey ships. The sale argument for the product should be for the costumer to obtain attitude estimates together with position/velocity estimates. The position estimates should be smoother than the raw, noise influenced, GPS measurements and be available at a higher sample rate than the GPS measurements. In addition, the navigation solution should also be able to provide estimates during small periods of GPS outages.

1.1 History and Principle of INS

For several centuries, navigation has been a concern for mankind.

In the last few decades, Global Navigation Satellite Systems (GNSS), such as GPS, has revolutionized navigation - both military and commercial. The essential feature of the GNSS is the ability to give measurement of the current position and velocity with bounded precision anywhere on the globe. However, in order to do this, the receiver needs clear view of at least 4 satellites, which can be a problem due to atmospherical disturbances causing small periods of GPS outage. Moreover, some applications need precision, higher than the one provided by the standalone GPS.

Due to these disadvantages, a field of research has been the usage of inertial sensors in combination with GPS to reduce the effect of these disadvantages.

1.1.1 Gimbled Inertial Navigation System

The first research on navigation on inertial sensors were based on gimbaled gyroscopes. The basic principle of a gimbaled gyroscope is illustrated in Fig. 1.1. The gyroscope has a rotor (a rotating mass) in its center which, due to the principals of moment of inertial, will maintain its orientation independent of the orientation of the gyroscope frame.

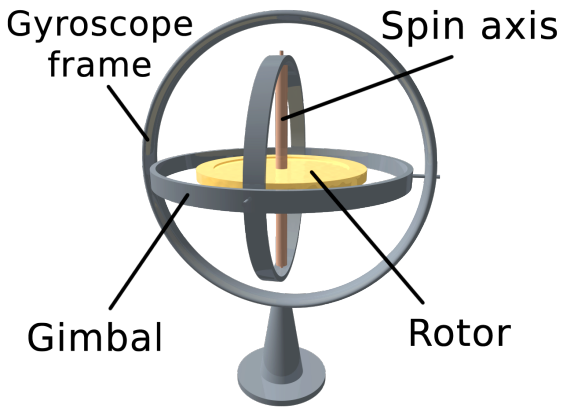

Figure 1.1: Basic gimbaled gyroscope

The basic principle of navigation using gimbaled gyroscopes is to have a 3-axis accelerometer alongside the rotor. Integration of the accelerometer will then directly realm the changes in velocity and position. A system consisting of this setup alone is termed an Inertial Navigation System (INS).

1.1.2 Strapdown Inertial Navigation System

In the late 1970s, the development of Strapdown Inertial Navigation Systems (SINS) started. Instead of relying on a gimbaled gyroscope to maintain a constant orientation, the basic principle in SINS is to use fixed mounted, angular rate measuring, gyroscopes to estimate the orientation. The acceleration measurements could then be rotated into a local navigation frame using this orientation information. By doing this the rotated accelerations could then be integrated to realm the changes in velocity and position.

Some of the advantages of using strap down systems, when compared to gimbaled, includes reduction of production price, size and reduction in required amount of maintenance due to the absence of mechanical parts.

The main disadvantage of the strap down is a requirement of more computational power - a requirement which still becomes decreasingly influential due to the improvement of processors.

The main advantage of using inertial sensors for navigation is that it, as opposed to GNSS, will not be subject of outage periods. Furthermore, the estimates will be available at a higher sample rate than the GNSS. The disadvantages however, is that different phenomenons such as measurement noise, measurement biases and gravity mismodeling will introduce an estimation error. This error will accumulate over time and will be unbounded. When comparing the advantages/disadvantages of inertial navigation with the ones of GNSS, it is clear that these are very complementary. Thus by combining these two technologies one could benefit from each of their advantageous properties while suppressing the effects of the bad properties.

1.2 Hardware

The low-cost hardware platform used in this thesis is the platform currently used for a AHRS product of CDL; MiniSense2 (MS2) [CDL 10]. Throughout this thesis, the hardware platform itself will be referred to as the MS2.

The MS2 is mainly based on a Analog Devices ADIS16362 Inertial Measurement Unit (IMU), which contains both 3-axis gyroscope and 3-axis accelerometer [Ana 11]. Furthermore, the MS2 contains a Honeywell HMC5830 3-axis magnetometer [Hon 11]. Additional, a Trimble MS750 GPS receiver [Tri 98] will be used as aiding.

Both the IMU and magnetometer are micro-electro-mechanical systems (MEMS) sensors. In recent years the use of MEMS sensors have been increasingly dominating in a variety of applications due to their low manufacturing price. This includes the MEMS gyroscopes and accelerometers which falls within the lowest price range of inertial sensors. These sensors are know to have considerable biases.

Further details regarding these sensors will be given in Chapter 4.

1.3 Approach Methods

In this section, the approach method laying basis for the rest of the thesis will be established. The extend of this thesis should be limited in such a way that it is reasonable for one student to complete it within the duration of one semester.

The issue of sensor fusing inertial sensor and GPS has been the topic for various papers. In the literature, in general, two different principal methods for the combining/fusion are widely utilized; loosely and tightly coupling [Titterton 04, 412-414].

1.3.1 Loosely Coupling

The loosely coupling method is simplified illustrated in Fig. 1.2.

In the loosely coupling method, the GPS utilizes an internal estimation filter to process the satellite data to achieve estimates of the position and velocity and output these. In order for the GPS to be able to estimates these states, it needs to be able to receive the broadcasted signals from at least 4 GPS satellites. In case of GPS outage, the sensors from the MS2 can be used to estimate the attitude and the accelerometers can be integrated to form a standalone SINS, with the introduction of an accumulating estimation error to follow. Contrary, if the MS2 fails, the GPS itself would still be able to provide position and velocity estimates, while GPS coverage is available.

1.3.2 Tightly Coupling

The tightly coupling method is simplified illustrated in Fig. 1.3.

As opposed to the loosely coupling, when using the tightly coupling, instead of getting the position and velocity estimates, the pseudo and delta ranges of the GPS are extracted and used as inputs for the filter. The pseudo ranges are the travel time between each satellite and the GPS receiver and the delta ranges are the derivatives of the pseudo ranges.

The delta ranges are not just calculated by differentiating the pseudo ranges, but by measuring the frequency shift in the carrier frequency and utilizing the Doppler principle, stating that

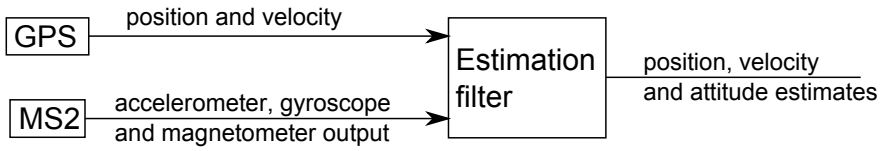

Figure 1.2: Loosely coupled integration

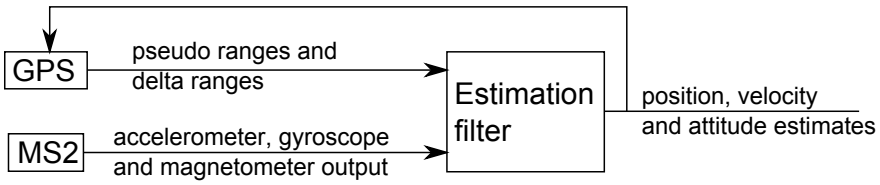

Figure 1.3: Tightly coupled integration

the frequency shift is due to the movement between the transmitting satellite and receiver. In the loosely coupling, the pseudo and delta ranges are internally utilized in the GPS to realm the position and velocity estimates.

Some GPSs accept external position/velocity estimates to help aid the internal filters, why this is fed back in the illustration in Fig. 1.3.

The advantage of using tight coupling, when compared to the loosely coupling, is that usable position/velocity information can be obtained from the GPS even though less than 4 GPS satellites are available. This design requires a GPS receiver which outputs the pseudo and delta ranges and possibly accepts position/velocity inputs as aid to the internal filters.

Coupling Choice

The loosely coupling method is considered the simplest of the two. Due to the desire of limiting the extend of this thesis, the loosely coupling method is chosen for the task of combining the GPS and MS2 measurements. Another reason for this choice is that in the real world data, which will be treated later, only the GPS position and velocity outputs are available - not the pseudo and delta ranges required for the tightly coupling.

1.3.3 Estimation Filter Choice

As it has been chosen to use the loosely coupling, the remaining concern of this thesis will be the design of the ”estimation filter” block in Fig. 1.2.

A very used category of filters in the field of estimation, is the Kalman filters. This category of filters is chosen as the subject of this thesis.

A normal linear Kalman filter will not be sufficient for this task as it only yields satisfying results in an small area of a single working point in the state space. This will not be feasible as the designed navigation solution should be usable over great areas.

An alternative approach is utilization of the extended Kalman filter. When utilizing the extended Kalman filter, instead of relaying on a single working point in the state space, a linearization of the nonlinear equation is conducted in each iteration of the filter. This is the principle of the extended Kalman filter.

The author is also familiar with articles utilizing the unscented Kalman filter for the purpose of integration between inertial sensor and GPS ie. [Crassidis].

Estimation Filter Choice

Both the extended Kalman filter and the unscented Kalman filter have been part of an estimation/sensor fusion course at Aalborg University which should be evaluated through this thesis.

Due to the desire of limiting the extend of this thesis, it has been chosen to base the estimation filter design on the structure of the extended Kalman filter structure, as it simpler than the unscented Kalman filter.

1.4 Thesis Structure

The part and chapter structure of the thesis will be described here.

In the remaining part of this chapter, the problem statement will be specified in Section 1.5, in which the subgoals and delimitation also will be described.

1.4.1 Part I: Modeling

This part will consist of the issue of modeling the world and sensors.

In Chapter 2, the different reference frames used throughout the thesis will be described. This includes a fixed inertial frame and a frame which is rotating with earth. Furthermore, a local navigation frame and sensor frame together with the rotation between these two will be described.

The equations for moving on the rotating earth will be outlined in Chapter 3 together with the expressions for the variables in the derived expressions.

Chapter 4 treats the subject of modeling the sensors of the MS2 platform and the GPS.

As it has been chosen to base this thesis on the extended Kalman filter, it is necessary to derive a linear expression for the local perturbation trajectory. This will be described in Chapter 5.

Chapter 6 contains the description of a developed simulation environment, which simulates a point mass moving in an inertial frame.

1.4.2 Part II: Estimation

In Part II, the design of the estimation filter will be described.

A procedure of stating the initial estimate values, including initial attitude, and the certainty of these estimates are given in Chapter 7.

The steps involved in an iteration of the filter is described in Chapter 8 and in Chapter 9, a pseudo code of the implemented filter is shown.

1.4.3 Part III: Closure

In Part III, the acceptance tests and conclusion will be treated.

A test which is conducted on simulated data is described in Chapter 10 while test results of a real world test are given in Chapter 11.

A conclusion of the thesis together with suggestions of future work are given in Chapter 12.

1.4.4 Appendix

In the appendix, material regarding rotational kinematics and DCM equations will be explained in Chapter A. Lastly, the derivation of the linear Kalman filter will be carried through in Chapter B.

1.5 Problem Statement

The scope of this thesis is to design a navigation system consisting of a CDL MiniSense2 and a GPS, based on the extended Kalman filter and the loosely coupling. The states of interest to be estimated should include the 3-dimensional attitude, position and velocity.

In the filter, estimates of the biases of the MS2 sensors should be included in order to correct for the effect of these.

The purpose of the project is stated in the following problem statement:

How can an estimation filter based on the extended Kalman filter be applied to form a navigation solution, consisting of a CDL MiniSense2, loosely coupled with a GPS, which corrects for sensor biases?

In general, the objective of this thesis is to archive as good estimates as possible. There is no reference system/algorithm to which the test results can be directly compared.

According to CDL, the primary property of the designed navigation solution should be an ability to smoothen the position measurements of the GPS. As a secondary property, the designed navigation solution should also be able to provide the position during short GPS outages.

1.5.1 Subgoals

This should be obtained by completing the following sub goals:

1. Derivation of the equations for traveling on a rotating Earth.
2. Derivation of models of the sensors in the MiniSense2 and GPS. These models should include the bias behavior of the gyroscopes, accelerometers and magnetometer of the MS2.
3. Design of an estimation filter, based on the extended Kalman filter, which can fuse the information for the various sensors into estimates of attitude, position and velocity.
4. Design of a simulation environment in order to have the advantage of knowing all true state values and error sources. The simulated object should have behavior comparable to the one of a maritime vessel at sea and known biases should be included in the simulation of the MS2 sensors.
5. Conduction of a real world experiment in which the MiniSense2 and GPS are installed in a host maritime vessel. During this real world experiment, the measurement data of the sensors of the MiniSense2 should be logged together with data from a GPS. Also, a high-grade navigation solution should be installed and logged simultaneously during the experiment.
6. Evaluation of the estimation performance on the implementation of the designed estimation filter. Here, two tests of the designed filter should be conducted; one using simulated data and one using the data obtained in the real world experiment. In the test on the simulated data, the real state values of the system are known for reference. In the test on the real world data, the available logged navigation data from the previously mentioned high-grade navigation system should be considered the true states of reference.

1.5.2 Delimitations

To limit the extend of the thesis, the following delimitations are made:

1. It is assumed that there is no fixed misalignment between the axis of the sensors and the axises of the host vehicle/vessel. This is further explained in Section 2.5.
2. Issues regarding navigation near the poles of the earth will not be considered.

Part I

Modeling

Chapter 2

Reference Frames

This section explains the different types of coordinate systems, that is reference frames which are used throughout the thesis to describe the states of the navigation solution.

Describing the sensor measurement in a given coordinate system wrt. a different coordinate systems will ease the calculation of the kinematic and dynamic equations. All the coordinate systems/reference frames stated below are right-handed Cartesian coordinate systems in 3-dimensions.

The described frames are:

- ECI - Earth Centered Initial Reference Frame
- ECEF - Earth Centered Earth Fixed Reference Frame
- NED - North East Down
- HVRF - Host Vehicle Reference Frame
- SRF - Sensor Reference Frame

Throughout this chapter and the rest of the thesis, Direct Cosines Matrices (DCMs) will be used to denote rotation between reference frames. A brief introduction to DCMs can be found in Appendix A.

2.1 Earth Centered Initial Reference Frame

The Earth Centered Initial Reference Frame (ECI) is defined relative to the rotation axis of the Earth, which's Z-axis points towards the geographic North Pole as shown in Fig. 2.1. The origin is placed in the center of the Earth, and the X-axis, which is perpendicular to the Z-axis, points towards the center of the sun one time each year at vernal equinox, which is illustrated in Fig. 2.1. The Y-axis is the cross product of the Z- and X-axises. In this way, the plane spanned by the X- and Y-axis is the equatorial plane. It should be noted that this frame does not rotate like the ECEF frame, because it is fixed relative to the sun. The ECI is denoted as i.

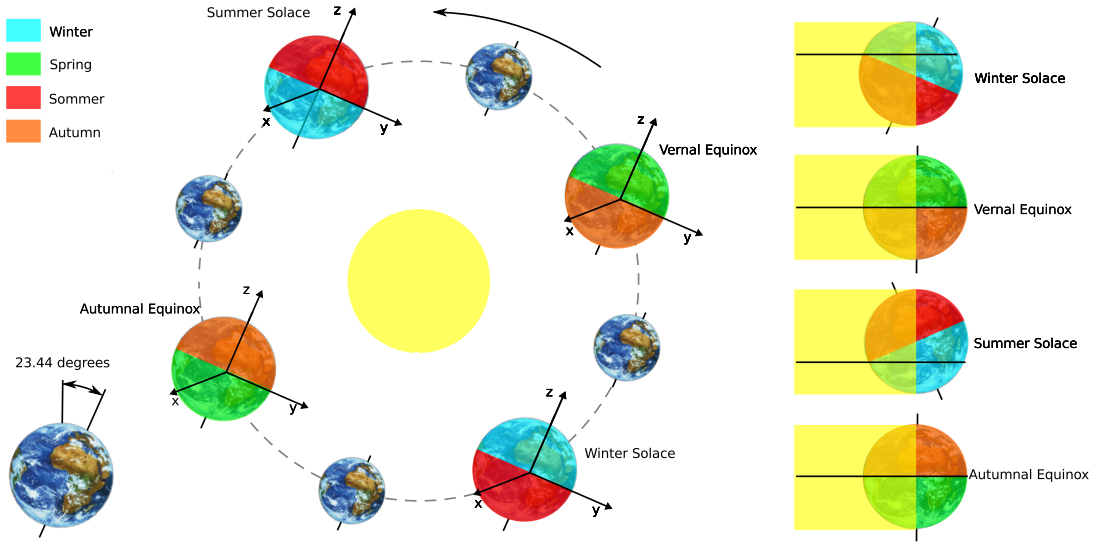

Figure 2.1: Earth Centered Initial Reference Frame, which is defined as the Z-axis pointing towards the north pole and X-axis pointing towards the center of the sun, one time each year at vernal equinox [of Electronic Systems 10]

2.2 Earth Centered Earth Fixed Reference Frame

Like the ECI reference frame, the ECEF has its origin in the center of the Earth and the Z-axis points in the direction of the geographic North Pole. This frame is fixed to the Earth in which the X-axis is defined as pointing towards the meeting point of Greenwich meridian and Equator (latitude and longitude = 0°), illustrated in Fig. 2.2. The Y-axis is the cross product of the Z- and X-axises. The ECRF is denoted as e.

The rotation rate between the ECI and the ECER is given as:

$$^{i}\omega_{ie} =^{e} \omega_{ie} = \begin{bmatrix} 0 & 0 & \omega_{earth} \end{bmatrix}^{T} \tag{2.1}$$

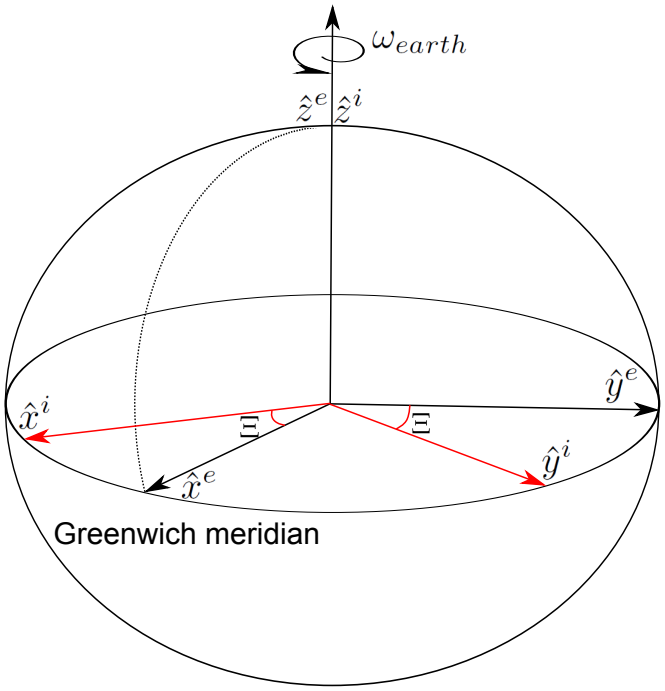

Figure 2.2: Earth Centered Earth Fixed Reference Frame, where the Z-axis points towards the North Pole, and the X-axis points towards the Greenwich meridian.

2.3 Navigation Reference Frame

The Navigation Reference Frame (NRF) is a reference frame which has its origin at the sensor denoted as $\boldsymbol{P}^n$.

The North East Down (NED) coordinates are very common to use as NRF. Another common choice for the NRF, is the East North Up (ENU) coordinates [Titterton 04]. As the name indicates, the NED will have the X-axis pointing towards the North pole, the Y-axis pointing east and consequently the Z-axis is pointing locally down. The NRF is denoted as n.

This NRF is illustrated in Fig. 2.3.

It can be seen that the NRF can be found by first rotating the ECRF 90° counterclockwise around its Y-axis, then rotating it the longitude around its X-axis and finally rotating it the latitude around the new Y-axis. These three successive rotations can be described by a DCM as:

$$\begin{aligned} {}^n\underline{\boldsymbol{C}}_e &= \underline{\boldsymbol{C}}(l)_y \, \underline{\boldsymbol{C}}(L)_x \, \underline{\boldsymbol{C}}(90^\circ)_y \\ &= \begin{bmatrix} \cos(l) & 0 & -\sin(l) \\ 0 & 1 & 0 \\ \sin(l) & 0 & \cos(l) \end{bmatrix} \begin{bmatrix} 1 & 0 & 0 \\ 0 & \cos(L) & \sin(L) \\ 0 & -\sin(L) & \cos(L) \end{bmatrix} \begin{bmatrix} \cos(90^\circ) & 0 & -\sin(90^\circ) \\ 0 & 1 & 0 \\ \sin(90^\circ) & 0 & \cos(90^\circ) \end{bmatrix} \\ &= \begin{bmatrix} -cos\,(L)\ sin\,(l) & sin\,(L)\ sin\,(l) & -cos\,(l) \\ sin\,(L) & cos\,(L) & 0 \\ cos\,(L)\ cos\,(l) & -sin\,(L)\ cos\,(l) & -sin\,(l) \end{bmatrix} \end{aligned} \tag{2.2}$$

If the elements of ${}^n\underline{\boldsymbol{C}}_e$ is denoted by row (r) and column (c) as C_{rc}, it can be seen from (2.2) that by knowing the ${}^n\underline{\boldsymbol{C}}_e$, the longitude and latitude can be extracted as:

$$\begin{aligned} L &= sin^{-1}(C_{12}) \\ l &= sin^{-1}(-C_{31}) \end{aligned} \tag{2.3}$$

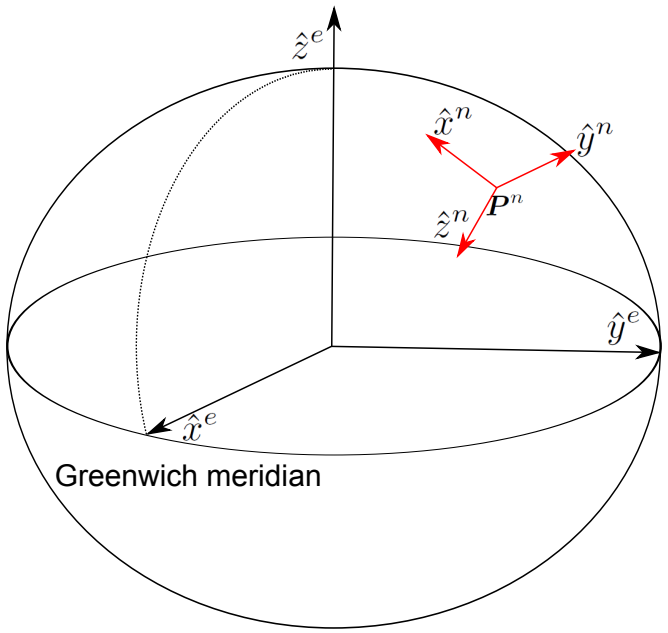

Figure 2.3: Navigation Reference Frame, where the X-axis points towards the North pole, and the Y-axis points towards East and the Z-axis points towards the center of the earth

2.4 Host Vehicle Reference Frame

The Host Vehicle Reference Frame (HVRF) has origin at the sensor and has its axis aligned with the body of the host vehicle. The axises are located in such a way that the vehicle roll is rotation around the X-axis, pitch is rotation around the Y-axis and yaw is around the Z-axis. The HVRF is denoted as b.

The HVRF is illustrated in Fig. 2.4 in which the roll (ϕ), pitch (θ) and yaw (ψ) axis are also illustrated. Positive rotation direction of roll, pitch and yaw is defined as being in clockwise direction when looking along the axis from the origin. The DCM describing the rotation from the NRF to the HVRF is defined as the result of a rotation firstly around the yaw-axis, then rotation around the pitch-axis and finally around the roll-axis (also known as a 3-2-1 rotation).

When denoting the values of the roll, pitch and yaw as ϕ, θ and ψ, this rotation can be described by using (A.13):

$$
{}^{b}\underline{\boldsymbol{C}}_{n} = \underline{\boldsymbol{C}}(\phi,\theta,\psi) = \begin{bmatrix} \cos(\theta)\cos(\psi) & \cos(\theta)\sin(\psi) & -\sin(\theta) \\ \sin(\phi)\sin(\theta)\cos(\psi) - \cos(\phi)\sin(\psi) & \sin(\phi)\sin(\theta)\sin(\psi) + \cos(\phi)\cos(\psi) & \sin(\phi)\cos(\theta) \\ \cos(\phi)\sin(\theta)\cos(\psi) + \sin(\phi)\sin(\psi) & \cos(\phi)\sin(\theta)\sin(\psi) - \sin(\phi)\cos(\psi) & \cos(\phi)\cos(\theta) \end{bmatrix} \tag{2.4}
$$

Furthermore, for small angle arguments, $cos(arg) \to 1$ and $sin(arg) \to arg$ are good approximations. By using this approximation (2.4) can be approximated for small valued ϕ, θ and ψ. These small valued angels is here denoted as $\delta\phi$, $\delta\theta$ and $\delta\psi$ by which the approximation of (2.4) can be written as:

$$
{}^{b}\underline{\boldsymbol{C}}_{n} \approx \begin{bmatrix} 1 & \delta\psi & -\delta\theta \\ -\delta\psi & 1 & \delta\phi \\ \delta\theta & -\delta\phi & 1 \end{bmatrix} = \underline{\boldsymbol{I}} - \begin{bmatrix} 0 & -\delta\psi & \delta\theta \\ \delta\psi & 0 & -\delta\phi \\ -\delta\theta & \delta\phi & 0 \end{bmatrix} \tag{2.5}
$$

It should be noted that the last term of (2.5) is a skew symmetric form of a vector, here introduced as $\boldsymbol{\gamma}$:

$$\boldsymbol{\gamma} \equiv \begin{bmatrix} \delta\phi & \delta\theta & \delta\psi \end{bmatrix}^T \tag{2.6}$$

From (2.4) it can also be seen that the roll, pitch and yaw angles can be extracted from the ${}^b\underline{\boldsymbol{C}}_n$ DCM. By denoting the elements of ${}^b\underline{\boldsymbol{C}}_n$ by row and column as C_{rc}, the angle extraction is derived as:

$$\begin{aligned} \frac{C_{23}}{C_{33}} &= \frac{\sin(\phi)\cos(\theta)}{\cos(\phi)\cos(\theta)} \Leftrightarrow \phi = tan^{-1}\left(\frac{C_{23}}{C_{33}}\right) \\ C_{13} &= -\sin(\theta) \Leftrightarrow \theta = -sin^{-1}\left(C_{13}\right) \\ \frac{C_{12}}{C_{11}} &= \frac{\cos(\theta)\sin(\psi)}{\cos(\theta)\cos(\psi)} \Leftrightarrow \psi = tan^{-1}\left(\frac{C_{12}}{C_{11}}\right) \end{aligned} \tag{2.7}$$

2.5 Sensor Reference Frame

The Sensor Reference Frame (SRF) has origin at the sensor and has its axis fixed to the axises of the sensor.

As the sensor is not always perfectly aligned with the body frame, there can exist a fixed misalignment rotation between the SRF and the HVRF.

The SBRF is also illustrated in Fig. 2.4 in which a misalignment around the Z-axis, with a value of Ψ, is illustrated.

The SRF is denoted as s.

As previously mentioned, throughout this thesis, the HVRF is assumed to coincide with the SRF, why the rotation containing the attitude information of interest will always be ${}^n\underline{\boldsymbol{C}}_s$.

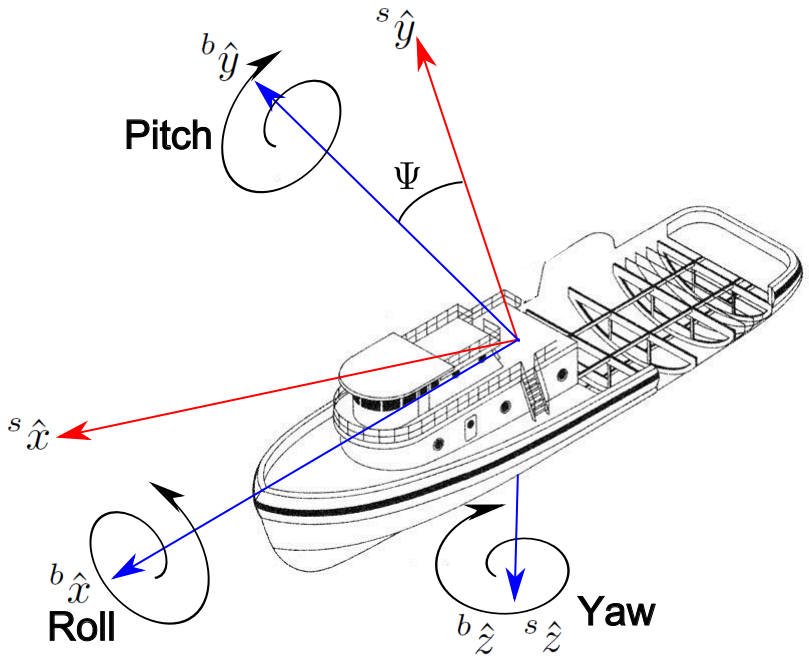

Figure 2.4: The HVRF axis, denoted with b and the SRF axis, here shown with a misalignment around the Z-axis with a value of Ψ

Chapter 3

Navigation Equations

The objective of this chapter is to derive expressions for the change of ground speed and position as a function of the current attitude, ground speed and position denoted in the NRF.

Newton's laws are only valid in inertial coordinate systems (such as the ECI frame). Newton's laws state that an object will only change direction or velocity if the sum of the forces affecting the object is different from 0 [Wikipedia 12a].

An object located at the position P^i and a vector (${}^i\boldsymbol{r}$) from the origin of the coordinate system (${}^iO$) to P^i is first defined in the ECI-frame. This is illustrated in Fig. 3.1.

When the object at P^i is in the vicinity of earth, the accelerations experienced by the object (${}^i\boldsymbol{a}$) will both be the ones caused by the gravitational field of the earth (${}^i\boldsymbol{g}$) and the accelerations of ${}^i\boldsymbol{r}$ when moving P^i around in the initial coordinate space (${}^i\ddot{\boldsymbol{r}}$). An accelerometer will measure both these accelerations as they are indistinguishable.

Thus, the acceleration of the object is given as:

$$\begin{aligned} {}^i\boldsymbol{a} &= {}^i\ddot{\boldsymbol{r}} + {}^i\boldsymbol{g} \\ &\Updownarrow \\ {}^i\ddot{\boldsymbol{r}} &= {}^i\boldsymbol{a} - {}^i\boldsymbol{g} \end{aligned} \tag{3.1}$$

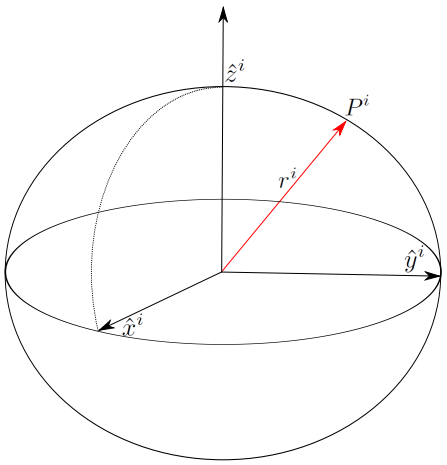

Figure 3.1: An object at position P^i and the vector ${}^i\boldsymbol{r}$ from the origin of the coordinate system to P^i

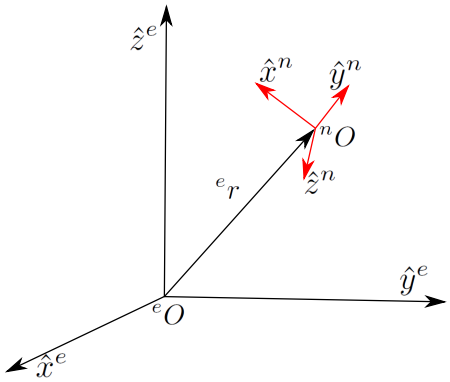

Figure 3.2: An object at position ${}^eP$ and the vector ${}^e\boldsymbol{r}$ from the origin of the coordinate system to ${}^eP$

As the navigation will take place on a rotating earth (in the ECRF), the relationship between the derivative of $\boldsymbol{r}$ when expressed in the ECI and ECRF is derived. This is done by first using the product rule followed by the insertion of the DCM kinematic rule (A.20):

$$
\begin{aligned}
{}^e\boldsymbol{r} &= {}^e\underline{\boldsymbol{C}}_i \; {}^i\boldsymbol{r} && (3.2)\\
&\Downarrow \\
{}^e\dot{\boldsymbol{r}} &= {}^e\dot{\underline{\boldsymbol{C}}}_i \; {}^i\boldsymbol{r} + {}^e\underline{\boldsymbol{C}}_i \; {}^i\dot{\boldsymbol{r}} \\
&= {}^e\underline{\boldsymbol{C}}_i \; {}^i\Omega_{ei} \; {}^i\boldsymbol{r} + {}^e\underline{\boldsymbol{C}}_i \; {}^i\dot{\boldsymbol{r}} && (3.3)
\end{aligned}
$$

For later use (3.3) is also rewritten to:

$$
{}^i\dot{\boldsymbol{r}} = {}^i\underline{\boldsymbol{C}}_e \; {}^e\dot{\boldsymbol{r}} - {}^i\Omega_{ei} \; {}^i\boldsymbol{r} \tag{3.4}
$$

Differentiating (3.3) again, and inserting (3.1), realms:

$$
\begin{aligned}
{}^e\ddot{\boldsymbol{r}} &= {}^e\dot{\underline{\boldsymbol{C}}}_i \; {}^i\Omega_{ei} \; {}^i\boldsymbol{r} + {}^e\underline{\boldsymbol{C}}_i \; {}^i\dot{\Omega}_{ei} \; {}^i\boldsymbol{r} + {}^e\underline{\boldsymbol{C}}_i \; {}^i\Omega_{ei} \; {}^i\dot{\boldsymbol{r}} + {}^e\dot{\underline{\boldsymbol{C}}}_i \; {}^i\dot{\boldsymbol{r}} + {}^e\underline{\boldsymbol{C}}_i \; {}^i\ddot{\boldsymbol{r}} \\
&= {}^e\underline{\boldsymbol{C}}_i \; {}^i\Omega_{ei} \; {}^i\Omega_{ei} \; {}^i\boldsymbol{r} + {}^e\underline{\boldsymbol{C}}_i \; {}^i\Omega_{ei} \; {}^i\dot{\boldsymbol{r}} + {}^e\underline{\boldsymbol{C}}_i \; {}^i\Omega_{ei} \; {}^i\dot{\boldsymbol{r}} + {}^e\underline{\boldsymbol{C}}_i \left({}^i\boldsymbol{a} - {}^i\boldsymbol{g}\right) \\
&= {}^e\underline{\boldsymbol{C}}_i \; {}^i\Omega_{ei} \; {}^i\Omega_{ei} \; {}^i\boldsymbol{r} + 2{}^e\underline{\boldsymbol{C}}_i \; {}^i\Omega_{ei} \; {}^i\dot{\boldsymbol{r}} - {}^e\boldsymbol{g} + {}^e\boldsymbol{a} \\
&= {}^e\underline{\boldsymbol{C}}_i \; {}^i\Omega_{ei} \; {}^i\Omega_{ei} \; {}^i\boldsymbol{r} + 2{}^e\underline{\boldsymbol{C}}_i \; {}^i\Omega_{ei} \; \left({}^i\underline{\boldsymbol{C}}_e \; {}^e\dot{\boldsymbol{r}} - {}^i\Omega_{ei} \; {}^i\boldsymbol{r}\right) - {}^e\boldsymbol{g} + {}^e\boldsymbol{a} \\
&= {}^e\underline{\boldsymbol{C}}_i \; {}^i\Omega_{ei} \; {}^i\Omega_{ei} \; {}^i\boldsymbol{r} + 2{}^e\underline{\boldsymbol{C}}_i \; {}^i\Omega_{ei} \; {}^i\underline{\boldsymbol{C}}_e \; {}^e\dot{\boldsymbol{r}} - 2{}^e\underline{\boldsymbol{C}}_i \; {}^i\Omega_{ei} \; {}^i\Omega_{ei} \; {}^i\boldsymbol{r} - {}^e\boldsymbol{g} + {}^e\boldsymbol{a} \\
&= 2{}^e\Omega_{ei} \; {}^e\dot{\boldsymbol{r}} - {}^e\underline{\boldsymbol{C}}_i \; {}^i\Omega_{ei} \; {}^i\Omega_{ei} \; {}^i\boldsymbol{r} - {}^e\boldsymbol{g} + {}^e\boldsymbol{a} && (3.5)
\end{aligned}
$$

Considering the host vehicle as moving around freely in the ECRF and a vector $({}^er)$ from the origin of the ECRF $({}^eO)$ to the origin of the NRF $({}^nO)$, as illustrated in Fig. 3.2.

The velocity experienced at ${}^nO$, represented in the NRF, is termed the ground speed and is denoted ${}^n\boldsymbol{v}$.

This velocity can be described as:

$$
{}^n\boldsymbol{v} = {}^n\underline{\boldsymbol{C}}_e \; {}^e\dot{\boldsymbol{r}} \tag{3.6}
$$

Which can be rearranged to:

$$
{}^e\dot{\boldsymbol{r}} = {}^e\underline{\boldsymbol{C}}_n \; {}^n\boldsymbol{v} \tag{3.7}
$$

Thus the ground acceleration in the NRF ($^n\dot{\boldsymbol{v}}$) can be found by differencing (3.6) using the product rule:

$$\begin{aligned} {}^n\dot{\boldsymbol{v}} &= {}^n\dot{\underline{\boldsymbol{C}}}_e \; {}^e\dot{\boldsymbol{r}} + {}^n\underline{\boldsymbol{C}}_e \; {}^e\ddot{\boldsymbol{r}} \\ &= {}^n\underline{\boldsymbol{C}}_e \; {}^e\Omega_{ne} \; {}^e\dot{\boldsymbol{r}} + {}^n\underline{\boldsymbol{C}}_e \; {}^e\ddot{\boldsymbol{r}} \\ &\Updownarrow \\ {}^e\ddot{\boldsymbol{r}} &= {}^e\underline{\boldsymbol{C}}_n \; {}^n\dot{\boldsymbol{v}} - {}^e\Omega_{ne} \; {}^e\dot{\boldsymbol{r}} \end{aligned} \tag{3.8}$$

First inserting (3.8) into (3.5), and afterwards inserting (3.7), realms:

$$\begin{aligned} {}^e\underline{\boldsymbol{C}}_n \; {}^n\dot{\boldsymbol{v}} - {}^e\Omega_{ne} \; {}^e\dot{\boldsymbol{r}} &= 2{}^e\Omega_{ei} \; {}^e\dot{\boldsymbol{r}} - {}^e\underline{\boldsymbol{C}}_i \; {}^i\Omega_{ei} \; {}^i\Omega_{ei} \; {}^i\boldsymbol{r} - {}^e\boldsymbol{g} + {}^e\boldsymbol{a} \\ &\Updownarrow \\ {}^n\dot{\boldsymbol{v}} &= 2{}^n\underline{\boldsymbol{C}}_e \; {}^e\Omega_{ei} \; {}^e\dot{\boldsymbol{r}} - {}^n\underline{\boldsymbol{C}}_e \; {}^e\underline{\boldsymbol{C}}_i \; {}^i\Omega_{ei} \; {}^i\Omega_{ei} \; {}^i\boldsymbol{r} - {}^n\underline{\boldsymbol{C}}_e \; {}^e\boldsymbol{g} + {}^n\underline{\boldsymbol{C}}_e \; {}^e\boldsymbol{a} + {}^n\underline{\boldsymbol{C}}_e \; {}^e\Omega_{ne} \; {}^e\dot{\boldsymbol{r}} \\ &= 2{}^n\underline{\boldsymbol{C}}_e \; {}^e\Omega_{ei} \; {}^e\underline{\boldsymbol{C}}_n \; {}^n\boldsymbol{v} - {}^n\underline{\boldsymbol{C}}_i \; {}^i\Omega_{ei} \; {}^i\Omega_{ei} \; {}^i\boldsymbol{r} - {}^n\boldsymbol{g} + {}^n\boldsymbol{a} + {}^n\underline{\boldsymbol{C}}_e \; {}^e\Omega_{ne} \; {}^e\underline{\boldsymbol{C}}_n \; {}^n\boldsymbol{v} \\ &= 2{}^n\Omega_{ei} \; {}^n\boldsymbol{v} - {}^n\underline{\boldsymbol{C}}_i \; {}^i\Omega_{ei} \; {}^i\Omega_{ei} \; {}^i\boldsymbol{r} - {}^n\boldsymbol{g} + {}^n\boldsymbol{a} + {}^n\Omega_{ne} \; {}^n\boldsymbol{v} \\ &= ({}^n\Omega_{ne} + 2{}^n\Omega_{ei})^n \, \boldsymbol{v} + {}^n\boldsymbol{a} - {}^n\boldsymbol{g} - {}^n\underline{\boldsymbol{C}}_i \; {}^i\Omega_{ei} \; {}^i\Omega_{ei} \; {}^i\boldsymbol{r} \end{aligned} \tag{3.9}$$

It is very common to denote the gravity and centripetal acceleration as a combined gravity term ($^n\breve{\boldsymbol{g}}$) [Titterton 04]:

$${}^n\breve{\boldsymbol{g}} = {}^n\underline{\boldsymbol{C}}_i \; {}^i\Omega_{ei} \; {}^i\Omega_{ei} \; {}^i\boldsymbol{r} + {}^n\boldsymbol{g} \tag{3.10}$$

$^n\breve{\boldsymbol{g}}$ is referred to as the "plum bob" gravity or apparent gravity [Titterton 04].

Applying (3.10) to (3.9) gives:

$${}^n\dot{\boldsymbol{v}} = ({}^n\Omega_{ne} + 2{}^n\Omega_{ei})^n \, \boldsymbol{v} + {}^n\boldsymbol{a} - {}^n\breve{\boldsymbol{g}} \tag{3.11}$$

(3.11) is the navigation equation, which describes the change of the ground speed as a function of several variables. As mentioned, it is desired that the final equation should only be a function of the attitude, position and velocity, which is why equations will be set up for these variables in the following sections.

3.1 Derivation of Navigation Variables

In this section, the expression for the variables used in (3.11) will be described. This includes the expressions for $^n\Omega_{ei}$, $^n\boldsymbol{a}$, $^n\Omega_{ne}$ and the gravity term ($^n\breve{\boldsymbol{g}}$).

3.1.1 $^n\Omega_{ei}$

The first variable is $^n\Omega_{ei}$ which is the rotation vector of earth described in the navigation frame in skew symmetric form. The vector form of this can be found as:

$${}^n\omega_{ei} = {}^n\underline{\boldsymbol{C}}_e \, (-{}^e\omega_{ie}) = \begin{bmatrix} \omega_{earth} cos(l) & 0 & \omega_{earth} sin(l) \end{bmatrix}^T \tag{3.12}$$

(3.12) is derived by using $^n\underline{\boldsymbol{C}}_e$ which is derived as a function of position in (2.2) on page 10 and $^e\omega_{ie}$ which is given in (2.1) on page 9.

3.1.2 $^n\boldsymbol{a}$

$^n\boldsymbol{a}$ is the acceleration experienced by the object, which is measured by the accelerometers. The models of the accelerometers themselves are discussed further in Chapter 4. The acceleration measurements are obtained in the SRF (as $^s\boldsymbol{a}$). From this $^n\boldsymbol{a}$ can be found, by rotating it into the NRF, as:

$${}^n\boldsymbol{a} = {}^n\underline{\boldsymbol{C}}_s \; {}^s\boldsymbol{a} \tag{3.13}$$

In which the attitude $^n\underline{\boldsymbol{C}}_s$ will be described in Section 3.2.

3.1.3 ${}^{n}\Omega_{ne}$

Another variable in (3.11) is ${}^{n}\Omega_{ne}$.

According to [Titterton 04, p. 47], ${}^{n}\omega_{ne}$ can be described as:

$$ {}^{n}\omega_{ne} = \begin{bmatrix} \dot{L}cos(l) & -\dot{l} & -\dot{L}sin(l) \end{bmatrix}^{T} \tag{3.14} $$

It is desired to have a navigation equation which is only a function of ground speed and the position. Thus, expressions for the time derivative of the latitude and longitude in terms of ground speed and position should be derived.

For further reference, the different components of the ground speed term in the NRF is denoted as:

$$ {}^{n}\boldsymbol{v} = \begin{bmatrix} V_N & V_E & V_D \end{bmatrix}^{T} \tag{3.15} $$

If the earth is assumed to be a perfect sphere with the radius R_0 and the sensor is placed at a distance h above the sea level, expressions for the time derivative of the latitude, longitude and height above sea level can be derived as:

$$ \begin{aligned} \dot{l} &= \frac{V_N}{R_0 + h} \\ \dot{L} &= \frac{V_E}{(R_0 + h)\, cos(l)} = \frac{V_E\, sec(l)}{R_0 + h} \\ \dot{h} &= -V_D \end{aligned} \tag{3.16} $$

The $cos(l)$ term in (3.16) is due to the fact that when moving east or west on the earth, there is less distance between the longitudes closer to the poles than at the equator.

The above equations were all based on the earth being a perfect sphere. Because of the centripetal acceleration, the shape of the earth is much better approximated as being an ellipsoid.

If introducing the notation of the semi-major axis radius as R_M (the radius at the equator) and the semi-minor axis radius as R_m (the radius at the poles), an expression for the flattening f_{earth} and the major eccentricity e_{earth} is given as [Titterton 04, p. 49]:

$$ f_{earth} = \frac{R_M - R_m}{R_M} \tag{3.17} $$

$$ e_{earth} = \sqrt{f_{earth}(2 - f_{earth})} \tag{3.18} $$

Two important geometric aspects of the earth are the meridional and the normal radius of curvature. These are defined as the radius of the circle one would travel in, if one continued ones current curve. The meridional radius of curvature (R_{NS}) is the radius of the circle one would follow if one traveled directly north or south. This radius is illustrated in Fig. 3.3. The normal radius of curvature (R_{EW}) is the radius of the circle if one traveled directly east or west.

The radiuses of curvature is given as [Titterton 04, p. 49], which is refering to the WGS-84 standard ellipsoid:

$$ R_{NS} = \frac{R_M \left(1 - e_{earth}^2\right)}{\left(1 - e_{earth}^2\, sin^2(l)\right)^{3/2}} \tag{3.19} $$

$$ R_{EW} = \frac{R_M}{\left(1 - e_{earth}^2\, sin^2(l)\right)^{1/2}} \tag{3.20} $$

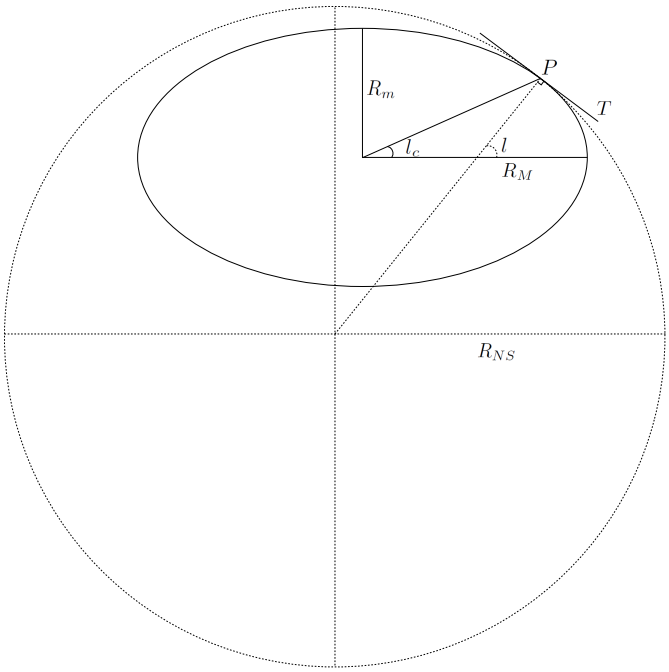

Figure 3.3: The earth and its radius of north-south curvature at P

Inserting (3.20) into (3.16):

$$\begin{aligned} \dot{l} &= \frac{V_N}{R_{NS} + h} \\ \dot{L} &= \frac{V_E \, sec(l)}{R_{EW} + h} \\ \dot{h} &= -V_D \end{aligned} \tag{3.21}$$

For further reference, the position vector is defined as:

$$\boldsymbol{p} \equiv \begin{bmatrix} l \\ L \\ h \end{bmatrix} \qquad \Rightarrow \dot{\boldsymbol{p}} = \begin{bmatrix} \dot{l} \\ \dot{L} \\ \dot{h} \end{bmatrix} \tag{3.22}$$

By inserting (3.21) back into (3.14), the final term for ${}^{n}\omega_{ne}$ is obtained as:

$$\begin{aligned} {}^{n}\omega_{ne} &= \begin{bmatrix} \frac{V_E \, sec(l)}{R_{EW}+h} \, cos(l) & -\frac{V_N}{R_{NS}+h} & -\frac{V_E sec(l)}{R_{EW}+h} \, sin(l) \end{bmatrix}^T \\ &= \begin{bmatrix} \frac{V_E}{R_{EW}+h} & -\frac{V_N}{R_{NS}+h} & -\frac{V_E}{R_{EW}+h} \, tan(l) \end{bmatrix}^T \end{aligned} \tag{3.23}$$

3.1.4 Gravity Model

As the Z-axis of the navigation frame is always pointing downwards, the plum bob gravitational acceleration can be approximated as always only being present in this axis.

The magnitude of the plum bob gravity at sea level can be described as [Titterton 04, p. 57]:

$$\breve{g_0}(l) = 9.780318 \left(1 + 5.3024 \cdot 10^{-3} \, sin^2(l) - 5.9 \cdot 10^{-6} \, sin^2(2l)\right) \; [m/s^2] \tag{3.24}$$

Furthermore, the magnitude of the plum bob gravity at a specific height (h) above the sea level can be described as:

$$\breve{g}(h,l) = \breve{g_0}(l) - h \cdot 3.0877 \cdot 10^{-6} \left(1 - 1.39 \cdot 10^{-3}\, sin^2(l)\right) \ [^m/_{s^2}] \tag{3.25}$$

Thus, given that the gravity is only present in the Z-axis of the navigation frame, the gravity vector has the expression:

$$^n\breve{\boldsymbol{g}} = \begin{bmatrix} 0 \\ 0 \\ \breve{g}(h) \end{bmatrix} \tag{3.26}$$

3.2 Attitude Expression

$^n\underline{\boldsymbol{C}}_s$ is the DCM describing the attitude of the sensor. As in this thesis fixed sensor alignment errors are not considered, it is assumed that:

$$^n\underline{\boldsymbol{C}}_s = ^n\, \underline{\boldsymbol{C}}_b \tag{3.27}$$

$^s\omega_{si}$ is the rate which can be estimated from the measurements from the gyroscopes. The model of the gyroscopes themselves are discussed further in Chapter 4.

$$\begin{aligned}
^n\dot{\underline{\boldsymbol{C}}}_s &= ^n\, \underline{\boldsymbol{C}}_s\ ^s\Omega_{ns} \\
&= ^n\, \underline{\boldsymbol{C}}_s\, (^s\Omega_{se} - ^s\, \Omega_{ne}) \\
&= ^n\, \underline{\boldsymbol{C}}_s\, (^s\Omega_{si} - ^s\, \Omega_{ei} - ^s\, \Omega_{ne}) \\
&= ^n\, \underline{\boldsymbol{C}}_s\, (^s\Omega_{si} - ^s\, \underline{\boldsymbol{C}}_n\, (^n\Omega_{ei} - ^n\, \Omega_{ne})^n\, \underline{\boldsymbol{C}}_s) \\
&= ^n\, \underline{\boldsymbol{C}}^s_s\Omega_{si} - (^n\Omega_{ei} - ^n\, \Omega_{ne})^n\, \underline{\boldsymbol{C}}_s
\end{aligned} \tag{3.28}$$

3.3 Chapter Summery

In this chapter the fundamental navigation equation, which describes the change of ground velocity, has been derived as:

$$^n\dot{\boldsymbol{v}} = (^n\Omega_{ne} + 2^n\Omega_{ei})^n\, \boldsymbol{v} + ^n\, \boldsymbol{a} - ^n\, \breve{\boldsymbol{g}} \tag{3.29}$$

Derivations have been preformed to describe this as a function of measured variables and the present location and velocity. For instances $^n\Omega_{ne}$ has been derived as the skew-symmetric representation of:

$$^n\omega_{ne} = \begin{bmatrix} \frac{V_E}{R_{EW}+h} & -\frac{V_N}{R_{NS}+h} & -\frac{V_E}{R_{EW}+h}\, tan(l) \end{bmatrix}^T \tag{3.30}$$

The term $^n\breve{\boldsymbol{g}}$ can be obtained from a model given the present location. This is described in Subsection 3.1.4.

Furthermore, the following term for the position has been derived:

$$\begin{aligned}
\dot{l} &= \frac{V_N}{R_{NS} + h} \\
\dot{L} &= \frac{V_E\, sec(l)}{R_{EW} + h} \\
\dot{h} &= -V_D
\end{aligned} \tag{3.31}$$

And the position vector was introduced, which were defined as:

$$\boldsymbol{p} \equiv \begin{bmatrix} l \\ L \\ h \end{bmatrix} \tag{3.32}$$

The change of attitude was determined to be described as:

$$^{n}\underline{\dot{\boldsymbol{C}}}_{s} = ^{n}\ \underline{\boldsymbol{C}}_{s}^{s}\Omega_{si} - (^{n}\Omega_{ei} - ^{n}\ \Omega_{ne})^{n}\ \underline{\boldsymbol{C}}_{s} \tag{3.33}$$

Chapter 4

Sensor Modeling

As previously described, the sensors used in this navigation application are an IMU unit (a unit consisting of a 3-axises gyroscope and 3-axises accelerometer), a 3-axises magnetometer and a GPS unit.
In this chapter, these sensors and their models are described.

As mentioned, the scope of this thesis is to be basis for a commercial low-cost navigation product. As with all components, their parameter values will vary. In this price range it is not likely cost-effective to do an individual estimation of the parameters on each unit. Because of this it is chosen to use the parameter values given in the data sheets, when possible, as opposed to conducting tests in order to derive own parameter values which might be a better fit for the specific tested unit, but might be a very bad fit for other MiniSense2 units.

4.1 Gyroscopes

Within the IMU [Ana 11] used in the MiniSense2, is a gyroscope which measures the angular velocity vector of the sensor relative to the IRF at a sample rate of 51.2 Hz. This measurement is denoted as: ${}^s\widetilde{\boldsymbol{\omega}}_{is}$. The gyroscope measurement will be corrupted by factors such as misalignments in the sensor, biases and measurement noise.

In the model in this thesis, it is assumed that the measurement error is only caused by biases and uncorrelated measurement noise. The model is stated as:

$$ {}^s\widetilde{\boldsymbol{\omega}}_{is} = {}^s\,\boldsymbol{\omega}_{is} + {}^s\,\boldsymbol{b}_{gyro} + \boldsymbol{v}_{gyro} \tag{4.1} $$

In which $\boldsymbol{v}_{gyro}$ is the term for the measurement noise which is regarded to be white Gaussian distributed white noise.

In the datasheet [Ana 11, 3] it is informed that the Angular Random Walk coefficient $K_{ARW_{gyro}}$ is 2.0 $^\circ/\sqrt{hr} = 33 \cdot 10^{-3\circ}/\sqrt{s}$.

The relation between Random Walk Coefficients (K_{RW}) and the standard deviation of the underlaying noise (σ_v) is given as [Totu 02, p. 20]:

$$ \sigma_v = \frac{K_{RW}}{\sqrt{TS}} \tag{4.2} $$

In which TS is the sample periode.

Using (4.2), it is found that the standard deviation of $\boldsymbol{v}_{gyro}$ is 0.238 $^\circ/s$.

In (4.1), the bias term is denoted as ${}^s\boldsymbol{b}_{gyro}$.

A common method to model the bias is to consider it as being a standard Brownian motion [Pifu Zhang 05] [Totu 02, p. 40]. A Brownian motion is the integration of a Gaussian distributed white noise process [Wikipedia 12b]:

$$^{s}\boldsymbol{b}_{gyro} = \int \boldsymbol{w}_{\boldsymbol{b}_{gyro}} \tag{4.3}$$

Where $\boldsymbol{w}_{\boldsymbol{b}_{gyro}}$ is Gaussian distributed white noise.

A suitable bias model notation is obtained by differentiating (4.3) as:

$$^{s}\dot{\boldsymbol{b}}_{gyro} = \boldsymbol{w}_{\boldsymbol{b}_{gyro}} \tag{4.4}$$

The determination of the standard variation of $\boldsymbol{w}_{\boldsymbol{b}_{gyro}}$ is described in Subsection 4.1.1.

Another thing to consider is the turn-on to turn-on bias stability. This is the variation of the initial bias when the gyroscope is turned on. The standard deviation of the initial bias is informed to be 3 $^{\circ}/_{s}$. This will be used later in the thesis when initializing the estimation filter and when selecting the bias values for the simulation environment.

4.1.1 Determination of Gyroscope Bias Variation

As mentioned, the bias is modeled as integrated white noise - known as a Brownian motion.

In the datasheets for some gyroscope, a value for this random walk is specified as the Rate Random Walk (RRW). However, in the data sheet for the IMU used in this thesis, this is not specified. But, both for the gyroscope and accelerometer, the Allan Variance plot is specified.

Allan Variance Plot

An Allan variance plot is a tool commonly used in the field of gyroscope parameter determination.

The Allan variance plot is obtained by doing a longterm test in which the sensor is placed stationary while the sensor is sampled.

The data is then divided into equal sized subintervals of data of a specified time interval (τ) and the mean value is calculated for each set of data. The standard deviation of these mean values are then calculated. This is repeated for a range of different time intervals.

The resulting standard deviations at the different intervals are then plotted into a graph. This graph contains a great amount of information regarding the parameter values of the sensor.

An example of a gyroscope Allan variance plot is shown in Fig. 4.1 in which the axises are log-log. In Fig. 4.1, indications of how different gyroscope noise terms will appear in the Allan variance plot are shown. According to [Gyro 97, Appendix C, p. 71], experience shows that in most cases, different noise terms appear in different regions of the Allan variance plot.

The Rate Random Walk coefficient K_{RRW} is represented by a slope of $+1/2$ on a log-log plot, which in a log-log plot is given by the equation [Gyro 97, Appendix C, p. 66]:

$$\sigma^2(\tau) = \frac{K_{RRW}^2 \cdot \tau}{3} \tag{4.5}$$

The value K_{RRW} of be obtained by extending the $+1/2$ slope and find the intersection point of this slope and the $\tau = 3$ line.

By observing (4.5) it can be seen that K_{RRW} can then be obtained by the standard deviation at this point. An example of this is indicated by the dotted lines on Fig. 4.1.

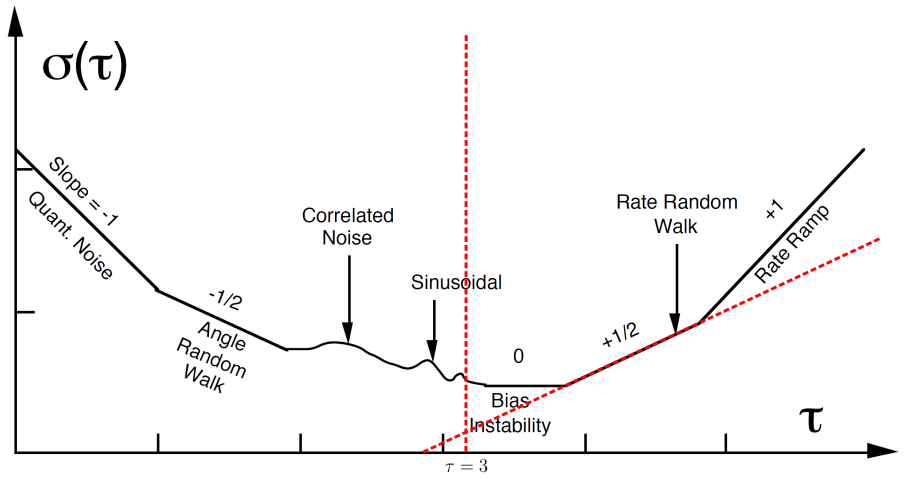

Figure 4.1: An example of a typical Allan variance plot [Gyro 97, Appendix C, p. 71] with added dotted lines indicating the procedure of finding K_{RRW}. The axises here are log-log.

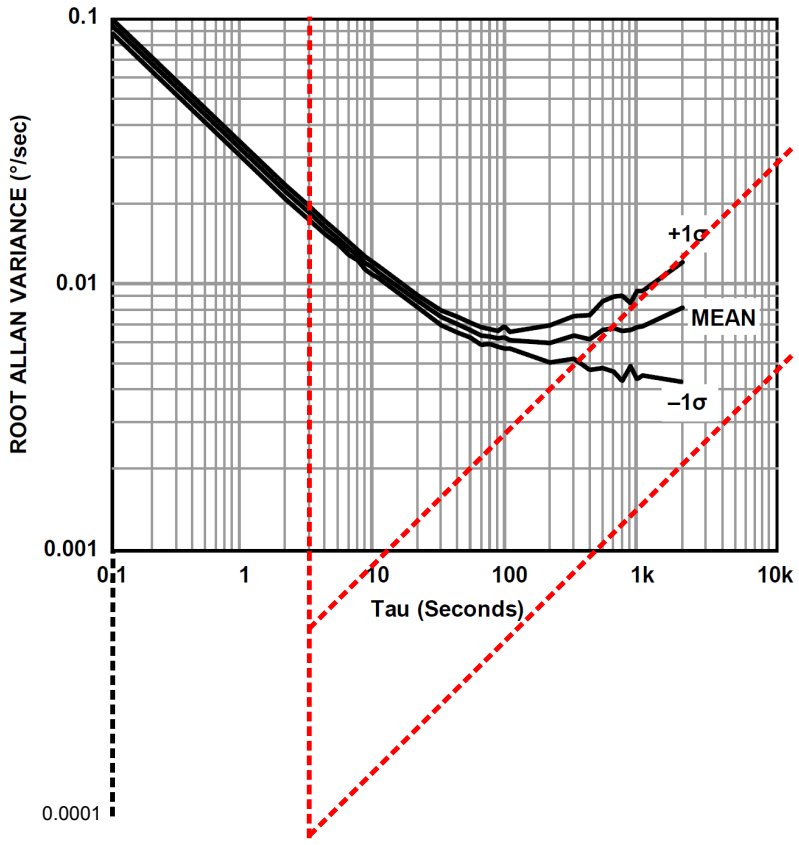

Figure 4.2: The Allan variance plot for the IMU's gyroscope [Ana 11] with extended Y-axis together with dotted line indicating the procedure of finding $K_{RRW_{gyro}}$

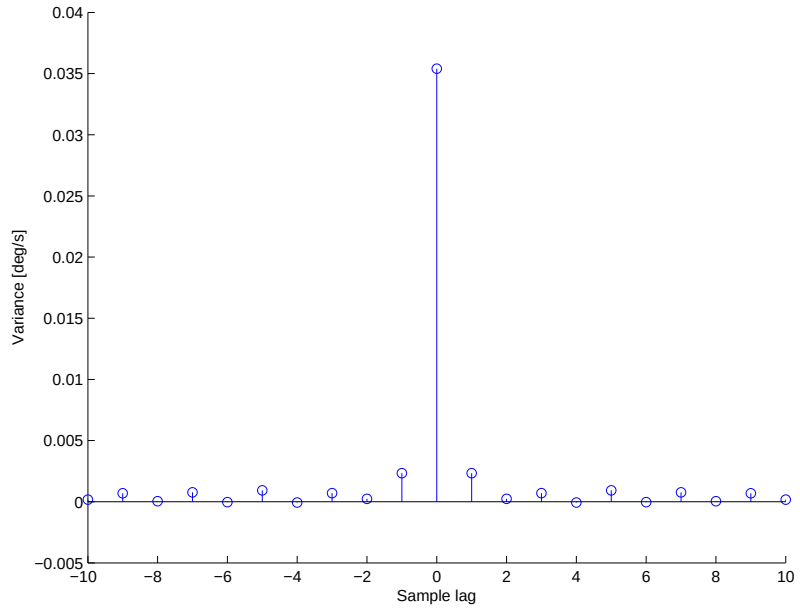

Figure 4.3: Covariance of gyroscope measurement of a 2 *min* stationary test

Determination of $K_{RRW_{gyro}}$ Using Allan Variance Plot

In Fig. 4.2, the Allan variance plot from the gyroscope data sheet is shown.

Two lines with a $+1/2$ slope has been added to the original plot. It is seen that this Allan variance plot does not contain any part with a $+1/2$ slope. Furthermore, it is seen that, presumably due to variations in the production of the IMUs, the right part of the plot is dominated by increasingly uncertainty.

It has been attempted to assess the 1 σ range of the $+1/2$ slope and draw lines to $\tau = 3$, knowing that this is a cruel approximation as the original $-\sigma$ graph does not seem to have a tendency to start increasing into a $+1/2$ slope.

Using this approach, it is roughly assessed that the 1 σ confidence range of $K_{RRW_{gyro}}$ is between $0.08 \cdot 10^{-3}$ and $0.5 \cdot 10^{-3}$ $^\circ/\sqrt{s^3}$. The $K_{RRW_{gyro}}$ value is selected as the average value of these two, which is $0.29 \cdot 10^{-3}$ $^\circ/\sqrt{s}$.

By utilizing (4.2) it is found that the standard deviation of $\boldsymbol{w}_{\boldsymbol{b}_{gyro}}$ is $2.1 \cdot 10^{-3}$ $^\circ/s^2$.

4.1.2 Correlation of Gyroscope Measurement Noise

It is commonly seen that sensors experience correlation of the measurements.

To analyze this, an experiment has been conducted in which the gyroscope has been placed stationary while a sample series has been obtained.

The cross-covariance has been calculated from a series of 2 *min* of 51.2 Hz stationary measurements from one of the gyroscope axises. The result of this is shown in Fig. 4.3.

In Fig. 4.3 it is seen that the measurement series is not dominantly correlated. However, at 1 sample lag there is a slight correlation.

In the time domain, this will mean that the sensor is experiencing a slight low pass effect.

In order to include a low pass effect in the system model for each axis of the gyroscope, three additional system states are required with concomitant extra computational load to follow.

As the low pass effect is very slight it is assessed that it is not justifiable to add this extra computational load and model complexity.

A histogram of the 2 *min* sample was also conducted, but is not shown here. It was seen that the assumption of the noise being Gaussian distributed was highly justified.

4.2 Accelerometer

The accelerometers within the IMU is modeled in a very similar way to the gyroscopes. The accelerometers measure the acceleration in the IRF, due to movement and the gravitational field. Like with the gyroscopes, these measurements are available at a sample rate of 51.2 Hz

As mentioned, the accelerometer model it very similar to the one of the gyroscope, in the way that it is assumed that the measurement (${}^s\widetilde{\boldsymbol{a}}$) is the function of the actual acceleration, a slow changing bias and measurement noise.

The measurement model is described as:

$$ {}^s\widetilde{\boldsymbol{a}} = {}^s\,\boldsymbol{a} + {}^s\,\boldsymbol{b}_{acc} + \boldsymbol{v}_{acc} \tag{4.6} $$

In which $\boldsymbol{v}_{acc}$ is the term for the measurement noise which is regarded to be Gaussian distributed white noise.

In the datasheet [Ana 11, 3] it is informed that the Velocity Random Walk Coefficient $K_{VRW_{acc}}$ is 0.09 $\frac{m/s}{\sqrt{hr}} = 1.5 \cdot 10^{-3} m/\sqrt{s^3}$.

By utilizing (4.2) it is found that the standard deviation of $\boldsymbol{v}_{acc}$ is $10.73 \cdot 10^{-3}$ m/s^2.

The model for the bias term (${}^s\boldsymbol{b}_{acc}$) is similar to the gyroscope bias as is also modeled as a Brownian motion.

The dynamic model of the bias is described as:

$$ {}^s\dot{\boldsymbol{b}}_{acc} = \boldsymbol{w}_{\boldsymbol{b}_{acc}} \tag{4.7} $$

The determination of the standard variation of $\boldsymbol{w}_{\boldsymbol{b}_{gyro}}$ is described in Subsection 4.2.1.

Again, the turn-on to turn-on bias variance, which is the variation of the initial bias when the accelerometer is turned on, should be considered. The standard deviation of the initial bias of the accelerometer is informed to be 6 mg. This will be used later in the thesis when initializing the estimation filter and when selecting the bias values for the simulation environment.

4.2.1 Determination of Accelerometer Bias Variation and Correlation of Measurement Noise

Like the gyroscope, a value for the random walk of the bias is not directly specified. But the Allan variance plot is provided in the data sheet and illustrated in Fig. 4.4.

The same procedure, as was used when dealing with the gyroscope parameter $K_{RRW_{gyro}}$ is utilized to determine the Acceleration Random Walk coefficient ($K_{ARW_{acc}}$) of the accelerometer.

Using the same cruel assumptions, it is roughly assessed that the 1 σ confidence range of $K_{ARW_{acc}}$ is between $0.7 \cdot 10^{-6}$ and $4 \cdot 10^{-6}$ $g/\sqrt{s}$. For later use, the $K_{ARW_{acc}}$ value is selected as the average value of these two, which is $2.35 \cdot 10^{-6}$ $g/\sqrt{s} = 23.03 \cdot 10^{-6}$ $m/\sqrt{s^4}$.

By utilizing (4.2) it is found that the correspondent standard deviation of $\boldsymbol{w}_{\boldsymbol{b}_{acc}}$ is $164 \cdot 10^{-6}$ m/s^3.

Again it is known that this is a cruel approximation as the original $-\sigma$ graph does not seem to have a tendency to start increasing into a $+1/2$ slope.

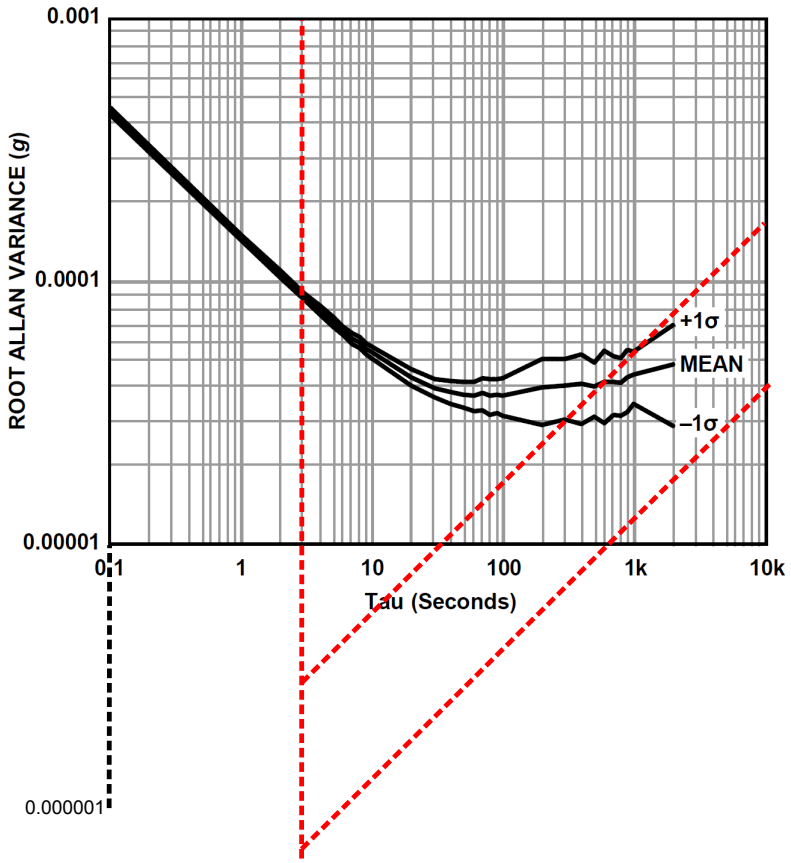

Figure 4.4: The Allan variance plot for the IMU's accelerometer [Ana 11] with extended Y-axis together with dotted line indicating the procedure of finding $K_{RRW_{acc}}$

As for the gyroscope, the correlation of the accelerometer measurements should also be analyzed.

The cross-covariance has been calculated from a series of 2 min of 51.2 Hz stationary measurement from one of the accelerometer axises. The result of this is shown in Fig. 4.5.

Again, a very slight correlation at 1 sample lag is detected.

Again, it is assessed that it is not justifiable to add extra system model states to model this effect.

A histogram of the 2 min sample was also conducted, but is not shown here. It was seen that the assumption of the noise being Gaussian distributed was highly justified.

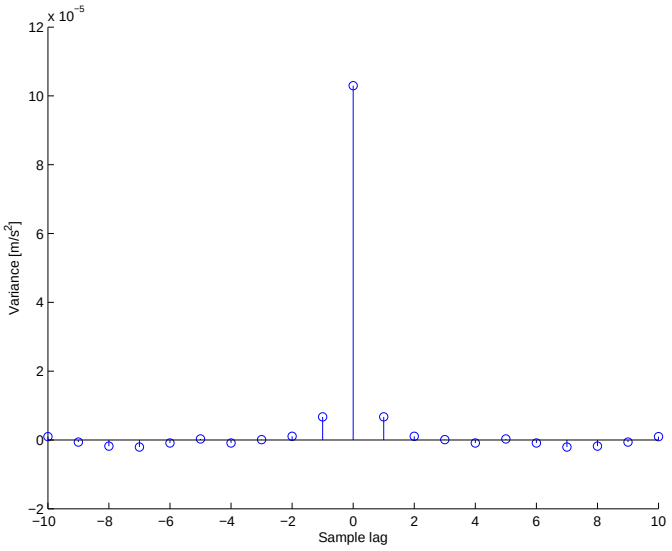

Figure 4.5: Covariance of accelerometer measurement of a 2 min stationary test

4.3 Magnetometer

The MiniSense2 is equipped with a 3-axises magnetometer [Hon 11], which measures the magnetic field in the SBR with a sample rate of 51.2 Hz.

Given a location, models are available to give an expected value of the current local magnetic field vector in the NRF (${}^{n}\breve{\boldsymbol{m}}$). The idea is then to compare this expected magnetic field vector with vector field measured by the magnetometers in the SRF (${}^{s}\widetilde{\boldsymbol{m}}$) in order to aid the attitude estimation.

In the applications of the MiniSense2 unit, it is often placed on a metal vessel with other electronics in the vicinity of the unit. Metal structures surrounding the unit can cause reshaping of the vector field and nearby electronic units can generate their own magnetic fields. It is assessed that both these two phenomenons can be modeled as being a constant or slowly changing additive measurement bias ${}^{s}\boldsymbol{b}_{mag}$.

Furthermore, as all other sensors, the magnetometer has measurement noise $\boldsymbol{v}_{mag}$. In the data sheet, the standard deviation of the measurement noise is informed to be 2 mG.

$$ {}^{s}\widetilde{\boldsymbol{m}} = {}^{s}\underline{\boldsymbol{C}}_{n}\, {}^{n}\breve{\boldsymbol{m}} + {}^{s}\boldsymbol{b}_{mag} + \boldsymbol{v}_{mag} \tag{4.8} $$

As the bias is modeled as being slowly changing, it is modeled like the gyroscope and accelerometer bias. The bias state ${}^{s}\boldsymbol{b}_{mag}$ is augmented in the state vector and modeled as:

$$ {}^{s}\dot{\boldsymbol{b}}_{mag} = \boldsymbol{w}_{\boldsymbol{b}_{mag}} \tag{4.9} $$

In which $\boldsymbol{w}_{\boldsymbol{b}_{mag}}$ is white Gaussian noise.

As the change in bias is actually not caused by the sensor itself, but by the environment, the standard deviation of the bias driving noise is regarded a tuning parameter as it cannot be found empirically for the general application.

In the MiniSense2 manual for the user [CDL 10], it is described how the magnetometer should be calibrated when applied to a vessel. This involves rotating the application around the spherical working region of the vessel. For many applications this is not possible (or very troublesome), such as ships. It can only be expected that the magnetometer has been roughly calibrated.

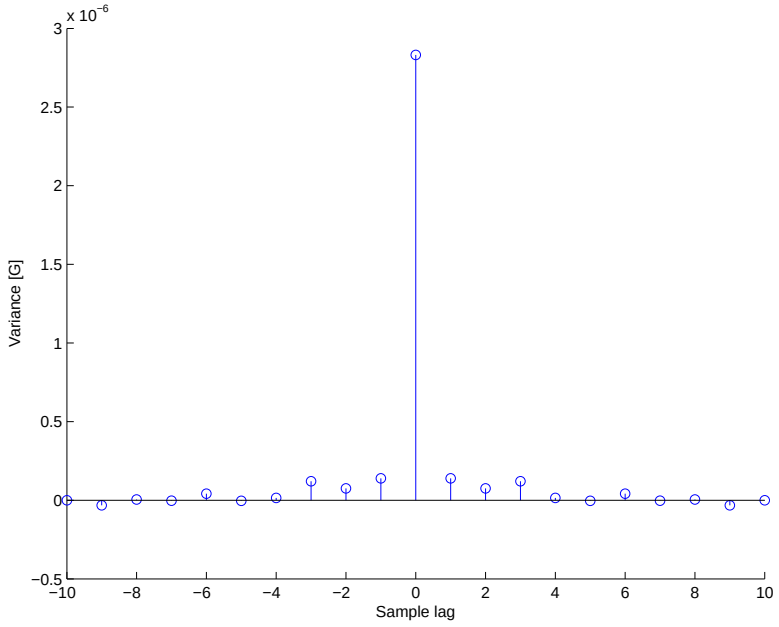

Figure 4.6: Covariance of magnetometer measurement of a 2 *min* stationary test

4.3.1 Analysis of Correlation of Magnetometer Measurement Noise

As for the previously described sensors, the correlation of the measurements should also be analyzed.

The cross-covariance has been calculated from a series of 2 *min* of 51.2 *Hz* stationary measurement from one of the magnetometer axises. The result of this is shown in Fig. 4.6.

In this magnetometer data series, a very slight correlation is detected at the first few sample lags.

But it is assessed that it is not justifiable to add extra system model states to model this effect at the expense of increased computational load.

A histogram of the 2 *min* sample was also conducted, but is not shown here. It was seen that the assumption of the noise being Gaussian distributed was highly justified.

4.3.2 Earth Magnetic Field Model

Near the vicinity of earth, the magnetic field can be roughly approximated as a dipole magnet going through the earth as illustrated in Fig. 4.7.

It should be noted in Fig. 4.7 that the geodetic (true) north and magnetic north does not coincide. There is a known, very slowly changing, rotation between these.

The magnetic field of the earth can be approximated by the International Geomagnetic Reference Field (IGRF) model, maintained by organization International Association of Geomagnetism and Aeronomy (IAGA) [of Geomagnetism 12].

The IGRF is based on a collection of contributions from different institutes who gathered magnetic field data from observatories and surveys around the world and from satellites like Champ and Ørsted [of Geomagnetism 12].

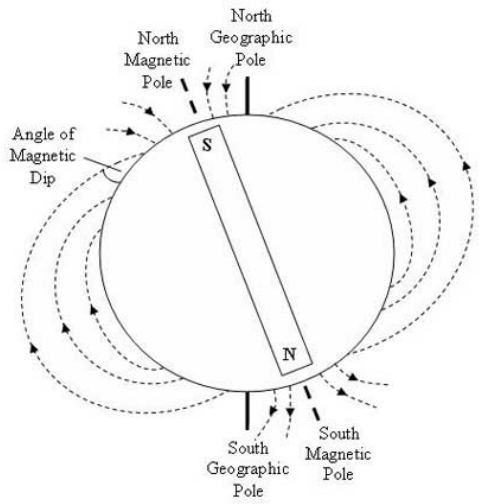

Figure 4.7: A simple model of the magnetic field of the earth

The annual rate of change of the Main Field is also incorporated in the IGRF and the model is assumed to be linear over five-year intervals. The latest model valid for 2010-2015 is called the IGRF 11th generation model (IGRF11).

IGRF provides an open source C-based function to get the magnetic field vectors denoted in the NED frame, given the latitude, longitude and height above sea level.

4.4 GPS

A GPS receiver unit is also available. The big advantage of having GPS measurements is that it measures the position and velocity with bounded precisions, which as mentioned in Chapter 1 is in contrast to the estimates of the pure INS.

One of the disadvantages, however, is that it can be unavailable for periods of time though the outage periods will generally be fairly short. [Simonsen 12] states that 99 % of the outages have a duration of less than 25 s.

Another disadvantage of GPS is a fairly slow measurement rate. In the later used test data, the GPS has a measurement rate of 1 Hz in contrast to the faster sample rate of the MS2 sensors of 51.2 Hz.

Furthermore, the position is only absolutely precise to within approximately 10 meters. A big part of the position inaccuracy is caused by various disturbances in the atmosphere which will cause a slowly varying bounded offset of the position measurement. A possible solution to this problem is to use differential GPS (DGPS). In DGPS, a special GPS base station is placed at a known fixed location in the vicinity of the mobile GPS receivers. The receiver of this fixed GPS base station, with known location, will receive the same atmospherical disturbances as the mobile units. This can be used to correct the position estimate of the mobile units by transmitting this information from the base station to the mobile units.

In the navigation solution scoped by this thesis, DGPS is not assumed. But when using low-cost initial components, it will not be achievable to be able to account for the slow varying offset caused by the atmospherical disturbances.

4.4.1 GPS Position Model

When GPS measurements are available it is possible to obtain a measurement of the current latitude and longitude ($\widetilde{l}$ and $\widetilde{L}$), together with a measurement of the current height ($\widetilde{h}$) above sea level.

The model for the position measurement is stated as:

$$^{n}\widetilde{\boldsymbol{p}}_{GPS} = \boldsymbol{p} + \boldsymbol{v}_{\boldsymbol{p}_{GPS}} \tag{4.10}$$

$$\tag{4.11}$$

$v_{\boldsymbol{p}_{GPS}}$ is here the measurement noise of the position which is modeled as being white Gaussian distributed noise. It is known that it is a fairly cruel assumption to approximate the measurement error as only being white as the GPS positions, as mentioned previously, are known to have a fairly correlated error due to e.g. factors as the atmospherical disturbances.

But it was also mentioned earlier, that it will not be achievable to account for this slow varying offset in the navigation solution. It is then assumed that the remaining measurement noise can be reasonable described as white Gaussian distributed noise. The standard deviation of this noise is assumed to be the stated position accuracy of the GPS when used in a DGPS setup.

In the data sheet of the GPS used in the real world experiment, the position accuracy is stated to have a standard deviation of 1 m when using DGPS [Tri 98], thus this is used as the noise parameter.

4.4.2 GPS Velocity Model

When a GPS unit measures the velocity, several standardized GPS output formats are available.

Unfortunately, the output format of the GPSs commonly used within maritime application is the National Marine Electronics Association (NMEA 0184) output format. The big disadvantage of using the format is that the measured velocity is only outputted as a horizontal heading and a magnitude, thus no information regarding the vertical velocity is outputted. The measured heading and magnitude can be transformed into measurements of the north and east components ($\widetilde{V}_{N_{GPS}}$ and $\widetilde{V}_{E_{GPS}}$).

As the primary applications for the navigation solution are maritime, it can be assumed that the vertical velocity is very small. It has been chosen to insert a fake measurement of the vertical velocity as being 0, with justification by the knowledge of this being very small in the target applications.

As described in Chapter 3, the accelerometer measures both the acceleration due to displacement and the gravity. The gravity has to be obtained using a model of the gravitational field which is described in Subsection 3.1.4. There is known to be a limited accuracy of this model as it is fairly simple. The calculated gravity magnitude will not be exactly, and when operating near mountains the direction can also slightly deviate from the downward axis of the NRF. By observing (3.29), it can be seen that the error due to the magnitude mismodeling causes a drift in the vertical velocity channel.

A big advantage of having the extra fake vertical measurement is that the velocity measurement bounds this drift. The vertical velocity would also be bounded by the vertical position measurement, but it is assessed that the vertical fake measurement is advantageous to have in order to further minimize this drift.

An other smaller advantage of inserting the fake vertical velocity measurement, is that it will be very simple to change the system in case a GPS unit with vertical velocity measurement output is used.

As the vertical channel has been assumed close to 0, the GPS velocity measurement vector is defined as:

$$ {}^{n}\widetilde{\boldsymbol{v}}_{GPS} = \begin{bmatrix} \widetilde{V}_{N_{GPS}} \\ \widetilde{V}_{E_{GPS}} \\ 0 \end{bmatrix} \tag{4.12} $$

The common way for GPS units to measure the velocity, is by utilizing the Doppler principle. Because the receiver moves relative to the GPS satellites, the transmission frequency received is shifted from the broadcast frequency. By having knowledge about the velocity of the satellites relative to the earth, the velocity of the receivers can be deduced. This method is not as affected by atmospherical disturbances as the position measurement [B. Hoffmann-Wellenhof 01, 6].

According to [Prasad 05, 53] the standard deviation of the velocity measurement of GPS is 0.1 $^{m}/_{s}$. It is assessed that this uncertainty, fairly, can be assumed to be Gaussian distributed white noise.

The model of the GPS velocity measurement can then be described as:

$$ {}^{n}\widetilde{\boldsymbol{v}}_{GPS} = {}^{n}\boldsymbol{v} + \boldsymbol{v}_{\boldsymbol{v}_{GPS}} \tag{4.13} $$

In which $v_{\boldsymbol{v}_{GPS}}$ is the measurement noise of the velocity which is modeled as being white Gaussian distributed noise.

4.5 Chapter Summary/Measurement Model

To summarize, the following models for the sensors have been stated in this chapter:

$$ \widetilde{\boldsymbol{y}} = \begin{bmatrix} \widetilde{\boldsymbol{p}}_{GPS} \\ {}^{n}\widetilde{\boldsymbol{v}}_{GPS} \\ {}^{s}\widetilde{\boldsymbol{\omega}}_{is} \\ {}^{s}\widetilde{\boldsymbol{a}} \\ {}^{s}\widetilde{\boldsymbol{m}} \end{bmatrix} = \begin{bmatrix} \boldsymbol{p} + \boldsymbol{v}_{\boldsymbol{p}_{GPS}} \\ {}^{n}\boldsymbol{v} + \boldsymbol{v}_{\boldsymbol{v}_{GPS}} \\ {}^{s}\boldsymbol{\omega}_{is} + {}^{s}\boldsymbol{b}_{gyro} + \boldsymbol{v}_{gyro} \\ {}^{s}\boldsymbol{a}_{ext} + {}^{s}\boldsymbol{b}_{acc} + \boldsymbol{v}_{acc} \\ {}^{s}\underline{\boldsymbol{C}}_{n}\, {}^{n}\breve{\boldsymbol{m}} + {}^{s}\boldsymbol{b}_{mag} + \boldsymbol{v}_{mag} \end{bmatrix} \tag{4.14} $$

It has also been described that the GPS and the MS2 sensors does not have the same sample rate as the GPS only outputs a measurement with a rate of 1 Hz while the gyroscopes, accelerometers and magnetometers have a sample rate of 51.2 Hz.

It should be noted in (4.14) that all of the equations are linearly except the expression for ${}^{s}\widetilde{\boldsymbol{m}}$.

4.5.1 Alternative Measurement Model Notation

As all the additive noise terms are Gaussian noise, (4.14) can be alternatively written as:

$$ \begin{aligned} \widetilde{\boldsymbol{y}} &= \begin{bmatrix} \widetilde{\boldsymbol{p}}_{GPS} \\ {}^{n}\widetilde{\boldsymbol{v}}_{GPS} \\ {}^{s}\widetilde{\boldsymbol{\omega}}_{is} \\ {}^{s}\widetilde{\boldsymbol{a}} \\ {}^{s}\widetilde{\boldsymbol{m}} \end{bmatrix} = \begin{bmatrix} \boldsymbol{p} \\ {}^{n}\boldsymbol{v} \\ {}^{s}\boldsymbol{\omega}_{is} + {}^{s}\boldsymbol{b}_{gyro} \\ {}^{s}\boldsymbol{a}_{ext} + {}^{s}\boldsymbol{b}_{acc} \\ {}^{s}\underline{\boldsymbol{C}}_{n}\, {}^{n}\breve{\boldsymbol{m}} + {}^{s}\boldsymbol{b}_{mag} \end{bmatrix} + \begin{bmatrix} \underline{\boldsymbol{\sigma}^{2}_{\boldsymbol{p}_{GPS}}} & \underline{\boldsymbol{0}} & \underline{\boldsymbol{0}} & \underline{\boldsymbol{0}} & \underline{\boldsymbol{0}} \\ \underline{\boldsymbol{0}} & \underline{\boldsymbol{\sigma}^{2}_{\boldsymbol{v}_{GPS}}} & \underline{\boldsymbol{0}} & \underline{\boldsymbol{0}} & \underline{\boldsymbol{0}} \\ \underline{\boldsymbol{0}} & \underline{\boldsymbol{0}} & \underline{\boldsymbol{\sigma}^{2}_{\boldsymbol{v}_{gyro}}} & \underline{\boldsymbol{0}} & \underline{\boldsymbol{0}} \\ \underline{\boldsymbol{0}} & \underline{\boldsymbol{0}} & \underline{\boldsymbol{0}} & \underline{\boldsymbol{\sigma}^{2}_{\boldsymbol{v}_{acc}}} & \underline{\boldsymbol{0}} \\ \underline{\boldsymbol{0}} & \underline{\boldsymbol{0}} & \underline{\boldsymbol{0}} & \underline{\boldsymbol{0}} & \underline{\boldsymbol{\sigma}^{2}_{\boldsymbol{v}_{mag}}} \end{bmatrix} \boldsymbol{v} \\ &= \begin{bmatrix} \boldsymbol{p} \\ {}^{n}\boldsymbol{v} \\ {}^{s}\boldsymbol{\omega}_{is} + {}^{s}\boldsymbol{b}_{gyro} \\ {}^{s}\boldsymbol{a}_{ext} + {}^{s}\boldsymbol{b}_{acc} \\ {}^{s}\underline{\boldsymbol{C}}_{n}\, {}^{n}\breve{\boldsymbol{m}} + {}^{s}\boldsymbol{b}_{mag} \end{bmatrix} + \underline{\boldsymbol{\Lambda}}\boldsymbol{v} \end{aligned} \tag{4.15} $$

In which, $\underline{\boldsymbol{\sigma_{sensor}}}$ are diagonal matrices with the standard deviation of the correspondent sensor. $\boldsymbol{v}$ is a vector with independent white Gaussian distributed noise elements, all with unitary standard deviation.

4.5.2 Reduced Measurement Model

As mentioned, the GPS and the other sensors have different sample rates.

Even though the MS2 sample rate of 51.2 Hz does not divide perfectly into the 1 Hz sample rate of the GPS it is assumed that every time a new GPS measurement is available, new measurements from the MS2 sensors are available too. In practice, the estimation filter described later, will be run at the same rate as the fastest available sensor, why a check for a new GPS measurement will only be conducted when new MS2 measurements are available.

(4.15) is the measurement model when all sensors are available. For later reference it is desired also to have a measurement model describing the system when no new GPS measurement is available.

By removing the GPS terms from (4.15), the reduced measuring model is given as:

$$\begin{aligned}\widetilde{\boldsymbol{y}}_{no\,GPS} &= \begin{bmatrix} {}^{s}\widetilde{\boldsymbol{\omega}}_{is} \\ {}^{s}\widetilde{\boldsymbol{a}} \\ {}^{s}\widetilde{\boldsymbol{m}} \end{bmatrix} = \begin{bmatrix} {}^{s}\boldsymbol{\omega}_{is} + {}^{s}\boldsymbol{b}_{gyro} \\ {}^{s}\boldsymbol{a}_{ext} + {}^{s}\boldsymbol{b}_{acc} \\ {}^{s}\underline{\boldsymbol{C}}_{n}\,{}^{n}\breve{\boldsymbol{m}} + {}^{s}\boldsymbol{b}_{mag} \end{bmatrix} + \begin{bmatrix} \underline{\boldsymbol{\sigma}^{2}_{v_{gyro}}} & \underline{\boldsymbol{0}} & \underline{\boldsymbol{0}} \\ \underline{\boldsymbol{0}} & \underline{\boldsymbol{\sigma}^{2}_{v_{acc}}} & \underline{\boldsymbol{0}} \\ \underline{\boldsymbol{0}} & \underline{\boldsymbol{0}} & \underline{\boldsymbol{\sigma}^{2}_{v_{mag}}} \end{bmatrix} \boldsymbol{v} \\ &= \begin{bmatrix} {}^{s}\boldsymbol{\omega}_{is} + {}^{s}\boldsymbol{b}_{gyro} \\ {}^{s}\boldsymbol{a}_{ext} + {}^{s}\boldsymbol{b}_{acc} \\ {}^{s}\underline{\boldsymbol{C}}_{n}\,{}^{n}\breve{\boldsymbol{m}} + {}^{s}\boldsymbol{b}_{mag} \end{bmatrix} + \underline{\boldsymbol{\Lambda}}_{no\,GPS}\boldsymbol{v}\end{aligned} \tag{4.16}$$

4.5.3 Added States

During this chapter, three biases have been introduced. All of these three biases have been modeled as being standard Brownian motions, thus their time derivatives are white Gaussian distributed noise. In order to include this in the model, these biases are included as states, which means that the dynamic equation will have to be augmented with these states. To summarize, the dynamics of the bias states were found as:

$$\begin{bmatrix} {}^{s}\dot{\boldsymbol{b}}_{gyro} \\ {}^{s}\dot{\boldsymbol{b}}_{acc} \\ {}^{s}\dot{\boldsymbol{b}}_{mag} \end{bmatrix} = \begin{bmatrix} \boldsymbol{w}_{\boldsymbol{b}_{gyro}} \\ \boldsymbol{w}_{\boldsymbol{b}_{acc}} \\ \boldsymbol{w}_{\boldsymbol{b}_{mag}} \end{bmatrix} \tag{4.17}$$

The standard deviation of $\boldsymbol{w}_{\boldsymbol{b}_{gyro}}$ and $\boldsymbol{w}_{\boldsymbol{b}_{acc}}$ were found in Subsection 4.1.1 and Subsection 4.2.1, while the standard deviation of $\boldsymbol{w}_{\boldsymbol{b}_{mag}}$ is considered a tuning parameter.

It should be noted that all the equations in (4.17) are linear.

Chapter 5

Small Perturbations Trajectory Model

As it has been chosen to base the design of the navigation solution on the extended Kalman filter a model, which is a linear description of how the time derivatives of the states change within a small region, is needed.

This is needed as the main principle of the extended Kalman filter, as mentioned in Subsection 1.3.3, is to conduct a linearization of the nonlinear differential equations in each iteration.

The object of this chapter is thus to derive this linear model which describes the trajectory of the states.

Furthermore, models describing the small perturbations trajectory effects on the measurement will also be derived as this is also needed in the extended Kalman filter.

5.1 Derivation Approach

Before actually deriving the small perturbations trajectory model, a few things regarding the model assumption and approach should be clarified.

5.1.1 Model Assumptions

In this chapter and throughout the thesis, a model that assumes that the vessel is having a constant acceleration and constant angular velocity will be used.

The reason for including this constant assumption is based on [J. Wendel], in which the results of this approach produced good results.

That is, like the bias models, the acceleration and angular velocity will be modeled as:

$$\begin{aligned} {}^{s}\dot{\boldsymbol{a}} &= \boldsymbol{w}_{\boldsymbol{a}} \\ {}^{s}\underline{\dot{\boldsymbol{\omega}}}_{si} &= \boldsymbol{w}_{{}^{s}\omega_{si}} \end{aligned} \tag{5.1}$$

In which $\boldsymbol{w}_{\boldsymbol{a}}$ and $\boldsymbol{w}_{{}^{s}\omega_{si}}$ are regarded as white Gaussian noise. Their standard deviation will be regarded as a turning parameter. As these states are directly measured, this assumption of constant terms will function as a low-pass filter and the chosen standard deviation of $\boldsymbol{w}_{\boldsymbol{a}}$ and $\boldsymbol{w}_{{}^{s}\omega_{si}}$ will determine the amount of filtering.

5.1.2 Error Approach

When deriving this small perturbation model, the normal approach is to perform a first order Taylor series approximation and subtract the work point. This equates to finding the partial derivative (the Jacobian matrix) of the expressing. Sometimes, as for DCMs, it is not possible

simply to calculate the Jacobian matrix using normal methods as ie. a symbolic math tool. When dealing with these cases, it is necessary to apply an error approach.

If first defining a state vector as $\boldsymbol{x}$ and a function describing the derivatives of this state vector as $\dot{\boldsymbol{x}} = f(\boldsymbol{x})$. The definition of the partial derivative can then be stated as:

$$\frac{\delta \dot{\boldsymbol{x}}}{\delta \boldsymbol{x}} = \frac{\delta f}{\delta \boldsymbol{x}} \equiv \lim_{\Delta \boldsymbol{x} \to 0} \frac{f(\boldsymbol{x} + \Delta \boldsymbol{x}) - f(x)}{(\boldsymbol{x} + \Delta \boldsymbol{x}) - x} \tag{5.2}$$

In which $\Delta \boldsymbol{x}$ is a small amount of the respectively units of the state vector.

If defining $\hat{\boldsymbol{x}} = \boldsymbol{x} + \Delta \boldsymbol{x}$ and $\hat{f} = f(\boldsymbol{x} + \Delta \boldsymbol{x}) - f(x)$, it can be seen from (5.2) that, if $\Delta \boldsymbol{x}$ is a small value, the terms δf and $\delta \boldsymbol{x}$ (and hence the partial derivative) can be approximated as:

$$\begin{aligned} \delta \boldsymbol{x} &= \hat{\boldsymbol{x}} - \boldsymbol{x} \\ \delta f &= f(\hat{\boldsymbol{x}}) - f(\boldsymbol{x}) \\ &\Updownarrow \\ \delta \dot{\boldsymbol{x}} &= \hat{\dot{\boldsymbol{x}}} - \dot{\boldsymbol{x}} \end{aligned} \tag{5.3}$$

By letting $\Delta \boldsymbol{x}$ go towards a limit of 0, this equals the partial differential.

This approach to find the partial differential is useful when deriving linear small perturbation models for rotation equations and will be utilized in the following subsection.

5.1.3 Small Angle Approach

Defining the small angle approximations of the rotation between the SRF and the NRF DCM in the same manner as the first line of (5.3):

$$\delta^n \underline{\boldsymbol{C}}_s \equiv^n \hat{\underline{\boldsymbol{C}}}_s -^n \underline{\boldsymbol{C}}_s \tag{5.4}$$

In Section 2.4, it was shown that for small angles, a rotation between the HVRF and NRF could be approximated by use the vector $\boldsymbol{\gamma}$, defined as:

$$\boldsymbol{\gamma} = \begin{bmatrix} \delta\phi \\ \delta\theta \\ \delta\psi \end{bmatrix} \tag{5.5}$$

Where $\delta\phi$, $\delta\theta$ and $\delta\psi$ are small misalignments in the roll, pitch and yaw axis. As the SRF and HVRF are assumed to coincide, this is also true of small rotations between the SRF and NRF.

According to [Titterton 04, p. 293] (and also see by (2.5)), $\delta^n \underline{\boldsymbol{C}}_s$ can thus be described as:

$${}^n\hat{\underline{\boldsymbol{C}}}_s = (\underline{\boldsymbol{I}} - \underline{\boldsymbol{\Gamma}})^n \underline{\boldsymbol{C}}_s \Leftrightarrow \delta^n \underline{\boldsymbol{C}}_s = -\underline{\boldsymbol{\Gamma}}^n \underline{\boldsymbol{C}}_s \tag{5.6}$$

In which $\underline{\boldsymbol{\Gamma}}$ is a skew-symmetric forms of $\boldsymbol{\gamma}$.

As γ is skew-symmetric (and thus only changes sign when transposed), the following is also given:

$$\begin{aligned} {}^s\hat{\underline{\boldsymbol{C}}}_n = ({}^n\hat{\underline{\boldsymbol{C}}}_s)^T &=^s \underline{\boldsymbol{C}}_n \, (\underline{\boldsymbol{I}} + \underline{\boldsymbol{\Gamma}}) \\ &\Updownarrow \\ \delta^s \underline{\boldsymbol{C}}_n &=^s \underline{\boldsymbol{C}}_n \, \Gamma \end{aligned} \tag{5.7}$$

5.1.4 Perturbations States

The result of the deviations in this chapter, should be a linear equation which describes the trajectory of a small perturbations state vector ($\delta\boldsymbol{x}$):

$$\dot{\delta\boldsymbol{x}} = \underline{\boldsymbol{F}}\delta\boldsymbol{x} + \underline{\boldsymbol{Q}}\boldsymbol{w} \tag{5.8}$$

In (5.8), $\boldsymbol{w}$ is a vector with independent Gaussian distributed noise elements, all with unitary standard deviation. $\underline{\boldsymbol{Q}}$ is the covariance matrix the added noise. $\underline{\boldsymbol{Q}}$ will be described later in this chapter.

It was seen that small perturbations within the attitude should be described with the vector $\boldsymbol{\gamma}$. Each of the other states, which have been introduced in the thesis so far, will have small signal appertaining components, denoted with added δ in front.

Throughout the rest of this thesis the small perturbation state vector will be defined as:

$$\delta\boldsymbol{x} = \begin{bmatrix} \delta\boldsymbol{p} \\ \delta^n\boldsymbol{v} \\ \boldsymbol{\gamma} \\ \delta^s\boldsymbol{a} \\ \delta^s\boldsymbol{\omega}_{is} \\ \delta^s\boldsymbol{b}_{acc} \\ \delta^s\boldsymbol{b}_{gyro} \\ \delta^s\boldsymbol{b}_{mag} \end{bmatrix} \tag{5.9}$$

Furthermore, a linear equation which describes the measurements due to small perturbations of the small perturbations state vector should be derived. This should be in the form of:

$$\delta\boldsymbol{y} = \underline{\boldsymbol{H}}\delta\boldsymbol{x} + \underline{\boldsymbol{\Lambda}}\boldsymbol{v} \tag{5.10}$$

In which the sensor noise term $\underline{\boldsymbol{\Lambda}}\boldsymbol{v}$ was described in Subsection 4.5.1. The equations for the sensor measurement of the system were described in (4.14) on page 30 in which the measurement vector components which were introduced. The measurement vector components will too have small signal appertaining components, denoted with added δ in front.

Throughout the rest of this thesis the small perturbation measurement vector will be defined as:

$$\delta\boldsymbol{z} = \begin{bmatrix} \delta\widetilde{\boldsymbol{p}}_{GPS} \\ \delta^n\widetilde{\boldsymbol{v}}_{GPS} \\ \delta^s\widetilde{\boldsymbol{\omega}}_{is} \\ \delta^s\widetilde{\boldsymbol{a}} \\ \delta^s\widetilde{\boldsymbol{m}} \end{bmatrix} \tag{5.11}$$

5.2 Position

The position is described by the latitude, longitude and height above sea level.

In Chapter 3, the equations for the change in these were found as:

$$\begin{aligned} \dot{l} &= \frac{V_N}{R_{NS} + h} \\ \dot{L} &= \frac{V_E\, sec(l)}{R_{EW} + h} \\ \dot{h} &= -V_D \end{aligned} \tag{5.12}$$

Also, the radiuses R_{EW} and R_{NS} were found as:

$$R_{NS} = \frac{R_M \left(1 - e_{earth}^2\right)}{\left(1 - e_{earth}^2 \, sin^2(l)\right)^{3/2}} \tag{5.13}$$

$$R_{EW} = \frac{R_M}{\left(1 - e_{earth}^2 \, sin^2(l)\right)^{1/2}} \tag{5.14}$$

Using the symbolic toolbox of MATLAB, the Jacobian of (5.12) was found as:

$$\begin{aligned}
\delta\dot{\boldsymbol{p}} = \begin{bmatrix} \delta\dot{l} \\ \delta\dot{L} \\ \delta\dot{h} \end{bmatrix} &= \begin{bmatrix} \frac{\delta\dot{l}}{\delta V_N} & \frac{\delta\dot{l}}{\delta V_E} & \frac{\delta\dot{l}}{\delta V_D} & \frac{\delta\dot{l}}{\delta h} & \frac{\delta\dot{l}}{\delta l} \\ \frac{\delta\dot{L}}{\delta V_N} & \frac{\delta\dot{L}}{\delta V_E} & \frac{\delta\dot{L}}{\delta V_D} & \frac{\delta\dot{L}}{\delta h} & \frac{\delta\dot{L}}{\delta l} \\ \frac{\delta\dot{h}}{\delta V_N} & \frac{\delta\dot{h}}{\delta V_E} & \frac{\delta\dot{h}}{\delta V_D} & \frac{\delta\dot{h}}{\delta h} & \frac{\delta\dot{h}}{\delta l} \end{bmatrix} \begin{bmatrix} \delta V_N \\ \delta V_E \\ \delta V_D \\ \delta h \\ \delta l \end{bmatrix} \\
&= \begin{bmatrix} a_1 & 0 & a_2 & a_3 & 0 & 0 \\ a_4 & 0 & a_5 & 0 & a_6 & 0 \\ 0 & 0 & 0 & 0 & 0 & a_7 \end{bmatrix} \begin{bmatrix} \delta l \\ \delta L \\ \delta h \\ \delta V_N \\ \delta V_E \\ \delta V_D \end{bmatrix} \\
&= \underline{\boldsymbol{A}}_1 \delta\boldsymbol{p} + \underline{\boldsymbol{A}}_2 \delta^n\boldsymbol{v}
\end{aligned} \tag{5.15}$$

in which:

$$\begin{aligned}
a_1 &= \frac{4 \, R_M \, V_N \, {e_{earth}}^2 \, cos\left(l\right) \, sin\left(l\right) \, \left({e_{earth}}^2 - 1\right)}{3 \left(h - \frac{R_M \left({e_{earth}}^2 - 1\right)}{\left(1 - {e_{earth}}^2 \, sin(l)^2\right)^{\frac{2}{3}}}\right)^2 \left(1 - {e_{earth}}^2 \, sin\left(l\right)^2\right)^{\frac{5}{3}}} \\
a_2 &= -\frac{V_N}{\left(h - \frac{R_M \left({e_{earth}}^2 - 1\right)}{\left(1 - {e_{earth}}^2 \, sin(l)^2\right)^{\frac{2}{3}}}\right)^2} \\
a_3 &= \frac{1}{h - \frac{R_M \left({e_{earth}}^2 - 1\right)}{\left(1 - {e_{earth}}^2 \, sin(l)^2\right)^{\frac{2}{3}}}} \\
a_4 &= \frac{V_E \, sin\left(l\right)}{cos\left(l\right)^2 \left(h + \frac{R_M}{\sqrt{1 - {e_{earth}}^2 \, sin(l)^2}}\right)} - \frac{R_M \, V_E \, {e_{earth}}^2 \, sin\left(l\right)}{\left(h + \frac{R_M}{\sqrt{1 - {e_{earth}}^2 \, sin(l)^2}}\right)^2 \left(1 - {e_{earth}}^2 \, sin\left(l\right)^2\right)^{\frac{3}{2}}} \\
a_5 &= -\frac{V_E}{cos\left(l\right) \left(h + \frac{R_M}{\sqrt{1 - {e_{earth}}^2 \, sin(l)^2}}\right)^2} \\
a_6 &= \frac{1}{cos\left(l\right) \left(h + \frac{R_M}{\sqrt{1 - {e_{earth}}^2 \, sin(l)^2}}\right)} \\
a_7 &= -1
\end{aligned} \tag{5.16}$$

5.3 Velocity

The velocity vector is describing the velocity over ground, given in the NRF-frame, thus the components of this vector is the velocity in the north, east and down direction.

In Chapter 3, the navigation equation describing the velocity was found as (here given in vector form):

$$ {}^n\dot{\boldsymbol{v}} = ({}^n\boldsymbol{\omega}_{ne} + 2{}^n\boldsymbol{\omega}_{ei}) \times^n \boldsymbol{v} +^n \underline{\boldsymbol{C}}_s \, {}^s\boldsymbol{a} -^n \breve{\boldsymbol{g}} \tag{5.17} $$

Defining two values for the change of velocity as $\dot{\boldsymbol{v}}$ and $\hat{\dot{\boldsymbol{v}}}$ and defining the error between them as:

$$ \delta^n\dot{\boldsymbol{v}} =^n \hat{\dot{\boldsymbol{v}}} -^n \dot{\boldsymbol{v}} \tag{5.18} $$

By inserting (5.17) into (5.18) one get:

$$ \begin{aligned}
\delta^n\dot{\boldsymbol{v}} &= ({}^n\hat{\boldsymbol{\omega}}_{ne} + 2{}^n\hat{\boldsymbol{\omega}}_{ei}) \times^n \hat{\boldsymbol{v}} +^n \hat{\underline{\boldsymbol{C}}}_s \, {}^s\hat{\boldsymbol{a}} -^n \hat{\breve{\boldsymbol{g}}} - ({}^n\boldsymbol{\omega}_{ne} + 2{}^n\boldsymbol{\omega}_{ei}) \times^n \boldsymbol{v} -^n \underline{\boldsymbol{C}}_s \, {}^s\boldsymbol{a} +^n \breve{\boldsymbol{g}} \\
&= ({}^n\boldsymbol{\omega}_{ne} + \delta^n\boldsymbol{\omega}_{ne} + 2{}^n\boldsymbol{\omega}_{ei} + 2\delta^n\boldsymbol{\omega}_{ei}) \times ({}^n\boldsymbol{v} + \delta^n\boldsymbol{v}) + ({}^n\underline{\boldsymbol{C}}_s + \delta^n\underline{\boldsymbol{C}}_s)\,({}^s\boldsymbol{a} + \delta^s\boldsymbol{a}) - \\
&\quad ({}^n\breve{\boldsymbol{g}} + \delta^n\breve{\boldsymbol{g}}) - ({}^n\boldsymbol{\omega}_{ne} + 2{}^n\boldsymbol{\omega}_{ei}) \times^n \boldsymbol{v} -^n \underline{\boldsymbol{C}}_s \, {}^s\boldsymbol{a} +^n \breve{\boldsymbol{g}} \\
&= ({}^n\boldsymbol{\omega}_{ne} + \delta^n\boldsymbol{\omega}_{ne} + 2{}^n\boldsymbol{\omega}_{ei} + 2\delta^n\boldsymbol{\omega}_{ei}) \times^n \boldsymbol{v} + ({}^n\boldsymbol{\omega}_{ne} + \delta^n\boldsymbol{\omega}_{ne} + 2{}^n\boldsymbol{\omega}_{ei} + 2\delta^n\boldsymbol{\omega}_{ei}) \times \delta^n\boldsymbol{v} \\
&\quad +^n \underline{\boldsymbol{C}}_s \, \delta^s\boldsymbol{a} + \delta^n\underline{\boldsymbol{C}}_s \, {}^s\boldsymbol{a} + \delta^n\underline{\boldsymbol{C}}_s \, \delta^s\boldsymbol{a} - \delta^n\breve{\boldsymbol{g}} - ({}^n\boldsymbol{\omega}_{ne} + 2{}^n\boldsymbol{\omega}_{ei}) \times^n \boldsymbol{v} \\
&= (\delta^n\boldsymbol{\omega}_{ne} + 2\delta^n\boldsymbol{\omega}_{ei}) \times^n \boldsymbol{v} + ({}^n\boldsymbol{\omega}_{ne} + 2{}^n\boldsymbol{\omega}_{ei}) \times \delta^n\boldsymbol{v} + (\delta^n\boldsymbol{\omega}_{ne} + 2\delta^n\boldsymbol{\omega}_{ei}) \times \delta^n\boldsymbol{v} \\
&\quad +^n \underline{\boldsymbol{C}}_s \, \delta^s\boldsymbol{a} + \delta^n\underline{\boldsymbol{C}}_s \, {}^s\boldsymbol{a} + \delta^n\underline{\boldsymbol{C}}_s \, \delta^s\boldsymbol{a} - \delta^n\breve{\boldsymbol{g}} \\
&\approx (\delta^n\boldsymbol{\omega}_{ne} + 2\delta^n\boldsymbol{\omega}_{ei}) \times^n \boldsymbol{v} + ({}^n\boldsymbol{\omega}_{ne} + 2{}^n\boldsymbol{\omega}_{ei}) \times \delta^n\boldsymbol{v} +^n \underline{\boldsymbol{C}}_s \, \delta^s\boldsymbol{a} + \delta^n\underline{\boldsymbol{C}}_s \, {}^s\boldsymbol{a} - \delta^n\breve{\boldsymbol{g}}
\end{aligned} \tag{5.19} $$

In the last line of (5.19), the terms which involves multiplication of two δ-values are neglected as these will be very small.

By inserting (5.6) into (5.19), the following is obtained:

$$ \begin{aligned}
\delta^n\dot{\boldsymbol{v}} &= (\delta^n\boldsymbol{\omega}_{ne} + 2\delta^n\boldsymbol{\omega}_{ei}) \times^n \boldsymbol{v} + ({}^n\boldsymbol{\omega}_{ne} + 2{}^n\boldsymbol{\omega}_{ei}) \times \delta^n\boldsymbol{v} +^n \underline{\boldsymbol{C}}_s \, \delta^s\boldsymbol{a} -^n \underline{\boldsymbol{\Gamma}}^n\underline{\boldsymbol{C}}_s \, {}^s\boldsymbol{a} - \delta^n\breve{\boldsymbol{g}} \\
&= (\delta^n\boldsymbol{\omega}_{ne} + 2\delta^n\boldsymbol{\omega}_{ei}) \times^n \boldsymbol{v} + ({}^n\boldsymbol{\omega}_{ne} + 2{}^n\boldsymbol{\omega}_{ei}) \times \delta^n\boldsymbol{v} +^n \underline{\boldsymbol{C}}_s \, \delta^s\boldsymbol{a} +^n \underline{\boldsymbol{C}}_s \, {}^s\boldsymbol{a} \times^n \boldsymbol{\gamma} - \delta^n\breve{\boldsymbol{g}} \\
&= ({}^n\underline{\boldsymbol{\Omega}}_{ne} + 2{}^n\underline{\boldsymbol{\Omega}}_{ei})\,\delta^n\boldsymbol{v} -^n \underline{\boldsymbol{v}}\,(\delta^n\boldsymbol{\omega}_{ne} + 2\delta^n\boldsymbol{\omega}_{ei}) +^n \underline{\boldsymbol{C}}_s \, \delta^s\boldsymbol{a} +^n \underline{\boldsymbol{C}}_s \, {}^s\underline{\boldsymbol{a}} \, {}^s\underline{\boldsymbol{C}}_n \, {}^n\boldsymbol{\gamma} - \delta^n\breve{\boldsymbol{g}}
\end{aligned} \tag{5.20} $$

In which ${}^n\underline{\boldsymbol{v}}$ and ${}^s\underline{\boldsymbol{a}}$ is the skew symmetric form of ${}^n\boldsymbol{v}$ and ${}^s\boldsymbol{a}$.

Expressions for $\delta^n\boldsymbol{\omega}_{ne}$, $\delta^n\boldsymbol{\omega}_{ei}$ and $\delta^n\breve{\boldsymbol{g}}$ are derived later in the chapter.

5.4 Attitude

The attitude is described as the DCM between the SRF and the NRF (${}^n\underline{\boldsymbol{C}}_s$).

In Chapter 3, the expression for the change in attitude was found as:

$$ \begin{aligned}
{}^n\dot{\underline{\boldsymbol{C}}}_s &=^n \underline{\boldsymbol{C}}_s \, ({}^s\underline{\boldsymbol{\Omega}}_{si} -^s \underline{\boldsymbol{C}}_n \, ({}^n\underline{\boldsymbol{\Omega}}_{ei} -^n \underline{\boldsymbol{\Omega}}_{ne})^n \underline{\boldsymbol{C}}_s) \\
&=^n \underline{\boldsymbol{C}}_s^s\underline{\boldsymbol{\Omega}}_{si} - ({}^n\underline{\boldsymbol{\Omega}}_{ei} -^n \underline{\boldsymbol{\Omega}}_{ne})^n \underline{\boldsymbol{C}}_s
\end{aligned} \tag{5.21} $$

By first differencing (5.6), one expression for the perturbation change of the attitude is obtained:

$$ \begin{aligned}
\delta^n\underline{\boldsymbol{C}}_s &= -^n\underline{\boldsymbol{\Gamma}}^n\underline{\boldsymbol{C}}_s \\
&\Downarrow \\
\delta^n\dot{\underline{\boldsymbol{C}}}_s &= -^n \dot{\underline{\boldsymbol{\Gamma}}}^n\underline{\boldsymbol{C}}_s -^n \underline{\boldsymbol{\Gamma}}^n\dot{\underline{\boldsymbol{C}}}_s
\end{aligned} \tag{5.22} $$

An alternative expression for the perturbation change of the attitude can be obtained by differentiating (5.4) and inserting (5.21) :

$$
\begin{aligned}
\delta^n\underline{\dot{\boldsymbol{C}}}_s =& {}^n\hat{\underline{\dot{\boldsymbol{C}}}}_s - {}^n\underline{\dot{\boldsymbol{C}}}_s \\
=& {}^n\hat{\underline{\boldsymbol{C}}}_s\, {}^s\hat{\underline{\boldsymbol{\Omega}}}_{si} - \left({}^n\hat{\underline{\boldsymbol{\Omega}}}_{ei} - {}^n\hat{\underline{\boldsymbol{\Omega}}}_{ne}\right)^n\hat{\underline{\boldsymbol{C}}}_s - {}^n\underline{\boldsymbol{C}}_s\, {}^s\underline{\boldsymbol{\Omega}}_{si} + ({}^n\underline{\boldsymbol{\Omega}}_{ei} - {}^n\underline{\boldsymbol{\Omega}}_{ne})^n\underline{\boldsymbol{C}}_s \\
=& ({}^n\underline{\boldsymbol{C}}_s + \delta^n\underline{\boldsymbol{C}}_s)\,({}^s\underline{\boldsymbol{\Omega}}_{si} + \delta^s\underline{\boldsymbol{\Omega}}_{si}) - ({}^n\underline{\boldsymbol{\Omega}}_{ei} + \delta^n\underline{\boldsymbol{\Omega}}_{ei} - {}^n\underline{\boldsymbol{\Omega}}_{ne} - \delta^n\underline{\boldsymbol{\Omega}}_{ne})\,({}^n\underline{\boldsymbol{C}}_s + \delta^n\underline{\boldsymbol{C}}_s) \\
& - {}^n\underline{\boldsymbol{C}}_s\, {}^s\underline{\boldsymbol{\Omega}}_{si} + ({}^n\underline{\boldsymbol{\Omega}}_{ei} - {}^n\underline{\boldsymbol{\Omega}}_{ne})^n\underline{\boldsymbol{C}}_s \\
=& {}^n\underline{\boldsymbol{C}}_s\, {}^s\underline{\boldsymbol{\Omega}}_{si} + {}^n\underline{\boldsymbol{C}}_s\,\delta^s\underline{\boldsymbol{\Omega}}_{si} + \delta^n\underline{\boldsymbol{C}}_s\, {}^s\underline{\boldsymbol{\Omega}}_{si} + \delta^n\underline{\boldsymbol{C}}_s\,\delta^s\underline{\boldsymbol{\Omega}}_{si} - ({}^n\underline{\boldsymbol{\Omega}}_{ei} - {}^n\underline{\boldsymbol{\Omega}}_{ne})^n\underline{\boldsymbol{C}}_s - ({}^n\underline{\boldsymbol{\Omega}}_{ei} - {}^n\underline{\boldsymbol{\Omega}}_{ne})\,\delta^n\underline{\boldsymbol{C}}_s \\
& - (\delta^n\underline{\boldsymbol{\Omega}}_{ei} - \delta^n\underline{\boldsymbol{\Omega}}_{ne})^n\underline{\boldsymbol{C}}_s - (\delta^n\underline{\boldsymbol{\Omega}}_{ei} - \delta^n\underline{\boldsymbol{\Omega}}_{ne})\,\delta^n\underline{\boldsymbol{C}}_s - {}^n\underline{\boldsymbol{C}}_s\, {}^s\underline{\boldsymbol{\Omega}}_{si} + ({}^n\underline{\boldsymbol{\Omega}}_{ei} - {}^n\underline{\boldsymbol{\Omega}}_{ne})^n\underline{\boldsymbol{C}}_s \\
=& {}^n\underline{\boldsymbol{C}}_s\,\delta^s\underline{\boldsymbol{\Omega}}_{si} + \delta^n\underline{\boldsymbol{C}}_s\, {}^s\underline{\boldsymbol{\Omega}}_{si} + \delta^n\underline{\boldsymbol{C}}_s\,\delta^s\underline{\boldsymbol{\Omega}}_{si} - ({}^n\underline{\boldsymbol{\Omega}}_{ei} - {}^n\underline{\boldsymbol{\Omega}}_{ne})\,\delta^n\underline{\boldsymbol{C}}_s \\
& - (\delta^n\underline{\boldsymbol{\Omega}}_{ei} - \delta^n\underline{\boldsymbol{\Omega}}_{ne})^n\underline{\boldsymbol{C}}_s - (\delta^n\underline{\boldsymbol{\Omega}}_{ei} - \delta^n\underline{\boldsymbol{\Omega}}_{ne})\,\delta^n\underline{\boldsymbol{C}}_s \\
\approx& {}^n\underline{\boldsymbol{C}}_s\,\delta^s\underline{\boldsymbol{\Omega}}_{si} - {}^n\underline{\boldsymbol{\Gamma}}^n\underline{\boldsymbol{C}}_s\, {}^s\underline{\boldsymbol{\Omega}}_{si} + ({}^n\underline{\boldsymbol{\Omega}}_{ei} - {}^n\underline{\boldsymbol{\Omega}}_{ne})^n\underline{\boldsymbol{\Gamma}}^n\underline{\boldsymbol{C}}_s - (\delta^n\underline{\boldsymbol{\Omega}}_{ei} - \delta^n\underline{\boldsymbol{\Omega}}_{ne})^n\underline{\boldsymbol{C}}_s
\end{aligned}
\tag{5.23}
$$

Equating (5.22) and (5.23), and then inserting (5.21) realms:

$$
\begin{aligned}
-{}^n\underline{\dot{\boldsymbol{\Gamma}}}^n\underline{\boldsymbol{C}}_s - {}^n\underline{\boldsymbol{\Gamma}}^n\underline{\dot{\boldsymbol{C}}}_s =& {}^n\underline{\boldsymbol{C}}_s\,\delta^s\underline{\boldsymbol{\Omega}}_{si} - {}^n\underline{\boldsymbol{\Gamma}}^n\underline{\boldsymbol{C}}_s\, {}^s\underline{\boldsymbol{\Omega}}_{si} + ({}^n\underline{\boldsymbol{\Omega}}_{ei} - {}^n\underline{\boldsymbol{\Omega}}_{ne})^n\underline{\boldsymbol{\Gamma}}^n\underline{\boldsymbol{C}}_s \\
& - (\delta^n\underline{\boldsymbol{\Omega}}_{ei} - \delta^n\underline{\boldsymbol{\Omega}}_{ne})^n\underline{\boldsymbol{C}}_s \\
& \Updownarrow \\
-{}^n\underline{\dot{\boldsymbol{\Gamma}}}^n\underline{\boldsymbol{C}}_s - {}^n\underline{\boldsymbol{\Gamma}}^n({}^n\underline{\boldsymbol{C}}^s_s\underline{\boldsymbol{\Omega}}_{si} - ({}^n\underline{\boldsymbol{\Omega}}_{ei} - {}^n\underline{\boldsymbol{\Omega}}_{ne})^n\underline{\boldsymbol{C}}_s) =& {}^n\underline{\boldsymbol{C}}_s\,\delta^s\underline{\boldsymbol{\Omega}}_{si} - {}^n\underline{\boldsymbol{\Gamma}}^n\underline{\boldsymbol{C}}_s\, {}^s\underline{\boldsymbol{\Omega}}_{si} + ({}^n\underline{\boldsymbol{\Omega}}_{ei} - {}^n\underline{\boldsymbol{\Omega}}_{ne})^n\underline{\boldsymbol{\Gamma}}^n\underline{\boldsymbol{C}}_s \\
& - (\delta^n\underline{\boldsymbol{\Omega}}_{ei} - \delta^n\underline{\boldsymbol{\Omega}}_{ne})^n\underline{\boldsymbol{C}}_s \\
& \Updownarrow \\
-{}^n\underline{\dot{\boldsymbol{\Gamma}}}^n\underline{\boldsymbol{C}}_s =& {}^n\underline{\boldsymbol{C}}_s\,\delta^s\underline{\boldsymbol{\Omega}}_{si} + ({}^n\underline{\boldsymbol{\Omega}}_{ei} - {}^n\underline{\boldsymbol{\Omega}}_{ne})^n\underline{\boldsymbol{\Gamma}}^n\underline{\boldsymbol{C}}_s \\
& - (\delta^n\underline{\boldsymbol{\Omega}}_{ei} - \delta^n\underline{\boldsymbol{\Omega}}_{ne})^n\underline{\boldsymbol{C}}_s - {}^n\underline{\boldsymbol{\Gamma}}^n({}^n\underline{\boldsymbol{\Omega}}_{ei} - {}^n\underline{\boldsymbol{\Omega}}_{ne})^n\underline{\boldsymbol{C}}_s \\
& \Updownarrow \\
{}^n\underline{\dot{\boldsymbol{\Gamma}}} =& -{}^n\underline{\boldsymbol{C}}_s\,\delta^s\underline{\boldsymbol{\Omega}}_{si}\, {}^s\underline{\boldsymbol{C}}_n + (\delta^n\underline{\boldsymbol{\Omega}}_{ei} - \delta^n\underline{\boldsymbol{\Omega}}_{ne}) \\
& + {}^n\underline{\boldsymbol{\Gamma}}\,({}^n\underline{\boldsymbol{\Omega}}_{ei} - {}^n\underline{\boldsymbol{\Omega}}_{ne}) - ({}^n\underline{\boldsymbol{\Omega}}_{ei} - {}^n\underline{\boldsymbol{\Omega}}_{ne})^n\underline{\boldsymbol{\Gamma}}
\end{aligned}
\tag{5.24}
$$

A problem with (5.24) is that the two last terms of the last line are both multiplications of the skew symmetric representation of the small value attitude perturbation with another skew symmetric vector. For the final equation, it is required to have it in a form in which the small value attitude perturbation is written in vector form and multiplied on a matrix.

This can be accomplished by applying the vector triple product. The vector triple product states that for three arbitrary vectors, the following holds:

$$
\boldsymbol{a}\times(\boldsymbol{b}\times\boldsymbol{c}) = (\boldsymbol{a}\cdot\boldsymbol{c})\cdot\boldsymbol{b} - (\boldsymbol{a}\cdot\boldsymbol{b})\cdot\boldsymbol{c} \tag{5.25}
$$

This can be used to rewrite the last line of (5.24). First, an arbitrary vector, denoted $\boldsymbol{q}$, is introduced. By multiplying with $\boldsymbol{q}$, expanding the expression and applying (5.25), the last two terms can be written as:

$$
\begin{aligned}
&({}^n\underline{\boldsymbol{\Gamma}}\,({}^n\underline{\boldsymbol{\Omega}}_{ei} - {}^n\,\underline{\boldsymbol{\Omega}}_{ne}) - ({}^n\underline{\boldsymbol{\Omega}}_{ei} - {}^n\,\underline{\boldsymbol{\Omega}}_{ne})^n\,\underline{\boldsymbol{\Gamma}})\,\boldsymbol{q} \\
&= \underbrace{{}^n\boldsymbol{\gamma}}_{\boldsymbol{a}} \times \left(\underbrace{({}^n\boldsymbol{\omega}_{ei} - {}^n\,\boldsymbol{\omega}_{ne})}_{\boldsymbol{b}} \times \underbrace{\boldsymbol{q}}_{\boldsymbol{c}} \right) - \underbrace{({}^n\boldsymbol{\omega}_{ei} - {}^n\,\boldsymbol{\omega}_{ne})}_{\boldsymbol{a}} \times \left(\underbrace{{}^n\boldsymbol{\gamma}}_{\boldsymbol{b}} \times \underbrace{\boldsymbol{q}}_{\boldsymbol{c}} \right) \\
&= ({}^n\boldsymbol{\gamma} \cdot \boldsymbol{q})\,({}^n\boldsymbol{\omega}_{ei} - {}^n\,\boldsymbol{\omega}_{ne}) - ({}^n\boldsymbol{\gamma} \cdot ({}^n\boldsymbol{\omega}_{ei} - {}^n\,\boldsymbol{\omega}_{ne}))\,\boldsymbol{q} \\
&\quad - (({}^n\boldsymbol{\omega}_{ei} - {}^n\,\boldsymbol{\omega}_{ne}) \cdot \boldsymbol{q})^n\,\boldsymbol{\gamma} + (({}^n\boldsymbol{\omega}_{ei} - {}^n\,\boldsymbol{\omega}_{ne}) \cdot^n \boldsymbol{\gamma})\,\boldsymbol{q} \\
&= \left(\underbrace{\boldsymbol{q}}_{\boldsymbol{a}} \cdot \underbrace{{}^n\boldsymbol{\gamma}}_{\boldsymbol{c}} \right) \underbrace{({}^n\boldsymbol{\omega}_{ei} - {}^n\,\boldsymbol{\omega}_{ne})}_{\boldsymbol{b}} - \left(\underbrace{\boldsymbol{q}}_{\boldsymbol{a}} \cdot \underbrace{({}^n\boldsymbol{\omega}_{ei} - {}^n\,\boldsymbol{\omega}_{ne})}_{\boldsymbol{b}} \right) \underbrace{{}^n\boldsymbol{\gamma}}_{\boldsymbol{c}} \\
&= \boldsymbol{q} \times (({}^n\boldsymbol{\omega}_{ei} - {}^n\,\boldsymbol{\omega}_{ne}) \times^n \boldsymbol{\gamma})
\end{aligned} \tag{5.26}
$$

As $\boldsymbol{q}$ can be an arbitrary vector, it is chosen as $\boldsymbol{q} = [1\ 1\ 1]^T$ in order to remove it from the expression.

By writing (5.24) in vector form and inserting (5.26), the final attitude expression is archived:

$$
\begin{aligned}
{}^n\dot{\boldsymbol{\gamma}} &= ({}^n\boldsymbol{\omega}_{ei} - {}^n\,\boldsymbol{\omega}_{ne}) \times^n \boldsymbol{\gamma} - \delta^n\boldsymbol{\omega}_{ei} + \delta^n\boldsymbol{\omega}_{ne} - {}^n\,\underline{\boldsymbol{C}}_s\,\delta^s\boldsymbol{\omega}_{si} \\
&= ({}^n\underline{\boldsymbol{\Omega}}_{ei} - {}^n\,\underline{\boldsymbol{\Omega}}_{ne})^n\,\boldsymbol{\gamma} - \delta^n\boldsymbol{\omega}_{ei} + \delta^n\boldsymbol{\omega}_{ne} - {}^n\,\underline{\boldsymbol{C}}_s\,\delta^s\boldsymbol{\omega}_{si}
\end{aligned} \tag{5.27}
$$

Expressions for $\delta^n\boldsymbol{\omega}_{ne}$ and $\delta^n\boldsymbol{\omega}_{ei}$ are derived later in following section.

5.5 Partial Derivations of Variables

In the derived expressions for $\delta\boldsymbol{p}$, $\delta^n\boldsymbol{v}$ and $\dot{\boldsymbol{\gamma}}$ it is observed that the variables $\delta^n\boldsymbol{\omega}_{ne}$, $\delta^n\boldsymbol{\omega}_{ei}$ and $\delta^n\breve{\boldsymbol{g}}$ appear. The focus of this section is to derive linear expressions for these variables which are functions of the perturbation states.

5.5.1 Partial Derivative of ${}^n\boldsymbol{\omega}_{ne}$

In (3.30), ${}^n\boldsymbol{\omega}_{ne}$ was found as:

$$
{}^n\boldsymbol{\omega}_{ne} = \begin{bmatrix} \frac{V_E}{R_{EW}+h} \\ -\frac{V_N}{R_{NS}+h} \\ -\frac{V_E}{R_{EW}+h}\,tan(l) \end{bmatrix} \tag{5.28}
$$

The expressions for R_{NS} and R_{EW} were refreshed in (5.14).

The Jacobian matrix of this equation was found using the MATLAB symbolic toolbox as:

$$
\begin{aligned}
\frac{\delta^n\boldsymbol{\omega}_{ne}}{\delta\boldsymbol{x}} &= \frac{\delta^n\boldsymbol{\omega}_{ne}}{\delta V_E} + \frac{\delta^n\boldsymbol{\omega}_{ne}}{\delta V_N} + \frac{\delta^n\boldsymbol{\omega}_{ne}}{\delta h} + \frac{\delta^n\boldsymbol{\omega}_{ne}}{\delta l} \\
&\Updownarrow \\
\delta^n\boldsymbol{\omega}_{ne} &= \begin{bmatrix} b_1 & 0 & b_2 & 0 & b_3 & 0 \\ b_4 & 0 & b_5 & b_6 & 0 & 0 \\ b_7 & 0 & b_8 & 0 & b_9 & 0 \end{bmatrix} \begin{bmatrix} \delta l \\ \delta L \\ \delta h \\ \delta V_N \\ \delta V_E \\ \delta V_D \end{bmatrix} \\
&= \underline{\boldsymbol{B}}_1\delta\boldsymbol{p} + \underline{\boldsymbol{B}}_2\delta^n\boldsymbol{v}
\end{aligned} \tag{5.29}
$$

in which:

$$
\begin{aligned}
b_1 &= -\frac{2\,R_M\,V_E\,{e_{earth}}^2\,cos\,(l)\;sin\,(l)}{3\left(h+\frac{R_M}{\left(1-{e_{earth}}^2\,sin(l)^2\right)^{\frac{1}{3}}}\right)^2\left(1-{e_{earth}}^2\,sin\,(l)^2\right)^{\frac{4}{3}}}\\
b_2 &= -\frac{V_E}{\left(h+\frac{R_M}{\left(1-{e_{earth}}^2\,sin(l)^2\right)^{\frac{1}{3}}}\right)^2}\\
b_3 &= \frac{1}{h+\frac{R_M}{\left(1-{e_{earth}}^2\,sin(l)^2\right)^{\frac{1}{3}}}}\\
b_4 &= -\frac{4\,R_M\,V_N\,{e_{earth}}^2\,cos\,(l)\;sin\,(l)\;\left({e_{earth}}^2-1\right)}{3\left(h-\frac{R_M\,({e_{earth}}^2-1)}{\left(1-{e_{earth}}^2\,sin(l)^2\right)^{\frac{2}{3}}}\right)^2\left(1-{e_{earth}}^2\,sin\,(l)^2\right)^{\frac{5}{3}}}\\
b_5 &= \frac{V_N}{\left(h-\frac{R_M\,({e_{earth}}^2-1)}{\left(1-{e_{earth}}^2\,sin(l)^2\right)^{\frac{2}{3}}}\right)^2}\\
b_6 &= -\frac{1}{h-\frac{R_M\,({e_{earth}}^2-1)}{\left(1-{e_{earth}}^2\,sin(l)^2\right)^{\frac{2}{3}}}}\\
b_7 &= \frac{2\,R_M\,V_E\,{e_{earth}}^2\,cos\,(l)\;sin\,(l)\;tan\,(l)}{3\left(h+\frac{R_M}{\left(1-{e_{earth}}^2\,sin(l)^2\right)^{\frac{1}{3}}}\right)^2\left(1-{e_{earth}}^2\,sin\,(l)^2\right)^{\frac{4}{3}}}-\frac{V_E\,\left(tan\,(l)^2+1\right)}{h+\frac{R_M}{\left(1-{e_{earth}}^2\,sin(l)^2\right)^{\frac{1}{3}}}}\\
b_8 &= \frac{V_E\,tan\,(l)}{\left(h+\frac{R_M}{\left(1-{e_{earth}}^2\,sin(l)^2\right)^{\frac{1}{3}}}\right)^2}\\
b_9 &= -\frac{tan\,(l)}{h+\frac{R_M}{\left(1-{e_{earth}}^2\,sin(l)^2\right)^{\frac{1}{3}}}}
\end{aligned}
\tag{5.30}
$$

5.5.2 Partial Derivative of ${}^n\boldsymbol{\omega}_{ei}$

Writing ${}^n\boldsymbol{\omega}_{ei}$ in vector form as:

$$
\begin{aligned}
{}^n\boldsymbol{\omega}_{ei} &= {}^n\underline{\boldsymbol{C}}_e\;{}^e\boldsymbol{\omega}_{ie}\\
&= \boldsymbol{\omega}_{earth}\begin{bmatrix} cos\,(l)\\ 0\\ sin\,(l)\end{bmatrix}
\end{aligned}
\tag{5.31}
$$

The Jacobian matrix of this equation was found using the MATLAB symbolic toolbox as:

$$
\begin{aligned}
\frac{\delta^n\boldsymbol{\omega}_{ei}}{\delta x} &= \frac{\delta^n\boldsymbol{\omega}_{ei}}{\delta l}\\
&\Updownarrow\\
\delta^n\boldsymbol{\omega}_{ei} &= \begin{bmatrix} c_1 & 0 & 0\\ 0 & 0 & 0\\ c_2 & 0 & 0\end{bmatrix}\begin{bmatrix}\delta l\\ \delta L\\ \delta h\end{bmatrix}\\
&= \underline{\boldsymbol{C}}\delta\boldsymbol{p}
\end{aligned}
\tag{5.32}
$$

in which:

$$\begin{aligned} c_1 &= -w_{earth}\, sin\,(l) \\ c_2 &= w_{earth}\, cos\,(l) \end{aligned} \tag{5.33}$$

5.5.3 Partial Derivative of ${}^n\breve{\boldsymbol{g}}$

In Chapter 3, an expression for the gravity magnitude in the Z-axis of the NRF, was given as:

$$\breve{g}_0(l) = \underbrace{9.780318}_{a}\left(1 + \underbrace{5.3024\cdot 10^{-3}}_{b}\, sin^2(l) - \underbrace{5.9\cdot 10^{-6}}_{c}\, sin^2(2l)\right)\ [m/s^2] \tag{5.34}$$

$$\breve{g}(h,l) = \breve{g}_0(l) - h\cdot \underbrace{3.0877\cdot 10^{-6}}_{d}\left(1 - \underbrace{1.39\cdot 10^{-3}}_{e}\, sin^2(l)\right)\ [m/s^2] \tag{5.35}$$

As the gravity is described by the height above sea level and the latitude, the partial derivative of the Z-axis gravity can be described as:

$$\begin{aligned} \frac{\delta\breve{g}}{\delta x} =& \frac{\delta\breve{g}}{\delta h} + \frac{\delta\breve{g}}{\delta l} \\ &\Updownarrow \\ \delta\breve{g} =& \begin{bmatrix} g_1 & 0 & g_2 \end{bmatrix} \begin{bmatrix} \delta l \\ \delta L \\ \delta h \end{bmatrix} \\ =& \underline{\boldsymbol{G}}\delta\boldsymbol{p} \end{aligned} \tag{5.36}$$

in which (obtained by using the MATLAB symbolic toolbox):

$$\begin{aligned} g_1 &= 2\,d\,e\,h\,cos\,(l)\ sin\,(l) - a\ (4\,c\,cos\,(2\,l)\ sin\,(2\,l) - 2\,b\,cos\,(l)\ sin\,(l)) \\ g_2 &= d\,\left(e\,sin\,(l)^2 - 1\right) \end{aligned} \tag{5.37}$$

5.6 Dynamics State Space Formulation

All the expressions derived in this chapter are linearly and can be combined and put in matrix state space form.

The new expressions found in Section 5.5, should first be inserted into the expression for $\delta\dot{\boldsymbol{p}}$, $\delta^n\dot{\boldsymbol{v}}$ and $\dot{\boldsymbol{\gamma}}$.

5.6.1 Position

As none of these variables appear in (5.15), the expression remains the same:

$$\delta\dot{\boldsymbol{p}} = \underline{\boldsymbol{A}}_1\delta\boldsymbol{p} + \underline{\boldsymbol{A}}_2\delta^n\boldsymbol{v} \tag{5.38}$$

5.6.2 Velocity

By inserting (5.29) and (5.32) into (5.20):

$$\begin{aligned} \delta\dot{\boldsymbol{v}} &= ({}^n\underline{\boldsymbol{\Omega}}_{ne} + 2{}^n\underline{\boldsymbol{\Omega}}_{ei})\,\delta^n\boldsymbol{v} - {}^n\,\underline{\boldsymbol{v}}\,(\delta^n\boldsymbol{\omega}_{ne} + 2\delta^n\boldsymbol{\omega}_{ei}) + {}^n\,\underline{\boldsymbol{C}}_s\,\delta^s\boldsymbol{a} + {}^n\,\underline{\boldsymbol{C}}_s\,{}^s\underline{\boldsymbol{a}}\,{}^s\underline{\boldsymbol{C}}_n\,{}^n\boldsymbol{\gamma} - \delta^n\breve{\boldsymbol{g}} \\ &= ({}^n\underline{\boldsymbol{\Omega}}_{ne} + 2{}^n\underline{\boldsymbol{\Omega}}_{ei})\,\delta^n\boldsymbol{v} - {}^n\,\underline{\boldsymbol{v}}\,(\underline{\boldsymbol{B}}_1\delta\boldsymbol{p} + \underline{\boldsymbol{B}}_2\delta^n\boldsymbol{v} + 2\underline{\boldsymbol{C}}\delta\boldsymbol{p}) + {}^n\,\underline{\boldsymbol{C}}_s\,\delta^s\boldsymbol{a} + {}^n\,\underline{\boldsymbol{C}}_s\,{}^s\underline{\boldsymbol{a}}\,{}^s\underline{\boldsymbol{C}}_n\,{}^n\boldsymbol{\gamma} - \underline{\boldsymbol{G}}\delta\boldsymbol{p} \\ &= (-{}^n\underline{\boldsymbol{v}}\underline{\boldsymbol{B}}_1 - 2{}^n\underline{\boldsymbol{v}}\underline{\boldsymbol{C}} - \underline{\boldsymbol{G}})\,\delta\boldsymbol{p} + ({}^n\underline{\boldsymbol{\Omega}}_{ne} + 2{}^n\underline{\boldsymbol{\Omega}}_{ei} - {}^n\,\underline{\boldsymbol{v}}\underline{\boldsymbol{B}}_2)\,\delta^n\boldsymbol{v} + {}^n\,\underline{\boldsymbol{C}}_s\,{}^s\underline{\boldsymbol{a}}\,{}^s\underline{\boldsymbol{C}}_n\,{}^n\boldsymbol{\gamma} + {}^n\,\underline{\boldsymbol{C}}_s\,\delta^s\boldsymbol{a} \end{aligned} \tag{5.39}$$

5.6.3 Attitude

In the same way, (5.29) and (5.32) are also inserted into:

$$
\begin{aligned}
{}^n\dot{\boldsymbol{\gamma}} &= \left({}^n\underline{\boldsymbol{\Omega}}_{ei} -{}^n \underline{\boldsymbol{\Omega}}_{ne}\right)^n \gamma - \delta^n\boldsymbol{\omega}_{ei} + \delta^n\boldsymbol{\omega}_{ne} -{}^n \underline{\boldsymbol{C}}_s\, \delta^s\boldsymbol{\omega}_{si} \\
&= \left({}^n\underline{\boldsymbol{\Omega}}_{ei} -{}^n \underline{\boldsymbol{\Omega}}_{ne}\right)^n \gamma - \underline{\boldsymbol{C}}\delta\boldsymbol{p} + \underline{\boldsymbol{B}}_1\delta\boldsymbol{p} + \underline{\boldsymbol{B}}_2\delta^n\boldsymbol{v} -{}^n \underline{\boldsymbol{C}}_s\, \delta^s\boldsymbol{\omega}_{si} \\
&= \left(\underline{\boldsymbol{B}}_1 - \underline{\boldsymbol{C}}\right)\delta\boldsymbol{p} + \underline{\boldsymbol{B}}_2\delta^n\boldsymbol{v} + \left({}^n\underline{\boldsymbol{\Omega}}_{ei} -{}^n \underline{\boldsymbol{\Omega}}_{ne}\right)^n \gamma -{}^n \underline{\boldsymbol{C}}_s\, \delta^s\boldsymbol{\omega}_{si}
\end{aligned} \tag{5.40}
$$

5.6.4 Matrix Form

Now, the position, velocity and attitude expressions (5.38), (5.39) and (5.40) are expressed in linear matrix form.

In Subsection 5.1.1, the assumption of constant acceleration and angular velocity was introduced with the addition of two extra vector states. As shown in (5.1) their trajectory were modeled as white noise.

In Subsection 4.5.3 the addition of three bias vector states was described. As shown in (4.17) their trajectory were also modeled as white noise.

These can be combined to form the state space matrix formulation, introduced as (5.8) in Subsection 5.1.4:

$$
\begin{aligned}
&\delta\dot{\boldsymbol{x}} = \underline{\boldsymbol{F}}\delta\boldsymbol{x} + \underline{\boldsymbol{Q}}\boldsymbol{w} \\
&\quad\Updownarrow \\
&\quad\dot{\begin{bmatrix} \delta\boldsymbol{p} \\ \delta^n\boldsymbol{v} \\ \gamma \\ \delta^s\boldsymbol{a} \\ \delta^s\boldsymbol{\omega}_{is} \\ \delta^s\boldsymbol{b}_{acc} \\ \delta^s\boldsymbol{b}_{gyro} \\ \delta^s\boldsymbol{b}_{mag} \end{bmatrix}} = \\
&\quad\begin{bmatrix}
\underline{\boldsymbol{A}}_1 & \underline{\boldsymbol{A}}_2 & \underline{\boldsymbol{0}} & \underline{\boldsymbol{0}} & \underline{\boldsymbol{0}} & \underline{\boldsymbol{0}} & \underline{\boldsymbol{0}} & \underline{\boldsymbol{0}} \\
-{}^n\underline{\boldsymbol{vB}}_1 - 2^n\underline{\boldsymbol{vC}} + \underline{\boldsymbol{G}} & {}^n\underline{\boldsymbol{\Omega}}_{ne} + 2^n\underline{\boldsymbol{\Omega}}_{ei} -{}^n \underline{\boldsymbol{vB}}_2 & {}^n\underline{\boldsymbol{C}}_s\,{}^s\underline{\boldsymbol{a}}\,{}^s\underline{\boldsymbol{C}}_n & {}^n\underline{\boldsymbol{C}}_s & \underline{\boldsymbol{0}} & \underline{\boldsymbol{0}} & \underline{\boldsymbol{0}} & \underline{\boldsymbol{0}} \\
\underline{\boldsymbol{B}}_1 - \underline{\boldsymbol{C}} & \underline{\boldsymbol{B}}_2 & {}^n\underline{\boldsymbol{\Omega}}_{ei} -{}^n \underline{\boldsymbol{\Omega}}_{ne} & \underline{\boldsymbol{0}} & -{}^n\underline{\boldsymbol{C}}_s & \underline{\boldsymbol{0}} & \underline{\boldsymbol{0}} & \underline{\boldsymbol{0}} \\
\underline{\boldsymbol{0}} & \underline{\boldsymbol{0}} & \underline{\boldsymbol{0}} & \underline{\boldsymbol{0}} & \underline{\boldsymbol{0}} & \underline{\boldsymbol{0}} & \underline{\boldsymbol{0}} & \underline{\boldsymbol{0}} \\
\underline{\boldsymbol{0}} & \underline{\boldsymbol{0}} & \underline{\boldsymbol{0}} & \underline{\boldsymbol{0}} & \underline{\boldsymbol{0}} & \underline{\boldsymbol{0}} & \underline{\boldsymbol{0}} & \underline{\boldsymbol{0}} \\
\underline{\boldsymbol{0}} & \underline{\boldsymbol{0}} & \underline{\boldsymbol{0}} & \underline{\boldsymbol{0}} & \underline{\boldsymbol{0}} & \underline{\boldsymbol{0}} & \underline{\boldsymbol{0}} & \underline{\boldsymbol{0}} \\
\underline{\boldsymbol{0}} & \underline{\boldsymbol{0}} & \underline{\boldsymbol{0}} & \underline{\boldsymbol{0}} & \underline{\boldsymbol{0}} & \underline{\boldsymbol{0}} & \underline{\boldsymbol{0}} & \underline{\boldsymbol{0}} \\
\underline{\boldsymbol{0}} & \underline{\boldsymbol{0}} & \underline{\boldsymbol{0}} & \underline{\boldsymbol{0}} & \underline{\boldsymbol{0}} & \underline{\boldsymbol{0}} & \underline{\boldsymbol{0}} & \underline{\boldsymbol{0}}
\end{bmatrix}
\begin{bmatrix} \delta\boldsymbol{p} \\ \delta^n\boldsymbol{v} \\ \gamma \\ \delta^s\boldsymbol{a} \\ \delta^s\boldsymbol{\omega}_{is} \\ \delta^s\boldsymbol{b}_{acc} \\ \delta^s\boldsymbol{b}_{gyro} \\ \delta^s\boldsymbol{b}_{mag} \end{bmatrix} \\
&\quad + \begin{bmatrix}
\underline{\boldsymbol{0}} & \underline{\boldsymbol{0}} & \underline{\boldsymbol{0}} & \underline{\boldsymbol{0}} & \underline{\boldsymbol{0}} & \underline{\boldsymbol{0}} & \underline{\boldsymbol{0}} & \underline{\boldsymbol{0}} \\
\underline{\boldsymbol{0}} & \underline{\boldsymbol{0}} & \underline{\boldsymbol{0}} & \underline{\boldsymbol{0}} & \underline{\boldsymbol{0}} & \underline{\boldsymbol{0}} & \underline{\boldsymbol{0}} & \underline{\boldsymbol{0}} \\
\underline{\boldsymbol{0}} & \underline{\boldsymbol{0}} & \underline{\boldsymbol{0}} & \underline{\boldsymbol{0}} & \underline{\boldsymbol{0}} & \underline{\boldsymbol{0}} & \underline{\boldsymbol{0}} & \underline{\boldsymbol{0}} \\
\underline{\boldsymbol{0}} & \underline{\boldsymbol{0}} & \underline{\boldsymbol{0}} & \underline{\boldsymbol{\sigma}^2_{{}^s\boldsymbol{a}}} & \underline{\boldsymbol{0}} & \underline{\boldsymbol{0}} & \underline{\boldsymbol{0}} & \underline{\boldsymbol{0}} \\
\underline{\boldsymbol{0}} & \underline{\boldsymbol{0}} & \underline{\boldsymbol{0}} & \underline{\boldsymbol{0}} & \underline{\boldsymbol{\sigma}^2_{{}^s\boldsymbol{\omega}_{is}}} & \underline{\boldsymbol{0}} & \underline{\boldsymbol{0}} & \underline{\boldsymbol{0}} \\
\underline{\boldsymbol{0}} & \underline{\boldsymbol{0}} & \underline{\boldsymbol{0}} & \underline{\boldsymbol{0}} & \underline{\boldsymbol{0}} & \underline{\boldsymbol{\sigma}^2_{{}^s\boldsymbol{b}_{acc}}} & \underline{\boldsymbol{0}} & \underline{\boldsymbol{0}} \\
\underline{\boldsymbol{0}} & \underline{\boldsymbol{0}} & \underline{\boldsymbol{0}} & \underline{\boldsymbol{0}} & \underline{\boldsymbol{0}} & \underline{\boldsymbol{0}} & \underline{\boldsymbol{\sigma}^2_{{}^s\boldsymbol{b}_{gyro}}} & \underline{\boldsymbol{0}} \\
\underline{\boldsymbol{0}} & \underline{\boldsymbol{0}} & \underline{\boldsymbol{0}} & \underline{\boldsymbol{0}} & \underline{\boldsymbol{0}} & \underline{\boldsymbol{0}} & \underline{\boldsymbol{0}} & \underline{\boldsymbol{\sigma}^2_{{}^s\boldsymbol{b}_{mag}}}
\end{bmatrix} \boldsymbol{w}
\end{aligned} \tag{5.41}
$$

As mentioned earlier in this chapter, $\boldsymbol{w}$ is here a vector with independent Gaussian distributed noise elements, all with unitary standard deviation. $\underline{\boldsymbol{\sigma_{state}}}$ are diagonal matrices with the stan-

dard deviation of the correspondent noise vector element.

(5.41) is the final linear equation, which describes the small perturbations trajectory model of the states. The expressions of the variables inside the matrix can be found throughout this chapter and Chapter 3.

5.7 Small Perturbations Measurement Model

As mentioned earlier, a linear small perturbations measurement model is also needed. As described in Section 4.5, two measurement model are available: one describing the system when all sensors have new measurements available and one describing the system when only new measurements of the MS2 are available.

The full measurement model, for when a new GPS measurement is available, were derived in Chapter 4 and can be seen in (4.14) on page 30. It was noted that the expression for ${}^s\widetilde{\boldsymbol{m}}$ was the only non-linearly expression in this model.

${}^s\widetilde{\boldsymbol{m}}$ was found to be:

$$ {}^s\widetilde{\boldsymbol{m}} = {}^s\underline{\boldsymbol{C}}_n \, {}^n\breve{\boldsymbol{m}} + {}^s\,\boldsymbol{b}_{mag} + \boldsymbol{v}_{mag} \tag{5.42} $$

Introducing the small measurement error:

$$ \delta^s\widetilde{\boldsymbol{m}} = {}^s\widehat{\widetilde{\boldsymbol{m}}} - {}^s\,\widetilde{\boldsymbol{m}} \tag{5.43} $$

Inserting (5.43) into (5.42):

$$ \begin{aligned} \delta^s\widetilde{\boldsymbol{m}} &= {}^s\hat{\underline{\boldsymbol{C}}}_n \, {}^n\hat{\breve{m}} + {}^s\,\hat{\boldsymbol{b}}_{mag} + \hat{\boldsymbol{v}}_{mag} - {}^s\,\underline{\boldsymbol{C}}_n \, {}^n\breve{\boldsymbol{m}} - {}^s\,\boldsymbol{b}_{mag} - \boldsymbol{v}_{mag} \\ &= ({}^s\underline{\boldsymbol{C}}_n + \delta^s\underline{\boldsymbol{C}}_n)\,({}^n\breve{\boldsymbol{m}} + \delta^n\breve{\boldsymbol{m}}) - {}^s\,\underline{\boldsymbol{C}}_n \, {}^n\breve{\boldsymbol{m}} + \delta^s\boldsymbol{b}_{mag} + \delta\boldsymbol{v}_{mag} \\ &= {}^s\underline{\boldsymbol{C}}_n \, \delta^n\breve{\boldsymbol{m}} + \delta^s\underline{\boldsymbol{C}}_n \, {}^n\breve{\boldsymbol{m}} + \delta^s\underline{\boldsymbol{C}}_n \, \delta^n\breve{\boldsymbol{m}} + \delta^s\boldsymbol{b}_{mag} + \delta\boldsymbol{v}_{mag} \end{aligned} \tag{5.44} $$

It will be very complex to derive an expression for the partial differential of $\delta^n\breve{m}$. Also, the magnetic field of the earth will vary very little within a small area.

Because of this, it is chosen to approximate ${}^n\breve{\boldsymbol{m}}$ as a constant within a small area, why $\delta^n\breve{\boldsymbol{m}}$ can be approximated as being 0.

Applying this approximation and neglecting 2nd order terms, (5.44) can be reduced to:

$$ \delta^s\widetilde{\boldsymbol{m}} = \delta^s\underline{\boldsymbol{C}}_n \, {}^n\breve{\boldsymbol{m}} + \delta^s\boldsymbol{b}_{mag} + \delta\boldsymbol{v}_{mag} \tag{5.45} $$

By inserting (5.7) into (5.45), it can be written in vector form as:

$$ \begin{aligned} \delta^s\widetilde{\boldsymbol{m}} &= {}^s\underline{\boldsymbol{C}}_n \, \underline{\boldsymbol{\Gamma}} \, {}^n\breve{\boldsymbol{m}} + \delta^s\boldsymbol{b}_{mag} + \delta\boldsymbol{v}_{mag} \\ &= -{}^s\,\underline{\boldsymbol{C}}_n \, {}^n\underline{\breve{\boldsymbol{m}}}\,\boldsymbol{\gamma} + \delta^s\boldsymbol{b}_{mag} + \delta\boldsymbol{v}_{mag} \end{aligned} \tag{5.46} $$

In which ${}^n\underline{\breve{\boldsymbol{m}}}$ is the skew symmetric representation of ${}^n\breve{\boldsymbol{m}}$.

Together with the measurement model found as (4.15) on page 30, the state space representation of the full local measurement model can be written as:

$$ \begin{aligned} \delta\boldsymbol{y} &= \underline{\boldsymbol{H}}\delta\boldsymbol{x} + \underline{\boldsymbol{\Lambda}}\boldsymbol{v} \\ &\Updownarrow \\ \begin{bmatrix} \delta\widetilde{\boldsymbol{p}}_{GPS} \\ \delta^n\widetilde{\boldsymbol{v}}_{GPS} \\ \delta^s\widetilde{\boldsymbol{a}} \\ \delta^s\widetilde{\boldsymbol{\omega}}_{is} \\ \delta^s\widetilde{\boldsymbol{m}} \end{bmatrix} &= \begin{bmatrix} \underline{\boldsymbol{I}} & \underline{\boldsymbol{0}} & \underline{\boldsymbol{0}} & \underline{\boldsymbol{0}} & \underline{\boldsymbol{0}} & \underline{\boldsymbol{0}} & \underline{\boldsymbol{0}} & \underline{\boldsymbol{0}} \\ \underline{\boldsymbol{0}} & \underline{\boldsymbol{I}} & \underline{\boldsymbol{0}} & \underline{\boldsymbol{0}} & \underline{\boldsymbol{0}} & \underline{\boldsymbol{0}} & \underline{\boldsymbol{0}} & \underline{\boldsymbol{0}} \\ \underline{\boldsymbol{0}} & \underline{\boldsymbol{0}} & \underline{\boldsymbol{0}} & \underline{\boldsymbol{I}} & \underline{\boldsymbol{0}} & \underline{\boldsymbol{I}} & \underline{\boldsymbol{0}} & \underline{\boldsymbol{0}} \\ \underline{\boldsymbol{0}} & \underline{\boldsymbol{0}} & \underline{\boldsymbol{0}} & \underline{\boldsymbol{0}} & \underline{\boldsymbol{I}} & \underline{\boldsymbol{0}} & \underline{\boldsymbol{I}} & \underline{\boldsymbol{0}} \\ \underline{\boldsymbol{0}} & \underline{\boldsymbol{0}} & -{}^s\underline{\boldsymbol{C}}_n \, {}^n\underline{\breve{\boldsymbol{m}}} & \underline{\boldsymbol{0}} & \underline{\boldsymbol{0}} & \underline{\boldsymbol{0}} & \underline{\boldsymbol{0}} & \underline{\boldsymbol{I}} \end{bmatrix} \begin{bmatrix} \delta\boldsymbol{p} \\ \delta^n\boldsymbol{v} \\ \boldsymbol{\gamma} \\ \delta^s\boldsymbol{a} \\ \delta^s\boldsymbol{\omega}_{is} \\ \delta^s\boldsymbol{b}_{acc} \\ \delta^s\boldsymbol{b}_{gyro} \\ \delta^s\boldsymbol{b}_{mag} \end{bmatrix} + \underline{\boldsymbol{\Lambda}}\boldsymbol{v} \end{aligned} \tag{5.47} $$

5.7.1 Reduced Small Perturbations Measurement Model

In Subsection 4.5.2, a reduced measurement model describing the system when no new GPS measurement is available was introduced.

A small perturbations measurement model for this reduced model is also needed. This model is equal to (5.47), but with the GPS dependent rows and columns removed.

This reduces (5.47) to:

$$
\begin{aligned}
\delta \boldsymbol{y} =& \underline{\boldsymbol{H}}_{no\,GPS}\delta \boldsymbol{x} + \underline{\boldsymbol{\Lambda}}_{no\,GPS}\boldsymbol{v} \\
&\Updownarrow \\
\begin{bmatrix} \delta^s \widetilde{\boldsymbol{a}} \\ \delta^s \widetilde{\boldsymbol{\omega}}_{is} \\ \delta^s \widetilde{\boldsymbol{m}} \end{bmatrix} =& \begin{bmatrix} \underline{\mathbf{0}} & \underline{\mathbf{0}} & \underline{\mathbf{0}} & \underline{\boldsymbol{I}} & \underline{\mathbf{0}} & \underline{\boldsymbol{I}} & \underline{\mathbf{0}} & \underline{\mathbf{0}} \\ \underline{\mathbf{0}} & \underline{\mathbf{0}} & \underline{\mathbf{0}} & \underline{\mathbf{0}} & \underline{\boldsymbol{I}} & \underline{\mathbf{0}} & \underline{\boldsymbol{I}} & \underline{\mathbf{0}} \\ \underline{\mathbf{0}} & \underline{\mathbf{0}} & -{}^s\underline{\boldsymbol{C}}_n\,{}^n\underline{\breve{\boldsymbol{m}}} & \underline{\mathbf{0}} & \underline{\mathbf{0}} & \underline{\mathbf{0}} & \underline{\mathbf{0}} & \underline{\boldsymbol{I}} \end{bmatrix} \begin{bmatrix} \delta \boldsymbol{p} \\ \delta^n \boldsymbol{v} \\ \boldsymbol{\gamma} \\ \delta^s \boldsymbol{a} \\ \delta^s \boldsymbol{\omega}_{is} \\ \delta^s \boldsymbol{b}_{acc} \\ \delta^s \boldsymbol{b}_{gyro} \\ \delta^s \boldsymbol{b}_{mag} \end{bmatrix} + \underline{\boldsymbol{\Lambda}}_{no\,GPS}\boldsymbol{v}
\end{aligned}
\tag{5.48}
$$

5.8 Computing Discrete Models

Previously in this chapter, (5.41) was derived, which states the continuous model:

$$\delta\dot{\boldsymbol{x}} = \underline{\boldsymbol{F}}\delta\boldsymbol{x} + \underline{\boldsymbol{Q}}\boldsymbol{w} \tag{5.49}$$

The estimation filter is run at a fixed discrete sample rate, why a model is needed which describes the change in the small perturbations in the next sample step instead of the time derivative (or trajectory).

A transformation is needed to obtain the discrete version of the model matrices $\underline{\boldsymbol{F}}$ and $\underline{\boldsymbol{Q}}$. The discrete versions of these matrices are denoted $\underline{\boldsymbol{\Phi}}$ and $\underline{\boldsymbol{\Sigma}}$.

The object is thus to find $\underline{\boldsymbol{\Phi}}$ and Σ to describe the discrete state propagation:

$$\delta\boldsymbol{x}[k+1] = \underline{\boldsymbol{\Phi}[k]}\delta\boldsymbol{x}[k] + \underline{\boldsymbol{\Sigma}}[k]\boldsymbol{w} \tag{5.50}$$

The discrete matrices can be obtained by utilizing Van Loan's discretization method [Grewal 08, 110]. Van Loan's method states that a matrix M should be constructed using the continuous linear model matrices, as shown in (5.51).

$$M = TS\begin{bmatrix} -\boldsymbol{F} & \boldsymbol{Q} \\ \underline{\boldsymbol{0}} & \underline{\boldsymbol{F}}^T \end{bmatrix} \tag{5.51}$$

In which TS is the sample rate of the estimation filter.

If M is constructed according to this, then (5.52) will be true.

$$exp(M) = \begin{bmatrix} \underline{\boldsymbol{\Upsilon}} & \underline{\boldsymbol{\Phi}}^{-1}\underline{\boldsymbol{\Sigma}} \\ \underline{\boldsymbol{0}} & \underline{\boldsymbol{\Phi}}^T \end{bmatrix} \tag{5.52}$$

In which $\underline{\boldsymbol{\Upsilon}}$ are not used for anything in this utilization of Van Loan's method.

The discrete model of the small state trajectory ($\underline{\boldsymbol{\Phi}}$ and the discrete noise matrix ($\underline{\boldsymbol{\Sigma}}$) can then easily be extracted from the resulting matrix in (5.52).

5.8.1 Discrete Measurement Models

In Section 5.7 the two continuous measurements were derived, with the result shown in (5.47) and (5.48).

No transformation is needed in order to obtain the discrete versions of these matrices, why the discrete version of the full measurement model is given as:

$$\delta\boldsymbol{y}[k] = \underline{\boldsymbol{H}}[k]\delta\boldsymbol{x}[k] + \underline{\boldsymbol{\Lambda}}\boldsymbol{v}[k] \tag{5.53}$$

And the reduced measurement model, for when no new GPS measurement is available, is given as:

$$\delta\boldsymbol{y}_{no\,GPS}[k] = \underline{\boldsymbol{H}}_{no\,GPS}[k]\delta\boldsymbol{x}[k] + \underline{\boldsymbol{\Lambda}}_{no\,GPS}\boldsymbol{v}[k] \tag{5.54}$$

Chapter 6

Simulation Environment

Prior to testing the estimation filter on actual real world data, it is preferable to first test it on simulated data. One of the advantages of working with simulated data is to have control with the whole environment including noise and error sources. Another advantage of testing the estimation filter on self generated data is that the true noiseless state values are available at all times. Finally, the simulation environment can serve as a simplification of the real world, leaving some physical phenomenons out. This can be advantageous to test the basic capabilities of the filter and to easier debug implementation errors.

Due to these reasons, a simulator has been constructed in Simulink. The scope of the simulation environment is to model a point mass which is moving somewhat like a boat does at sea.

As mentioned earlier, data is available from a sea trail in which high precision attitude estimations are also at disposal. From this attitude data, the frequency and amplitude of the motion could be seen. This motion is caused by input forces and moments such as the engine thrust together with the addition of waves, current and wind.

In the simulation it has been the objective to affect the point mass with such forces and momentums that it will execute rotational oscillations which are comparable to the oscillations seen in the real world data. It is not essential that it acts precisely as a boat does in the real world as the navigation solution should be relatively independent of what platform it is mounted on.

This simulation environment does not include the effects of moving on a rotating earth. These effects are not included in order to reduce the complexity and due to the fact that these effects are very small at the velocities carried out by the marine applications for which this navigation solution is intended.

An overview of the simulation environment is illustrated in Fig. 6.1.

The MATLAB aerospace toolbox includes a Simulink block, which simulates the kinematic behavior of a point mass. This is the central part of the simulation environment. It has been chosen to use the point mass simulation block from the MATLAB toolbox instead of composing a separate point mass simulation block from the basic standard components. This was chosen for two reasons; it would be less time consuming and it would be easier to avoid introducing extra sources for possible implementation errors.

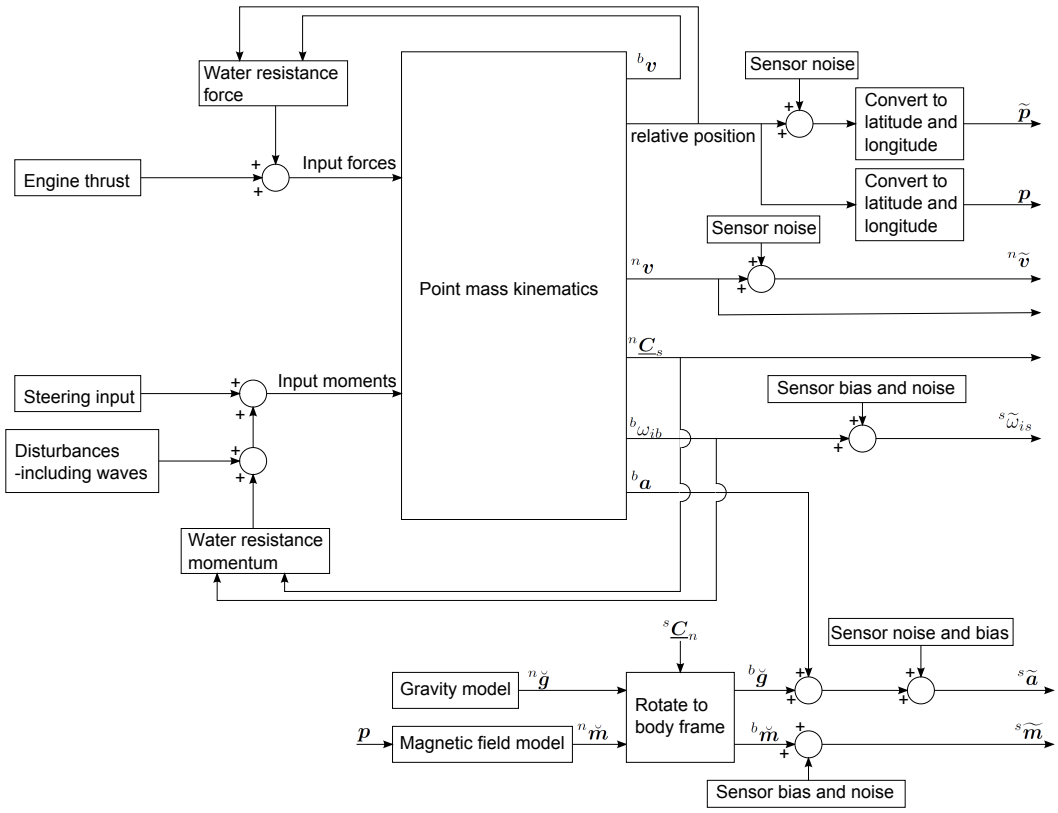

Figure 6.1: An overview of the simulation environment

6.1 Simulation Inputs

The point mass simulation block takes forces and angular momentums acting on the point as input.

It is not essential that the point mass moves precisely as a boat would do in the real world. Therefore there has not been put a lot of effort into studying literature regarding modeling of boat dynamics and maritime environments. The inputs have been generated based on the project group's assumptions of forces/momentums that would affect a boat in a maritime environment.

In order to imitate the thrust from the engine of the boat, a constant force in the forward X-axis direction is applied. As a boat will experience resistance from the water, this is added as a opposing force which has a magnitude that is proportional to the squared velocity. As the architecture of a boat causes a boat to have less water resistance at the front than at the sides, this is incorporated in the proportional coefficient vector, with the X-axis coefficient being smaller.

Due to the buoyancy of a boat, in calm waters, a boat would have a vertical equilibrium height at the water level. To simulate this, a force term has been included in the Z-axis which is proportional to the vertical offset from sea level.

In order to imitate the moment inflicted by the rudders of a boat, a steering input moment have been added as a controllable input. This is included as a moment acting around the Z-axis

of the point mass. As in a real boat, the steering moment and the forward thrust of the engine are the dominating forces/momentums, thus giving the user control of the route of the boat.

To mimic the rotational oscillations a boat is affected by, multiple momentum input terms are included. The momentums generated by ocean waves is simulated using different sinusoid signals with added white noise.

A boat would also experience a water resistance momentum when rotating. Due to this, a term which, like the water resistance force term, is proportional to the squared angular velocity is included.

Due to the buoyancy of a stable boat, is will experience stabilizing momentums when tilted around the roll or pitch axes. Thus a term which is proportional to the roll and pitch rotation angles has been included.

It is seen in the simulation that this design of the inputs causes physical real world phenomenons such as side slip when turning using the controllable steering input.

6.2 Sensor Simulation

As described in Chapter 4, the sensors of the system are assumed to be affected by different deviations from the true measurement values such as noise and biases.

Some of these deviation are included in an attempt to simulate the behavior of these sensors.

6.2.1 Gyroscopes

The gyroscopes measure the angular velocity of the point mass. But as described in Section 4.1, the sensor is also affected by noise and a bias.
In the simulation, the bias has been modeled as an added constant vector with the values: $\begin{bmatrix}-4 & 2 & -6\end{bmatrix}^T$ $^\circ/s$ which are within the 95% probability range of the run-to-run bias specified in the data sheet. The measurement noise is simulated as white noise with a mean value of the specified bias vector and a standard deviation of 0.8 $^\circ/s$ which is the standard deviation specified in the data sheet.

In Fig. 6.1, the gyroscope measuring is denoted as ${}^s\widetilde{\omega}_{ib}$.

6.2.2 Accelerometers

As mentioned in Chapter 3, the accelerometers will, indistinguishable, measure both the acceleration caused by motion of the platform and the gravitational acceleration. In the simulation environment it has, as a simplifying factor, been chosen to set the gravity acceleration to a constant downward acceleration of 9.82 $^m/_{s^2}$. Using the DCM generated by the point mass simulation block, this gravity is rotated into the body frame and added to the acceleration caused by motion of the point mass. In addition to this, the measurement is also affected by sensor noise and a bias.

In the simulation, the bias has been modeled as an added constant vector with the values: $\begin{bmatrix}4 & -10 & -3\end{bmatrix}^T$ mg which are within the 95% probability range of the run-to-run bias specified in the data sheet. The measurement noise is simulated as white zero mean noise with a mean value of the specified bias vector and a standard deviation of 5 mg which is the standard deviation specified in the data sheet.

In Fig. 6.1, the accelerometer measuring is denoted as ${}^n\widetilde{\boldsymbol{a}}$.

6.2.3 Magnetometers

In order to simulate the magnetometers, a simulation block from the MATLAB aerospace toolbox is used, which outputs the magnetic field in the NRF based on the current location. It should be

mentioned that this simulation block is based on the World Magnetic Model (WMM) as opposed to the IGRF model used in the estimation filter. But it has been seen that these two models differ very little, at least in the area in which the simulation is performed. The outputted magnetic field is rotated into the body frame using the DCM generated by the point mass simulation block. To the measurement is then added white measurement noise, with a standard deviation of 2 mG which is the standard deviation specified in the data sheet. A bias is modeled as a constant vector with the values: $\begin{bmatrix}-0.04 & 0.02 & 0.01\end{bmatrix}^T$ G. Which is applied to the measurement as being the mean value of the measurement noise.

In Fig. 6.1, the magnetometer measuring is denoted as ${}^s\widetilde{\boldsymbol{m}}$.

6.2.4 GPS

The GPS measures the position and the velocity in the NRF.

In the point mass simulation, the position is outputted as a relative distance to the starting point. Before this relative position is converted into latitude/longitude coordinates, noise is added to the state. This added noise is white to simulate random offsets.

As described in Section 1.5 and Section 4.4, the navigation solution scoped by this thesis will not achieve to be able to account for the slow varying offset caused by the atmospherical disturbances. Because of this, it has been assessed that it will be unsuitable to include a slow varying position measurement error in the simulation.

To simulate the GPS's measurement of the velocity, white noise is added to the velocity output from the point mass simulation block.

In Fig. 6.1, the position measuring of the GPS is denoted as $\widetilde{\boldsymbol{p}}$. In addition, the true position is available for comparison and is denoted $\boldsymbol{p}$. The velocity measuring of the GPS is denoted as ${}^n\widetilde{\boldsymbol{v}}$ and the true velocity is also available and is denoted in Fig. 6.1 as ${}^n\boldsymbol{v}$.

6.3 Simulation Navigation Equations Simplifications

As mentioned, this simulation environment does not include the effects of moving on a rotating earth.

This has the result that the equation developed throughout this thesis can be simplified when applied to data generated by the simulation, as the two terms ${}^n\omega_{ei}$ and ${}^n\omega_{ne}$ are zero in the simulation.

This has the impact that the main navigation equation (3.29) on 18 can be reduced to:

$$ {}^n\dot{\boldsymbol{v}} = {}^n\boldsymbol{a} - {}^n\breve{\boldsymbol{g}} \tag{6.1} $$

Furthermore, the equation describing the change attitude (3.33) on 19 can be reduced to:

$$ {}^n\dot{\underline{\boldsymbol{C}}}_s = {}^n\underline{\boldsymbol{C}}_s^s\Omega_{si} \tag{6.2} $$

These changes also affect the small perturbations trajectory model derived in Chapter 5 which too can be simplified. In addition to the two terms ${}^n\omega_{ei}$ and ${}^n\omega_{ne}$ being zero, another simplification made in the simulation environment is the implementation of the gravity of being constant.

This has the effect that the Jacobian matrix of these three terms are all zero matrices.

Thus, the matrix form of the small perturbations trajectory model (5.41) can be simplified to:

$$
\begin{gathered}
\delta\dot{\boldsymbol{x}} = \underline{\boldsymbol{F}}_{simu}\delta\boldsymbol{x} + \underline{\boldsymbol{Q}}\boldsymbol{w} \\
\Updownarrow \\
\dot{\begin{bmatrix} \delta\boldsymbol{p} \\ \delta^n\boldsymbol{v} \\ \boldsymbol{\gamma} \\ \delta^s\boldsymbol{a} \\ \delta^s\boldsymbol{\omega}_{is} \\ \delta^s\boldsymbol{b}_{acc} \\ \delta^s\boldsymbol{b}_{gyro} \\ \delta^s\boldsymbol{b}_{mag} \end{bmatrix}} = \begin{bmatrix} \underline{\boldsymbol{A}}_1 & \underline{\boldsymbol{A}}_2 & \underline{\mathbf{0}} & \underline{\mathbf{0}} & \underline{\mathbf{0}} & \underline{\mathbf{0}} & \underline{\mathbf{0}} & \underline{\mathbf{0}} \\ \underline{\mathbf{0}} & \underline{\mathbf{0}} & {}^n\underline{\boldsymbol{C}}_s\, {}^s\underline{\boldsymbol{a}}_{ext}\, {}^s\underline{\boldsymbol{C}}_n & {}^n\underline{\boldsymbol{C}}_s & \underline{\mathbf{0}} & \underline{\mathbf{0}} & \underline{\mathbf{0}} & \underline{\mathbf{0}} \\ \underline{\mathbf{0}} & \underline{\mathbf{0}} & \underline{\mathbf{0}} & \underline{\mathbf{0}} & -{}^n\underline{\boldsymbol{C}}_s & \underline{\mathbf{0}} & \underline{\mathbf{0}} & \underline{\mathbf{0}} \\ \underline{\mathbf{0}} & \underline{\mathbf{0}} & \underline{\mathbf{0}} & \underline{\mathbf{0}} & \underline{\mathbf{0}} & \underline{\mathbf{0}} & \underline{\mathbf{0}} & \underline{\mathbf{0}} \\ \underline{\mathbf{0}} & \underline{\mathbf{0}} & \underline{\mathbf{0}} & \underline{\mathbf{0}} & \underline{\mathbf{0}} & \underline{\mathbf{0}} & \underline{\mathbf{0}} & \underline{\mathbf{0}} \\ \underline{\mathbf{0}} & \underline{\mathbf{0}} & \underline{\mathbf{0}} & \underline{\mathbf{0}} & \underline{\mathbf{0}} & \underline{\mathbf{0}} & \underline{\mathbf{0}} & \underline{\mathbf{0}} \\ \underline{\mathbf{0}} & \underline{\mathbf{0}} & \underline{\mathbf{0}} & \underline{\mathbf{0}} & \underline{\mathbf{0}} & \underline{\mathbf{0}} & \underline{\mathbf{0}} & \underline{\mathbf{0}} \\ \underline{\mathbf{0}} & \underline{\mathbf{0}} & \underline{\mathbf{0}} & \underline{\mathbf{0}} & \underline{\mathbf{0}} & \underline{\mathbf{0}} & \underline{\mathbf{0}} & \underline{\mathbf{0}} \end{bmatrix} \begin{bmatrix} \delta\boldsymbol{p} \\ \delta^n\boldsymbol{v} \\ \boldsymbol{\gamma} \\ \delta^s\boldsymbol{a} \\ \delta^s\boldsymbol{\omega}_{is} \\ \delta^s\boldsymbol{b}_{acc} \\ \delta^s\boldsymbol{b}_{gyro} \\ \delta^s\boldsymbol{b}_{mag} \end{bmatrix} + \underline{\boldsymbol{Q}}\boldsymbol{w}
\end{gathered} \tag{6.3}
$$

Part II

Estimation

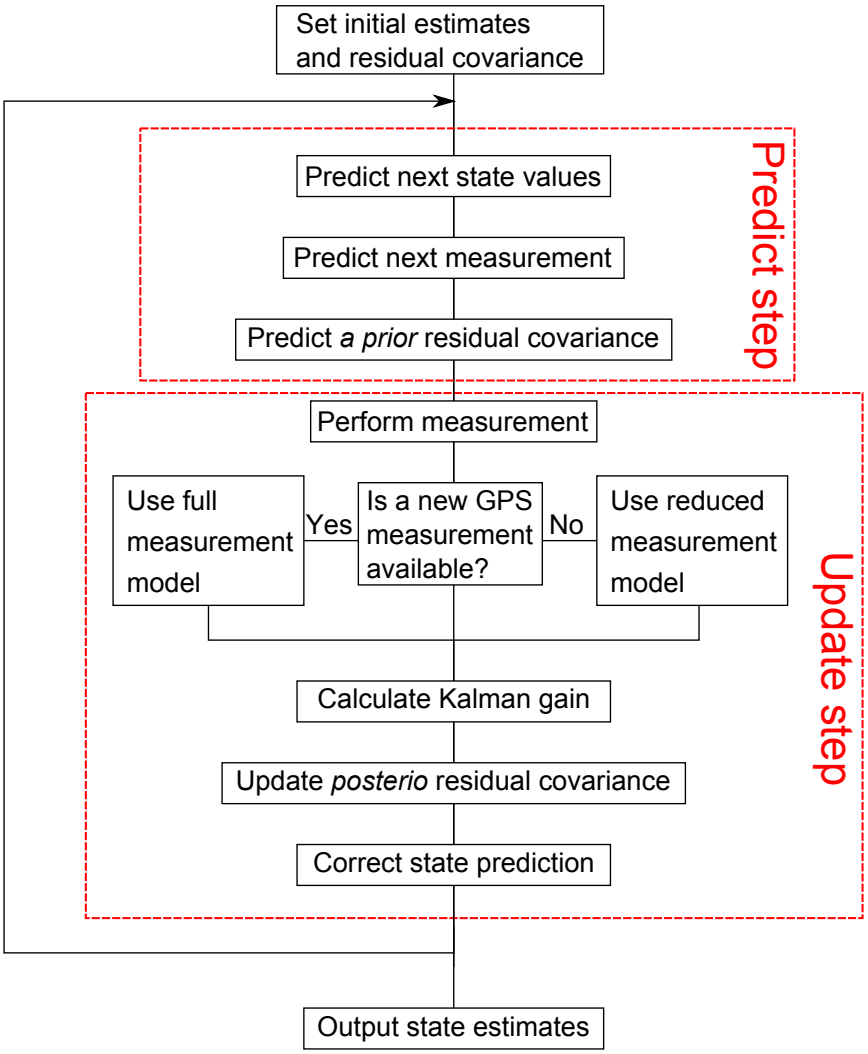

Figure 6.2: An overview of the estimation filter

In this part, the design of the estimation filter will be described. As mentioned, the used filter routine is based on the extended Kalman filter.

Throughout this part, it is assumed that the reader is familiar with the basics of the linear Kalman filter. The linear Kalman filter, and the deviation of it, is described in Appendix B.

The different steps of the estimation filter is shown in Fig. 6.2.

Before the estimation routine is started, a procedure is conducted to calculate initial estimates of the states. This procedure is described in Chapter 7.

Afterwards, the estimation routine itself is started, which consists of two main steps: a prediction step and an update step. These steps and the underlying subparts are described in Chapter 8.

Lastly, the pseudo code for the filter implementation is presented in Chapter 9.

Chapter 7

Filter Initialization

When starting the extended Kalman estimation filter, rough initial estimates of the states are required. The procedure of finding the initial attitude estimate is described in Section 7.1 while the obtaining of the initial values of the other states is described in Section 7.2.

For this, it is assumed that valid measurements are available from both the GPS and MS2 before the startup of the filter.

Lastly, the procedure of setting the initial values of the residual covariance terms is described in Section 7.3.

7.1 Course Alignment

The following course alignment procedure is based on the one of [Rogers 03, p. 216].

In order to calculate the initial estimate of the attitude between the NRF and SRF, two sets of vectors are required. In each vector set the vector represented both in the NRF and the SRF must be known.

By introducing the two vector set as the pairs ${}^n\boldsymbol{a}$ and ${}^s\boldsymbol{a}$ and ${}^n\boldsymbol{b}$ and ${}^s\boldsymbol{b}$, it can be seen that a third vector can be generated in each set by calculation the crossproduct of the vectors represented in both reference frames.

Knowing these three vectors represented in both reference frames, the mapping DCM, ${}^n\underline{\boldsymbol{C}}_s$ can be calculated as:

$$\begin{aligned} \begin{bmatrix} {}^n\boldsymbol{a} & {}^n\boldsymbol{b} & {}^n\boldsymbol{a} \times^n \boldsymbol{b} \end{bmatrix} &= {}^n\underline{\boldsymbol{C}}_s \begin{bmatrix} {}^s\boldsymbol{a} & {}^s\boldsymbol{b} & {}^s\boldsymbol{a} \times^s \boldsymbol{b} \end{bmatrix} \\ &\Updownarrow \\ {}^n\underline{\boldsymbol{C}}_s &= \begin{bmatrix} {}^n\boldsymbol{a} & {}^n\boldsymbol{b} & {}^n\boldsymbol{a} \times^n \boldsymbol{b} \end{bmatrix} \begin{bmatrix} {}^s\boldsymbol{a} & {}^s\boldsymbol{b} & {}^s\boldsymbol{a} \times^s \boldsymbol{b} \end{bmatrix}^{-1} \end{aligned} \tag{7.1}$$

It can be showed that the degree of orthogonality between the two vector sets leads to an increase in the precision of the alignment.

As described, in the navigation solution scoped in this thesis, two initial vectors is needed for this initial alignment. It is chosen to use the magnetic and gravitational field since, as previously described, models are available which can provide approximations of these vector fields in the NRF.

Assuming the initial measurement biases of the magnetometers are relatively small and the platform is not experiencing any big accelerations (ex. stationary), the magnetometers and accelerometers can provide the magnetic and gravitational field in the SRF.

These models and measurements should thus be inserted into (7.1).

So ${}^n\boldsymbol{a}$ is substituted with the modeled magnetic field vector ${}^n\breve{\boldsymbol{m}}$ and ${}^n\boldsymbol{a}$ is substituted with the measured magnetic field ${}^s\widetilde{\boldsymbol{m}}$.

${}^n\boldsymbol{b}$ is then substituted with the modeled gravitational field ${}^n\breve{\boldsymbol{g}}$ and lastly ${}^s\boldsymbol{a}$ is substituted with the accelerometer measurement ${}^s\widetilde{\boldsymbol{a}}$.

As a DCM transformation should not change the scale vectors (it should only rotate), the modeled and measured vectors are normalized.

By adding the normalization, this comes to the final attitude initialization equation:

$$ {}^n\underline{\boldsymbol{C}}_s = \left[|{}^n\breve{\boldsymbol{m}}| \quad |{}^n\breve{\boldsymbol{g}}| \quad |{}^n\breve{\boldsymbol{m}} \times {}^n\breve{\boldsymbol{g}}| \right] \left[|{}^s\widetilde{\boldsymbol{m}}| \quad |{}^s\widetilde{\boldsymbol{a}}| \quad |{}^s\widetilde{\boldsymbol{m}} \times {}^s\widetilde{\boldsymbol{a}}| \right]^{-1} \tag{7.2} $$

The ${}^n\underline{\boldsymbol{C}}_s$ calculated might not be completely orthogonal, why a reorthogonalityzation should be conducted before the start of the filter. The procedure of this reorthogonalityzation is described in Subsection A.4.3.

When using these vectors for the alignment procedure, the orthogonality issue described earlier leads to a decrease in precision near the poles. This is illustrated in Fig. 4.7 on page 28 in which it can be seen that the magnetic field lines are perpendicular to the surface of the earth at the poles and parallel with the surface at the equator. Because the gravity vector is always perpendicular to the surface of the earth, this leads to a decrease in precision closer to the poles as the two vectors becomes increasingly parallel. But as it was stated in Subsection 1.5.2 that issues regarding navigation near the poles will not be treated in this thesis, why this will not be of further concern.

7.1.1 Course Alignment Using High Grade Gyroscopes

In systems with high-grade gyroscopes, the angular velocity of the earth is often used instead of the magnetic field, as this can be measured if the platform is stationary. But the higher degree of measurement noise and gyro bias of the MS2 makes it improper to use this approach.

7.2 Initial Values of the Other States Estimates

In addition to the attitude, also the position, velocity, biases and the terms resulted from the constant assumption of acceleration and angular velocity (${}^s\boldsymbol{a}$ and ${}^s\boldsymbol{\omega}_{si}$) need initial estimate values.

As GPS measurements are assumed available before startup of the estimation filter, fairly precise initial estimates of the position and velocity can be obtained directly from this.

According to the run-to-run bias parameter of the datasheet [Ana 11], the accelerometer and gyroscope biases will vary each time the MS2 is booted. Due to this, these bias states are all initialized as being zero each time the filter is started.

As previously described, the magnetometer bias is mainly caused by nearby objects. Assuming that the MS2 is placed at a fixed position on the host vehicle, it might be advantageously to save the estimated magnetometer bias values in non-volatile memory as initial values for next boot up.

The initial estimate values of the two ${}^s\boldsymbol{a}$ and ${}^s\boldsymbol{\omega}_{si}$ vectors are set as the initial measurements of the accelerometer and gyroscope.

7.3 Initial Values of the Residual Covariance

The procedure of finding initial values of the state estimates has been described in this chapter. In the extended Kalman filter, initial values of the certainty of these initial estimates are also required. These are expressed in the initial residual covariance matrix $\underline{\boldsymbol{P}}_+[0]$.

$\underline{\boldsymbol{P}}_+[0]$ is designed as a diagonal matrix as, in which $\underline{\boldsymbol{\sigma^2_{state}}}[0]$ is a diagonal matrix with the corresponded residual variances:

$$\underline{\boldsymbol{P}}_+[0] = \begin{bmatrix} \underline{\boldsymbol{\sigma^2_p}}[0] & \underline{\mathbf{0}} & \underline{\mathbf{0}} & \underline{\mathbf{0}} & \underline{\mathbf{0}} & \underline{\mathbf{0}} & \underline{\mathbf{0}} & \underline{\mathbf{0}} \\ \underline{\mathbf{0}} & \underline{\boldsymbol{\sigma^2_{n_v}}}[0] & \underline{\mathbf{0}} & \underline{\mathbf{0}} & \underline{\mathbf{0}} & \underline{\mathbf{0}} & \underline{\mathbf{0}} & \underline{\mathbf{0}} \\ \underline{\mathbf{0}} & \underline{\mathbf{0}} & \underline{\boldsymbol{\sigma^2_{n\underline{C}_s}}}[0] & \underline{\mathbf{0}} & \underline{\mathbf{0}} & \underline{\mathbf{0}} & \underline{\mathbf{0}} & \underline{\mathbf{0}} \\ \underline{\mathbf{0}} & \underline{\mathbf{0}} & \underline{\mathbf{0}} & \underline{\boldsymbol{\sigma^2_{s_a}}}[0] & \underline{\mathbf{0}} & \underline{\mathbf{0}} & \underline{\mathbf{0}} & \underline{\mathbf{0}} \\ \underline{\mathbf{0}} & \underline{\mathbf{0}} & \underline{\mathbf{0}} & \underline{\mathbf{0}} & \underline{\boldsymbol{\sigma^2_{s_{\omega_{is}}}}}[0] & \underline{\mathbf{0}} & \underline{\mathbf{0}} & \underline{\mathbf{0}} \\ \underline{\mathbf{0}} & \underline{\mathbf{0}} & \underline{\mathbf{0}} & \underline{\mathbf{0}} & \underline{\mathbf{0}} & \underline{\boldsymbol{\sigma^2_{s_{b_{acc}}}}}[0] & \underline{\mathbf{0}} & \underline{\mathbf{0}} \\ \underline{\mathbf{0}} & \underline{\mathbf{0}} & \underline{\mathbf{0}} & \underline{\mathbf{0}} & \underline{\mathbf{0}} & \underline{\mathbf{0}} & \underline{\boldsymbol{\sigma^2_{s_{b_{gyro}}}}}[0] & \underline{\mathbf{0}} \\ \underline{\mathbf{0}} & \underline{\mathbf{0}} & \underline{\mathbf{0}} & \underline{\mathbf{0}} & \underline{\mathbf{0}} & \underline{\mathbf{0}} & \underline{\mathbf{0}} & \underline{\boldsymbol{\sigma^2_{s_{b_{mag}}}}}[0] \end{bmatrix} \tag{7.3}$$

$\underline{\boldsymbol{\sigma^2_p}}[0]$ and $\underline{\boldsymbol{\sigma^2_{n_v}}}[0]$ are selected as the variance of a GPS measurement, which is stated in Section 4.4. $\underline{\boldsymbol{\sigma^2_{n\underline{C}_s}}}[0]$ denotes the confidence in the initial course alignment which is has been chosen to set to $3\ ^\circ$. $\underline{\boldsymbol{\sigma^2_{s_{b_{acc}}}}}[0]$ and $\underline{\boldsymbol{\sigma^2_{s_{b_{gyro}}}}}[0]$ denotes the variance of the initial bias values of the inertial sensors. These are directly stated in the datasheet and are stated in Section 4.1 and Section 4.2.

$\underline{\boldsymbol{\sigma^2_{s_{b_{mag}}}}}[0]$ is the variance of the initial bias of the magnetometer. This parameter is regarded a tuning parameter which impacts the rate of which the magnetometer biases estimates converge.

$\underline{\boldsymbol{\sigma^2_{s_a}}}[0]$ and $\underline{\boldsymbol{\sigma^2_{s_{\omega_{is}}}}}[0]$ are also both considered as parameters of tuning. Both these should just be selected as high values as they will quickly converge due to the direct measurement of these states.

Chapter 8

Extended Kalman Filter

The extended Kalman filter is an extension of the linear Kalman filter. As the linear Kalman filter, it both outputs the estimate of the state vector and an estimate of the covariance of the residuals (the errors of the estimation). Like the linear Kalman filter, the extended Kalman filter consists of the two main steps: predict and update. These two steps will be described in details in the following subsections. The objective of these two steps is to calculate a correction vector, which will be used to update the last estimated state to an estimate of the present state.

In this estimation filter, the states will be kept track of using a full state which contains all the states of the system.

The full state vector is defined as:

$$\boldsymbol{x} = \begin{bmatrix} \boldsymbol{p} \\ {}^{n}\boldsymbol{v} \\ {}^{s}\underline{\boldsymbol{C}}_{n} \\ {}^{s}\boldsymbol{a} \\ {}^{s}\boldsymbol{\omega}_{is} \\ {}^{s}\boldsymbol{b}_{acc} \\ {}^{s}\boldsymbol{b}_{gyro} \\ {}^{s}\boldsymbol{b}_{mag} \end{bmatrix} \tag{8.1}$$

It should be noted that the only difference between the small perturbation state vector defined in (5.9) and the full state vector of (8.1) is the omission of δs and that the small angle approximation $\boldsymbol{\gamma}$ has been replaced by the full DCM (${}^{s}\underline{\boldsymbol{C}}_{n}$).

8.1 Prediction Step

In the prediction step, the derived system model is used to predict the most probable value of the state vector in the next sample step. This *a prior* estimate of the next state is denoted as $\boldsymbol{x}_{-}[k]$. Furthermore, based on the *a prior* state estimate, a prediction of the measurement is conducted. Lastly, an *a prior* estimate of the residual covariance is also calculated, which is denoted as $\underline{\boldsymbol{P}}_{-}[k]$.

One of the differences between the linear Kalman filter and the extended Kalman filter lies in the way that the prediction is performed. In the linear Kalman filter, the prediction is based on a set of linearized system equations while in the extended Kalman filter non-linear system equations can be utilized directly without the need of linearization. That is, based on the last *posterior* estimate of the state vector (denoted as $\boldsymbol{x}_{+}[k-1]$), the *a prior* state estimate is found as:

$$\boldsymbol{x}_{-}[k] = f\left(\boldsymbol{x}_{+}[k-1]\right) \tag{8.2}$$

$f()$ is here a function which maps the last *posterior* state estimate to the current *a prior* state estimate. In this estimation filter, the function $f()$ denotes an abstract function, which actually consists of multiple functions derived previously in this thesis.

8.1.1 The $f()$ Function

In the state vector defined in (8.1), the states ${}^{s}\boldsymbol{a}$ and ${}^{s}\boldsymbol{\omega}_{is}$ and all the bias states ${}^{s}\boldsymbol{b}_{acc}$, ${}^{s}\boldsymbol{b}_{gyro}$ and ${}^{s}\boldsymbol{b}_{mag}$ are all modeled as being constants with added white Gaussian noise why the most probable value in the next sample step would be the same as the *posterior* estimated in the previous sample step. Thus, this part of $f()$ just maps the last *posterior* state estimate of these states directly to the current *a prior* state estimate without any transformation.

Position and Velocity

The states $\boldsymbol{p}$ and ${}^{n}\boldsymbol{v}$ are predicted using a first order Euler approximation, which predict the next state value using the expressions:

$$\begin{aligned} \boldsymbol{p}_{-}[k] &= \boldsymbol{p}_{+}[k-1] + TS \cdot \dot{\boldsymbol{p}}_{+}[k-1] \\ {}^{n}\boldsymbol{v}_{-}[k] &= {}^{n}\boldsymbol{v}_{+}[k-1] + TS \cdot {}^{n}\dot{\boldsymbol{v}}_{+}[k-1] \end{aligned} \tag{8.3}$$

In which TS is the time interval with which the filter is run. The derivatives $\dot{\boldsymbol{p}}_{+}$ and ${}^{n}\dot{\boldsymbol{v}}_{+}$ are obtained directly using (3.31) and (3.29) and the previous *posterior* estimates.

Attitude

To predict the value of the attitude DCM (${}^{n}\underline{\boldsymbol{C}}_{s-}[k]$), ${}^{n}\dot{\underline{\boldsymbol{C}}}_{s+}[k]$ is first found using (3.33).

By knowing the previous *posterior* estimate (${}^{n}\underline{\boldsymbol{C}}_{s+}$) the discrete prediction can then be preformed by utilizing the method described in Section A.4.2, in which the prediction is done using:

$${}^{n}\underline{\boldsymbol{C}}_{s-}[k] = {}^{n}\underline{\boldsymbol{C}}_{s+}[k-1]\underline{\boldsymbol{\Pi}}[k] \tag{8.4}$$

in which $\underline{\boldsymbol{\Pi}}[k]$ is found using (A.23).

8.1.2 Prediction of Measurement

In every sample step, a new measurement of the MS2 sensors is conducted.

As described in Chapter 4, a new GPS measurements will not be available at each sample step, as it has a much slower sample rate than the MS2. This issue will be handled later in this section.

The full measurement vector, when a new GPS measurement is available, was defined in Section 4.5 as:

$$\widetilde{\boldsymbol{y}} = \begin{bmatrix} \widetilde{\boldsymbol{p}}_{GPS} \\ {}^{n}\widetilde{\boldsymbol{v}}_{GPS} \\ {}^{s}\widetilde{\omega}_{is} \\ {}^{s}\widetilde{a} \\ {}^{s}\widetilde{m} \end{bmatrix} \tag{8.5}$$

In the extended Kalman filter, the measurement values should be predicted. In this filter, the full measurement vector is always predicted using (4.14), as the check for a new GPS measurement is positioned in a later step.

This measurement prediction is denoted as $\tilde{\boldsymbol{y}}_{-}[k]$.

8.1.3 A Prior Residual Covariance

In the extended Kalman filter, the calculation of the *a prior* estimate of the residual covariance requires discrete linear equations, describing the small perturbation changes in a region.

The linear equations describing the perturbation trajectory was derived in Chapter 5 and the procedure to obtain the discrete versions of the small perturbation state matrix ($\underline{\mathbf{\Phi}}[k]$) and the process noise matrix ($\underline{\mathbf{\Sigma}}[k]$) was described in Section 5.8.

It should be noted, when calculating the continuous perturbation trajectory matrix $\underline{\boldsymbol{F}}$ using (5.41), that it is a function of the current full state vector elements. When calculating $\underline{\boldsymbol{F}}$, the *a prior* full state vector $\boldsymbol{x}_-[k]$, should be used as these required state vector elements.

The *a prior* estimate of the residual covariance can then be calculated using the normal linear Kalman equation as derived in (B.6):

$$\underline{\boldsymbol{P}}_-[k] = \underline{\mathbf{\Phi}}[k]\underline{\boldsymbol{P}}_+[k-1]\underline{\mathbf{\Phi}}[k]^T + \underline{\mathbf{\Sigma}}[k] \tag{8.6}$$

In which $\underline{\mathbf{\Sigma}}$ is the covariance of the noise terms of the model as shown in (5.41) on page 41.

By observing (8.6) it is obvious that this is where the initial residual covariance matrix ($\underline{\boldsymbol{P}}_+[0]$), described in Section 7.3, is required.

8.2 Update Step

After a new measurement have been received, the update step is conducted.

The update step is the step in which the new measurements are considered to form a *posterior* estimate of the current states. Furthermore, a *posterior* estimate of residual covariance is also calculated during this step.

When utilizing the extended Kalman filter, a linear equation describing the effect of the small perturbation states on the measurements is needed.

As described in Section 5.7, two different sets of small perturbation measuring matrices with appertaining noise matrices has been designed. Each of them describing the measurement, dependent of the existence of a new GPS measurement.

The two sets of matrices are the set $\underline{\boldsymbol{H}}$ and $\underline{\mathbf{\Lambda}}$ derived in (5.47) and the set $\underline{\boldsymbol{H}_{\boldsymbol{noGPS}}}$ and $\underline{\mathbf{\Lambda}_{\boldsymbol{noGPS}}}$ derived in (5.48).

As shown in Fig. 6.2, the first task in the update step is to check if the new measurement set contains a new GPS measurement. From the outcome of this check it is determined which of the measurement matrices to utilize.

The applicable set of measurement matrices are put into two temporary placeholders denoted as $\underline{\boldsymbol{H}}_{app}$ and $\underline{\mathbf{\Lambda}}_{app}$. These placeholders are introduced in order to simplify the description of the later equations.

In case no new GPS measurement is available, the GPS elements of the full measurement vector $\widetilde{\boldsymbol{y}}$ is removed, hence reducing it to $\widetilde{\boldsymbol{y}}_{noGPS}$. The applicable measurement vector is put into a temporary placeholders denoted as $\widetilde{\boldsymbol{y}}_{app}$ for simplification of later equations.

(5.47) contains elements of the full state vector, so as in the calculation of $\underline{\boldsymbol{F}}$, these elements should too be obtained from the *a prior* full state vector $\boldsymbol{x}_-[k]$.

Now, the Kalman gain matrix ($\underline{\bar{\boldsymbol{K}}}$) can be calculated using the normal linear Kalman filter equation, derived in (B.16):

$$\underline{\bar{\boldsymbol{K}}}[k] = \underline{\boldsymbol{P}}_-[k]\underline{\boldsymbol{H}}_{app}[k]^T \left[\underline{\boldsymbol{H}}_{app}\underline{\boldsymbol{P}}_-[k]\underline{\boldsymbol{H}}_{app}[k]^T + \underline{\mathbf{\Lambda}}_{app}\right]^{-1} \tag{8.7}$$

8.2.1 Posterior Residual Covariance

The obtained linear perturbation measurement model and Kalman gain can also be applied to calculate a *posterior* estimate of the residual covariance.

This is done using the normal linear Kalman filter equation, derived in (B.17):

$$\underline{\boldsymbol{P}}_{+}[k] = \left(\underline{\boldsymbol{I}} - \underline{\bar{\boldsymbol{K}}}[k]\underline{\boldsymbol{H}}_{app}[k]\right)\underline{\boldsymbol{P}}_{-}[k] \tag{8.8}$$

8.2.2 Posterior State Estimate

The obtained Kalman gain is then used to calculate a small state correction vector ($\delta\check{\boldsymbol{x}}[k]$).

With the new applicable measurement denoted as $\widetilde{\boldsymbol{y}}_{app}[k]$, the correction vector is found by multiplying the difference between this new measurement and the previously predicted measurement vector with the Kalman gain:

$$\delta\check{\boldsymbol{x}}[k] = \underline{\bar{\boldsymbol{K}}}[k]\left(\widetilde{\boldsymbol{y}}_{app}[k] - \tilde{\boldsymbol{y}}_{-}[k]\right) \tag{8.9}$$

The implementation of this step was the reason for the removal of the GPS terms from the full measurement vector in case of the absence of a new GPS measurement.

This obtained $\delta\check{\boldsymbol{x}}[k]$ is used to update the predicted full state estimates. For most states, the update is done by simply adding the correction value to the predicted state value:

$$\boldsymbol{x}_{+}[k] = \boldsymbol{x}_{-}[k] + \delta\check{\boldsymbol{x}}[k] \tag{8.10}$$

But $\delta\check{\boldsymbol{x}}[k]$ has the same form as (5.9), meaning that the attitude correction is given as the small angle correction $\check{\boldsymbol{\gamma}}$.

As the attitude full state is the DCM (${}^{n}\underline{\boldsymbol{C}}_{s}$), it cannot be updated by simply adding $\check{\boldsymbol{\gamma}}$.

Instead, by observing (5.6) on page 33, it can be seen that the full state state DCM can be updated by putting $\check{\boldsymbol{\gamma}}$ in its skew symmetric representation ($\check{\boldsymbol{\Gamma}}$) and using the equation:

$${}^{n}\underline{\boldsymbol{C}}_{s+}[k] = \left(\underline{\boldsymbol{I}} - \check{\boldsymbol{\Gamma}}\right){}^{n}\underline{\boldsymbol{C}}_{s-}[k] \tag{8.11}$$

When applying steps like the one of (8.11), numerical uncertainties and approximations can slowly cause the orthogonality of the DCM to be voided. To avoid this, a reorthogonalityzation should be conducted after the utilization of (8.11). The procedure of this reorthogonalityzation is described in Subsection A.4.3.

Chapter 9

Estimation Filter Pseudo Code

In this chapter, the pseudo code for the implementation of the designed estimation filter is given. This is shown in Table 9.1.

Init.:		
0.1	Initialize attitude estimate:	${}^{n}\underline{\boldsymbol{C}}_{s+}[0] = \left[\lvert {}^{n}\check{\boldsymbol{m}} \rvert \quad \lvert {}^{n}\check{\boldsymbol{g}} \rvert \quad \lvert {}^{n}\check{\boldsymbol{m}} \times {}^{n}\check{\boldsymbol{g}} \rvert \right] \left[\lvert {}^{s}\widetilde{\boldsymbol{m}} \rvert \quad \lvert {}^{s}\widetilde{\boldsymbol{a}} \rvert \quad \lvert {}^{s}\widetilde{\boldsymbol{m}} \times {}^{s}\widetilde{\boldsymbol{a}} \rvert \right]^{-1}$
0.2	Initialize position and velocity estimate:	$\boldsymbol{p}_{+}[0] = \widetilde{\boldsymbol{p}}_{GPS}$ and ${}^{n}\boldsymbol{v}_{+}[0] = {}^{n}\widetilde{\boldsymbol{v}}_{GPS}$
0.3	Initialize MS2 sensor bias estimates:	${}^{s}\boldsymbol{b}_{sensor+}[0] = \begin{bmatrix} 0 & 0 & 0 \end{bmatrix}^{T}$
0.4	Initialize constant assumption term states:	${}^{s}\boldsymbol{a}_{+}[0] = \widetilde{\boldsymbol{a}}$ and ${}^{s}\boldsymbol{\omega}_{si+}[0] = {}^{s}\widetilde{\boldsymbol{\omega}}_{si}$
0.5	Initialize residual covariance:	$\underline{\boldsymbol{P}}_{+}[0]$ using (7.3)
Predict:		
1.1	Predict the position:	$\boldsymbol{p}_{-}[k] = \boldsymbol{p}_{+}[k-1] + TS \cdot \dot{\boldsymbol{p}}_{+}[k-1]$ using (3.31)
1.2	Predict the velocity:	${}^{n}\boldsymbol{v}_{-}[k] = {}^{n}\boldsymbol{v}_{+}[k-1] + TS \cdot {}^{n}\dot{\boldsymbol{v}}_{+}[k-1]$ using (3.29)
1.3	Predict the attitude:	${}^{n}\underline{\boldsymbol{C}}_{s-}[k] = {}^{n}\underline{\boldsymbol{C}}_{s+}[k-1]\underline{\boldsymbol{\Pi}}[k]$ using (3.33) and (A.23)
1.4	Predict the biases and	${}^{s}\boldsymbol{b}_{sensor-}[k] = {}^{s}\boldsymbol{b}_{sensor+}[k-1]$
	constant assumption terms:	${}^{s}\boldsymbol{a}_{-}[k] = {}^{s}\boldsymbol{a}_{+}[k-1]$ and ${}^{s}\boldsymbol{\omega}_{si-}[k] = {}^{s}\boldsymbol{\omega}_{si+}[k-1]$
1.5	Predict the full measurement:	$\widetilde{\boldsymbol{y}}$ using (4.15)
1.6	Small perturbation model:	$\delta\dot{\boldsymbol{x}} = \underline{\boldsymbol{F}}\delta\boldsymbol{x} + \underline{\boldsymbol{Q}}\boldsymbol{w}$ using (5.41)
1.7	Discretized model:	$\delta\boldsymbol{x}[k+1] = \underline{\boldsymbol{\Phi}}[k]\delta\boldsymbol{x}[k] + \underline{\boldsymbol{\Sigma}}[k]\boldsymbol{w}$ using (5.52)
1.8	*A prior* covariance estimates	$\underline{\boldsymbol{P}}_{-}[k] = \underline{\boldsymbol{\Phi}}[k]\underline{\boldsymbol{P}}_{+}[k-1]\underline{\boldsymbol{\Phi}}[k]^{T} + \underline{\boldsymbol{\Sigma}}[k]$
Update:		
2.1	New GPS measurement check?:	If available, goto 2.2 else goto 2.3
2.2	Use full measurement model:	$\underline{\boldsymbol{H}}_{app}[k] = \underline{\boldsymbol{H}}[k]$ using (5.47)
		$\underline{\boldsymbol{\Lambda}}_{app}[k] = \underline{\boldsymbol{\Lambda}}[k]$
		$\tilde{\boldsymbol{y}}_{app-}[k] = \tilde{\boldsymbol{y}}_{-}[k]$, goto 2.4
2.3	Use reduced measurement model:	$\underline{\boldsymbol{H}}_{app}[k] = \underline{\boldsymbol{H}}_{no\,GPS}[k]$ using (5.48)
		$\underline{\boldsymbol{\Lambda}}_{app}[k] = \underline{\boldsymbol{\Lambda}}_{no\,GPS}[k]$
		$\tilde{\boldsymbol{y}}_{app-}[k] = \tilde{\boldsymbol{y}}_{no\,GPS-}[k]$
2.4	Kalman gain:	$\bar{\underline{\boldsymbol{K}}}[k] = \underline{\boldsymbol{P}}_{-}[k]\underline{\boldsymbol{H}}_{app}[k]^{T}\left[\underline{\boldsymbol{H}}_{app}\underline{\boldsymbol{P}}_{-}[k]\underline{\boldsymbol{H}}_{app}[k]^{T} + \underline{\boldsymbol{\Lambda}}_{app}\right]^{-1}$
2.5	*Posterior* covariance estimates:	$\underline{\boldsymbol{P}}_{+}[k] = \left(\underline{\boldsymbol{I}} - \bar{\underline{\boldsymbol{K}}}[k]\underline{\boldsymbol{H}}_{app}[k]\right)\underline{\boldsymbol{P}}_{-}[k]$
2.6	Correction vector:	$\delta\check{\boldsymbol{x}}[k] = \bar{\underline{\boldsymbol{K}}}[k]\left(\widetilde{\boldsymbol{y}}[k] - \tilde{\boldsymbol{y}}_{-}[k]\right)$
2.7	Apply correction vector to ${}^{n}\underline{\boldsymbol{C}}_{s-}[k]$:	${}^{n}\underline{\boldsymbol{C}}_{s+}[k] = \left(\underline{\boldsymbol{I}} - \check{\boldsymbol{\Gamma}}\right){}^{n}\underline{\boldsymbol{C}}_{s-}[k]$
2.8	Apply correction vector to other states:	$\boldsymbol{x}_{+}[k] = \boldsymbol{x}_{-}[k] + \delta\check{\boldsymbol{x}}[k]$
2.9	Perform reorthogonalityzation of ${}^{n}\underline{\boldsymbol{C}}_{s+}[k]$:	Using procedure of Subsection A.4.3
2.10	Output state estimates of interest:	$\boldsymbol{p}_{+}[k]$, ${}^{n}\boldsymbol{v}_{+}[k]$ and ${}^{n}\underline{\boldsymbol{C}}_{s+}[k]$
2.11	Repeat:	Go to 1.1 and iterate filter every time step TS

Table 9.1: Pseudo code for the designed estimation filter.

Part III

Closure

Two accept tests of the designed navigation system have been conducted. The first test, for which the results are described in Chapter 10, has been conducted using simulated data.

The second test was conducted using sensor data from an actual boat trip. The result from this is described in Chapter 11.

Lastly, a summative conclusion and suggestions of future work are given in Chapter 12.

Chapter 10

Simulation Acceptance Test

As mentioned, the first accept test is based on simulated sensor data. These 40 *min* of data has been generated using the designed simulation environment described in Chapter 6.

In the data, three GPS outages have been inserted. These all have a duration of 1 *min* and are located 15 *min* (900 *s*), 26 *min* (1560 *s*) and 37.5 *min* (2250 *s*) after the start.

All the graphs shown throughout this chapter are also available as zoomable MATLAB fig-files on the enclosed DVD, in the folder: `\images\simu_accept`.

One of the the big advantages of using simulated data is that the true state values are available at all times. Among other, the true value of the sensor biases are available, enabling the possibility of evaluating the ability of the filter to estimate these biases correctly.

An other advantage of using simulated data is the absence of effects from non-include phenomenons even though this might not correspond to the case of the actual real world system. The evaluation on a simplified simulation can give an indication of whether the basic concept of the solution works and whether it can be used as basic for future work.

An overview of the simulated boat trip is shown in Fig. 10.1.

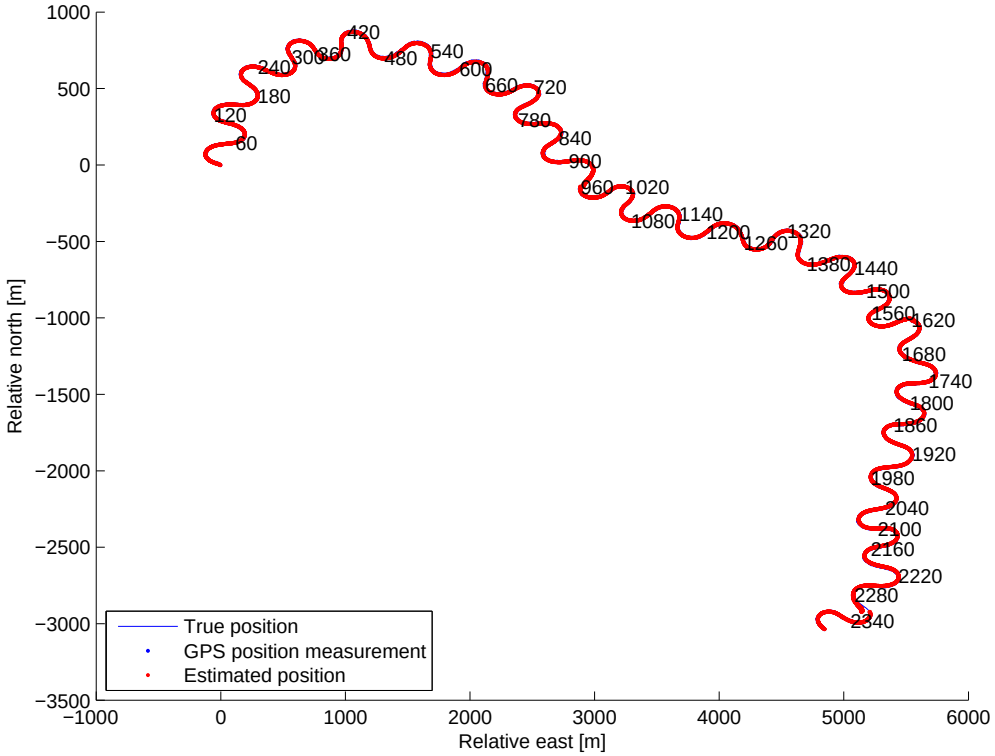

Figure 10.1: Overview of the simulated route

Unfortunately, the big scale of Fig. 10.1 makes it difficult to see details. Due to this, zooms of the area around the three GPS outage periods are shown in Fig. 10.2, Fig. 10.3 and Fig. 10.4.

In the three zooms, position estimates prior to the GPS outages can be seen together with the simulated GPS measurements. It can be seen here that the filter is able to acceptably smoothen the GPS measurements, thus satisfying the primary wish of CDL.
Furthermore, during the GPS outages, the filter is able to successfully follow the curve of the turns.

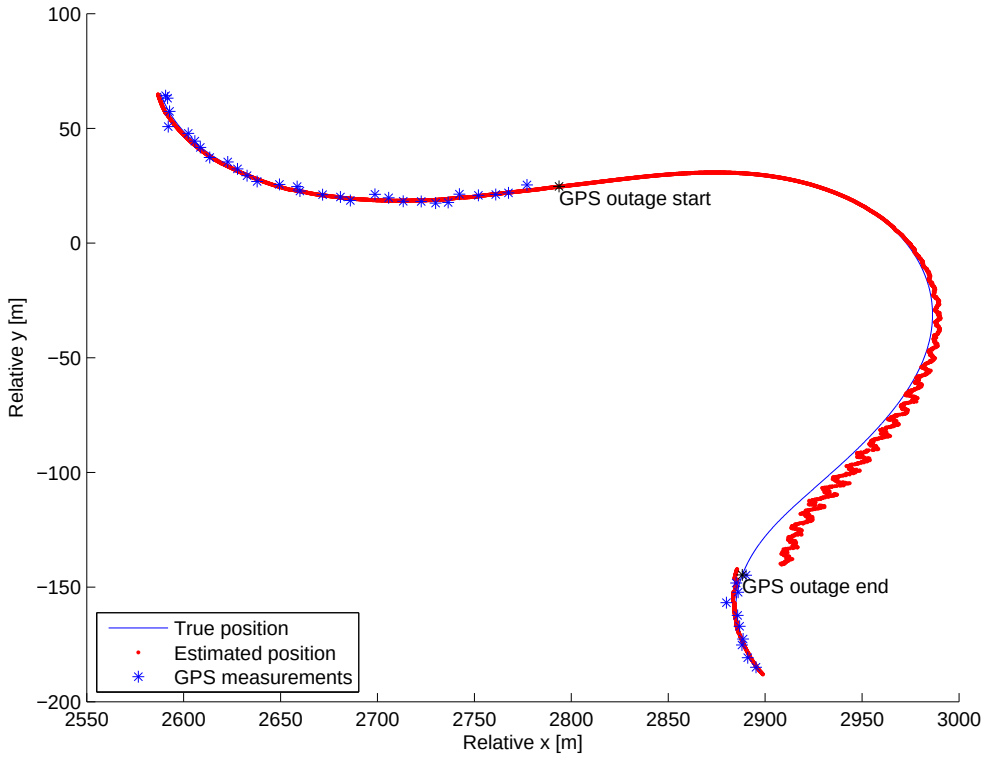

Figure 10.2: Zoom of the first GPS outage

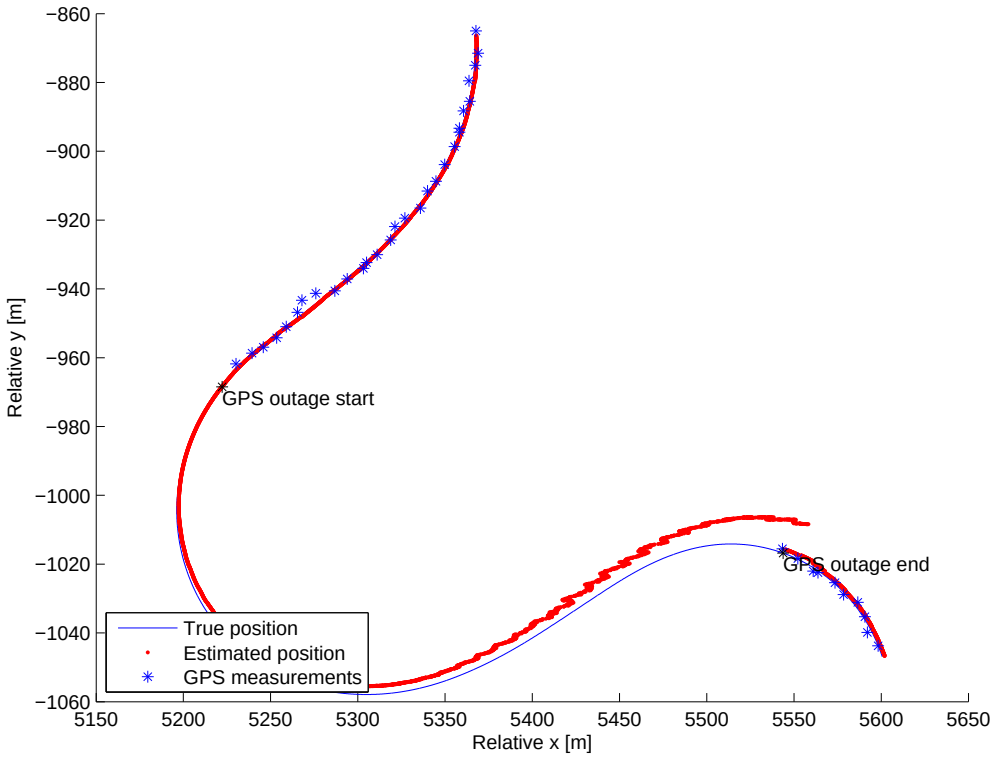

Figure 10.3: Zoom of the second GPS outage

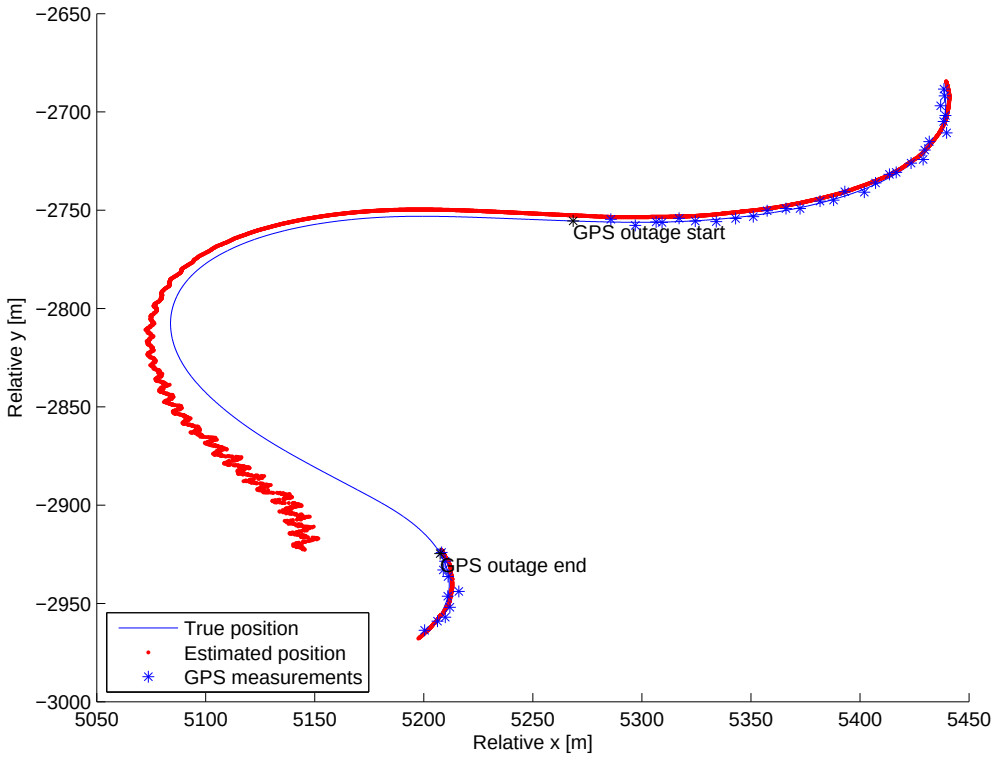

Figure 10.4: Zoom of the third GPS outage

10.1 Estimation Errors

In Fig. 10.5, the attitude estimation errors are illustrated.

The mean value of the absolute attitude errors of the roll and pitch axises, after the initial settle time, are approximately 0.08° while the yaw axis error is approximately 0.26°.

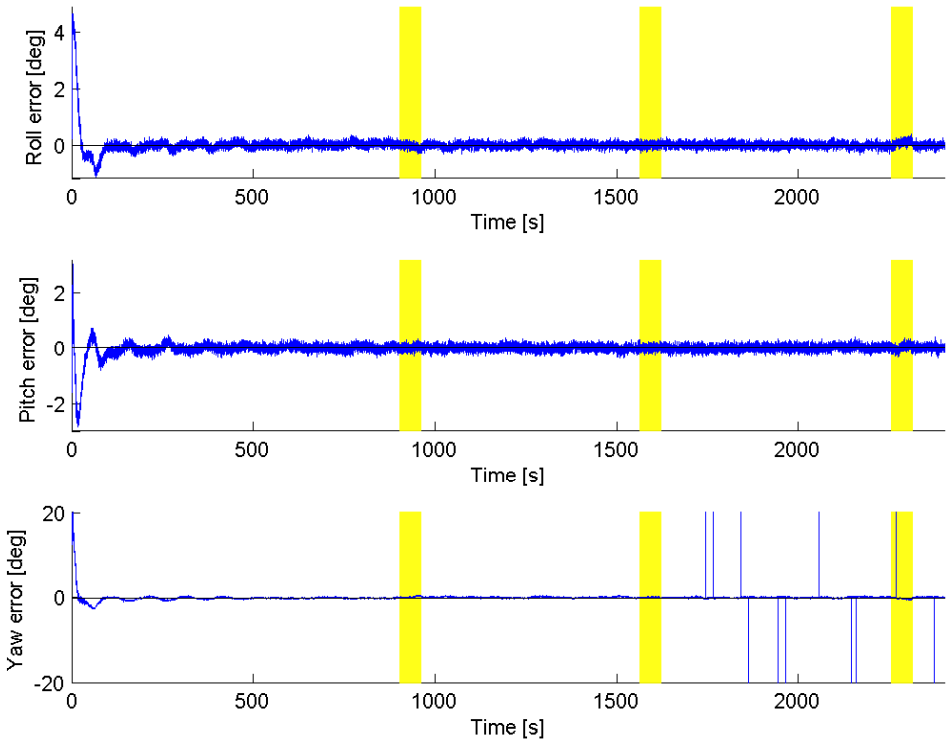

Figure 10.5: The attitude estimation errors. The highlighted areas are the GPS outage periods.

The velocity estimation errors are shown in Fig. 10.6 in which it can be seen that the estimation errors in the horizontal axis are at much larger magnitude than the vertical.

This is due to the fact that the accelerometers measures both acceleration due to movement and due to gravity. Because by studying (3.29) on page 18, it is seen that the gravity is attempted compensated by rotating the measured acceleration into the NRF and subtracting the modeled gravity.

But errors in the attitude estimation leads to errors in this compensation. This erroneous gravity compensation is a large contribution to the velocity errors.

Another error source is unestimated accelerometer biases.

It has been seen by different simulation runs, that the exact start locations of the GPS outages have a big effect on the magnitude of the velocity error. This is probably due to the nature of the sinus yaw input momentum in the test run.

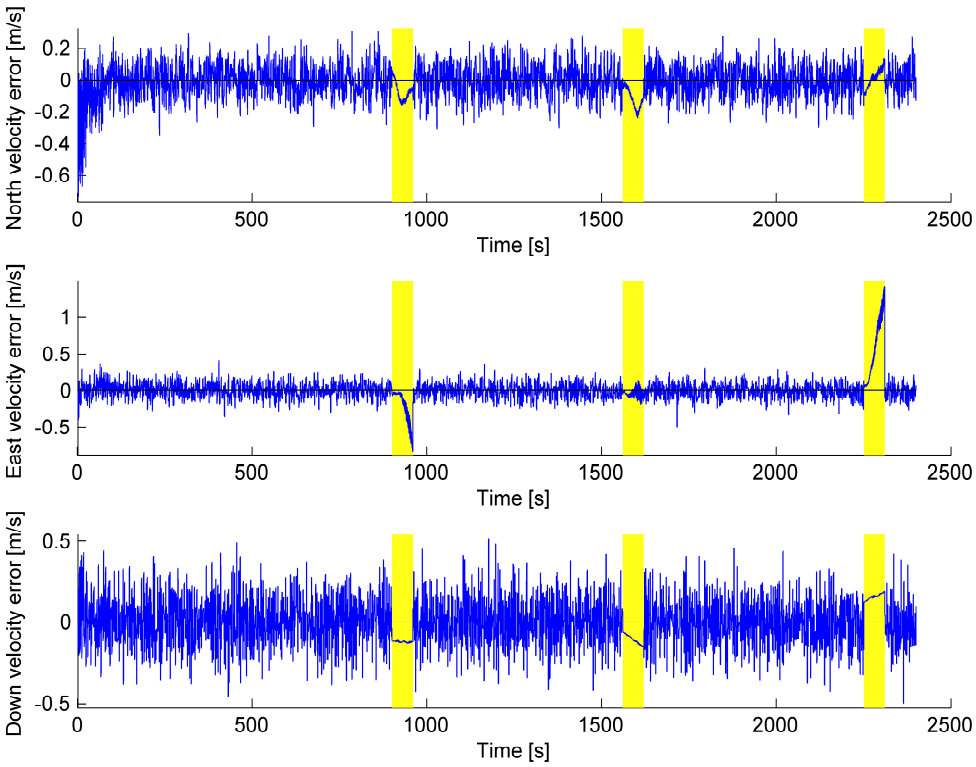

Figure 10.6: The velocity estimation errors of the NRF axises. The highlighted areas are the GPS outage periods.

To further evaluate the ability to estimate the position during GPS outages, the error of the position is plotted and shown in Fig. 10.7. During GPS outages, the position is estimated only by propagating the velocity estimates through the model. Because of this, the position estimation errors have the same tendencies as the velocity errors.

The magnitude of the position errors during the GPS outages are considered to be acceptable.

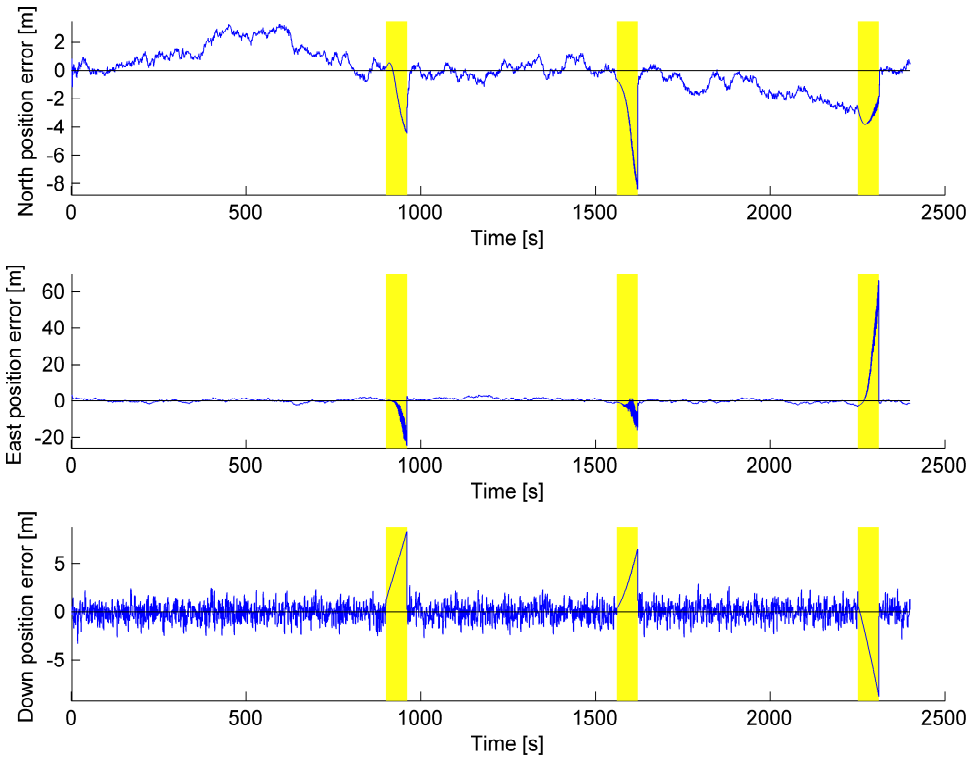

Figure 10.7: The position error of the different NRF axises. The highlighted areas are the GPS outage periods.

10.2 Bias Estimation

As described in Chapter 6, constant biases are added to the output of the gyroscope, magnetometer and accelerometer in the simulation environment.

The estimated and true values of the gyroscopes biases are shown in Fig. 10.8. It is here seen that the gyroscope bias estimates very quickly converge to the correct bias values. The biases of the roll and pitch axises converge in less than 30 s, while the yaw axis has converged in less than 2 min.

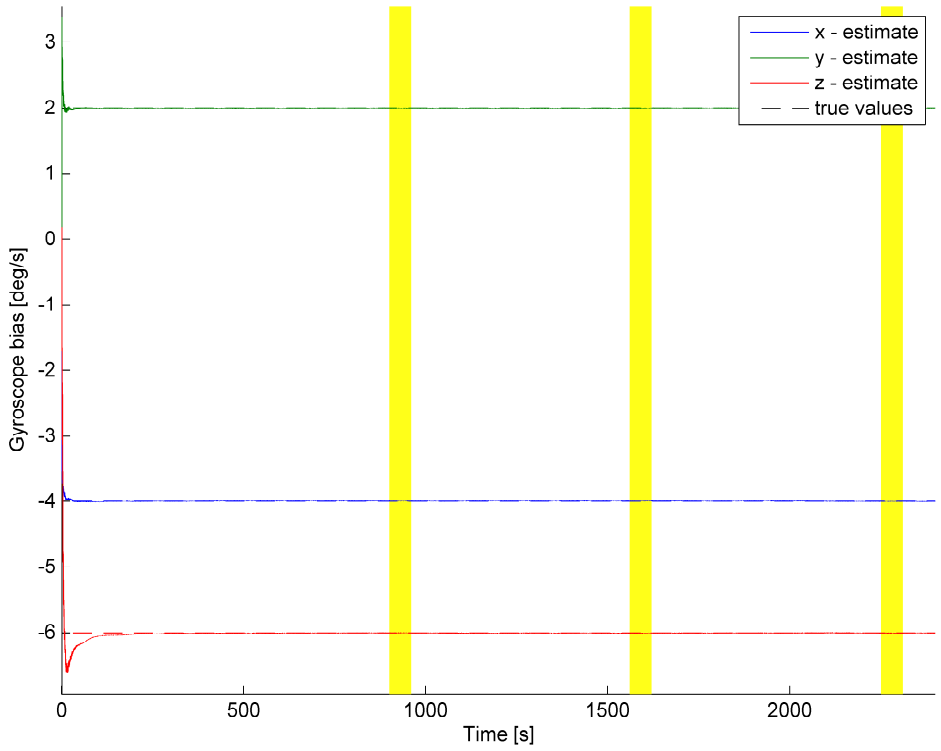

Figure 10.8: The estimated gyroscope biases. The dotted lines are the true constant bias values. The highlighted areas are the GPS outage periods.

The estimated and true values of the magnetometers biases are shown in Fig. 10.9 in which it is seen that these biases also converge. It takes about 7 *min* (420 *s*) for all the biases to converge.

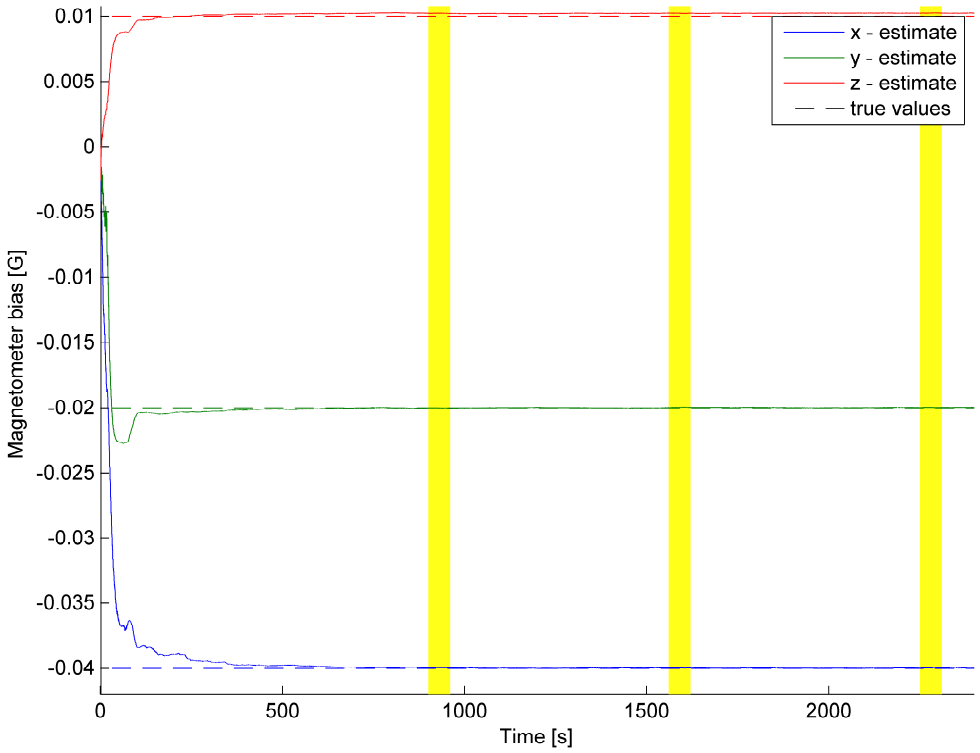

Figure 10.9: The estimated magnetometer biases. The dotted lines are the true constant bias values. The highlighted areas are the GPS outage periods.

The estimated and true values of the accelerometers bias are shown in Fig. 10.9 in which it is seen that these biases are also converging. But it is seen that this happens more slowly than the biases of the other sensors. It is also noticed that the accelerometer bias estimates seem to be more inflicted by noise than the bias estimates of the other MS2 sensors.

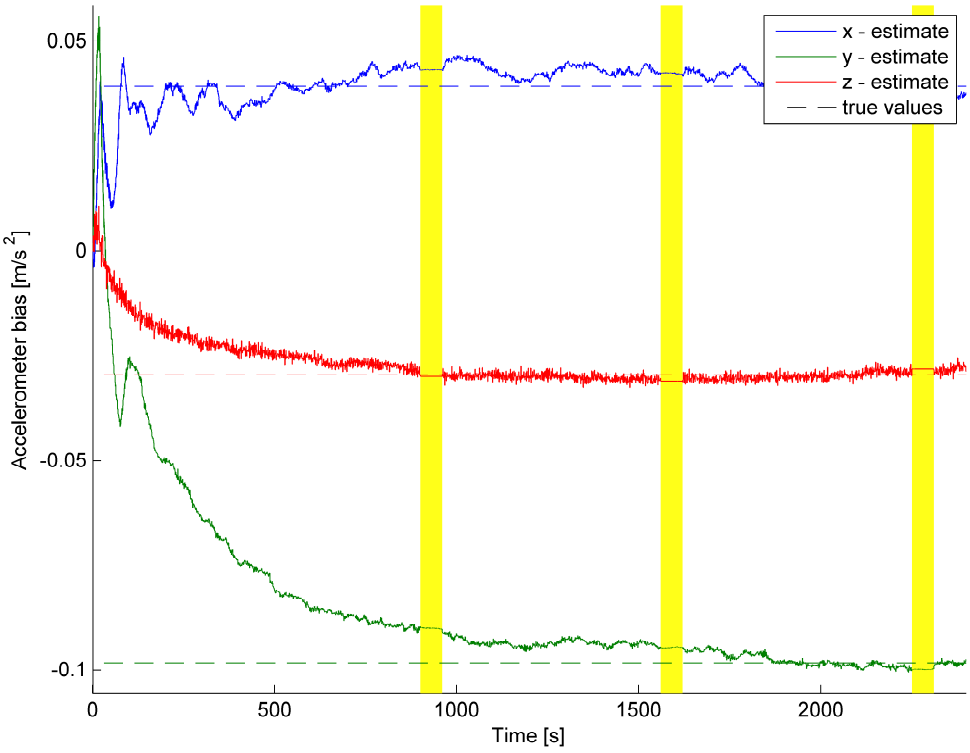

Figure 10.10: The estimated accelerometer biases. The dotted lines are the true constant bias values. The highlighted areas are the GPS outage periods.

10.3 Test Conclusion

In the test on the simulated data the performance of the designed estimation filter was assessed as being acceptable.

It was seen that the filter was able to acceptably smoothen the GPS measurements.
The filter was also able to estimate all the additive sensor biases and compensate for these, though the accelerometer bias estimates were slow to converge and seemed more noisy than the other bias estimates.

The estimation errors during the GPS outages were also acceptable. It was assessed that the errors in the estimated velocity and position during GPS outage is primarily due to erroneous gravity compensation.

From this, it is concluded that the basic concept of the designed solution works and that it can be used as basic for future work.

Chapter 11

Real World Data Acceptance Test

CDL have provided data from a boat trip in which the MS2 and and a GPS was logged. A 40 *min* cutout of this trip is here used for the evaluation of the designed navigation solution.

A high-grade T24 ADHS, which provides attitude estimates was also installed on the boat and logged during the trip. These attitude estimates will be used as reference when calculating the attitude estimation errors.

The true position and velocity are not available from any extern reference system. It has been chosen to interpolate the position and velocity measurements of the GPS using a spline interpolation and use this as reference when calculating the estimation errors of these states.

Again, three GPS outages have been inserted with a duration of 1 *min*, located at the same points in time as in the test on the simulation data.

All the graphs shown throughout this chapter are also available as MATLAB fig-files on the enclosed DVD, in the folder: `\images\ms2_accept`

An overview of the boat trip cutout is shown in Fig. 11.1.

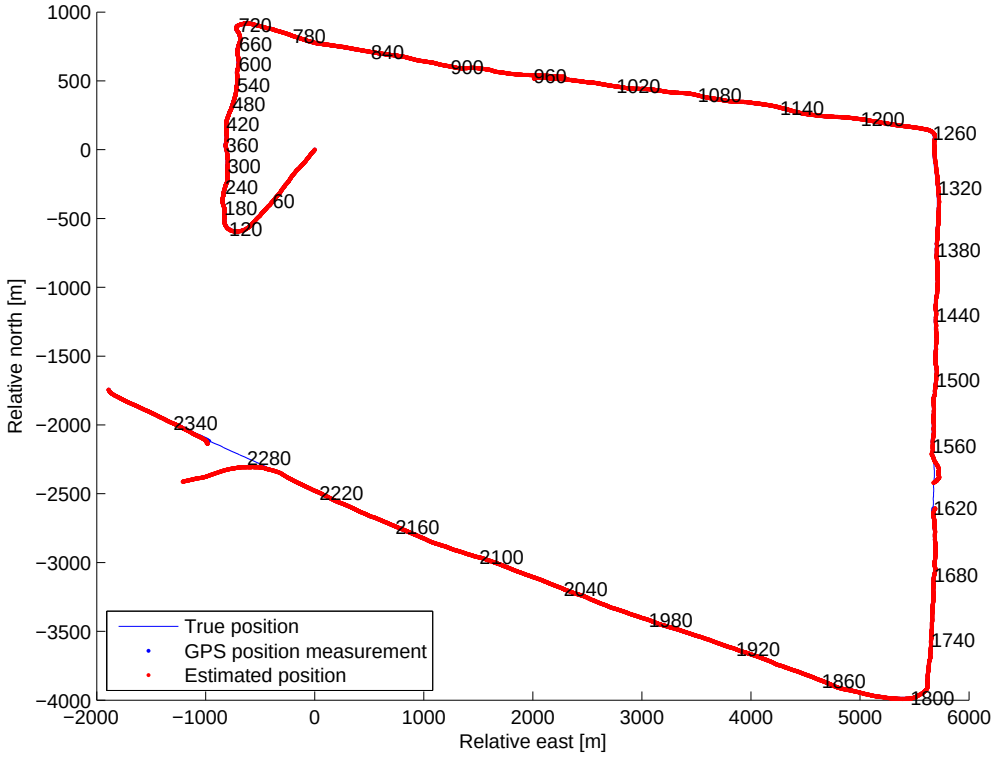

Figure 11.1: Overview of the real world boat trip cutout route

Again, zooms of the area around the three GPS outage periods have been included and are shown in Fig. 11.2, Fig. 11.3 and Fig. 11.4.

In the three zooms, position estimates prior to the GPS outages can be seen together with the simulated GPS measurements. It can be seen that before the first and the third GPS outage, the filter is here able to acceptable smoothen the GPS measurements during GPS coverage. But before the second GPS outage in which the boat is subject to a more curvy path, the position estimates are not acceptable.

Furthermore, during the last two GPS outages, the position estimates does not follow the path direction of the true position.

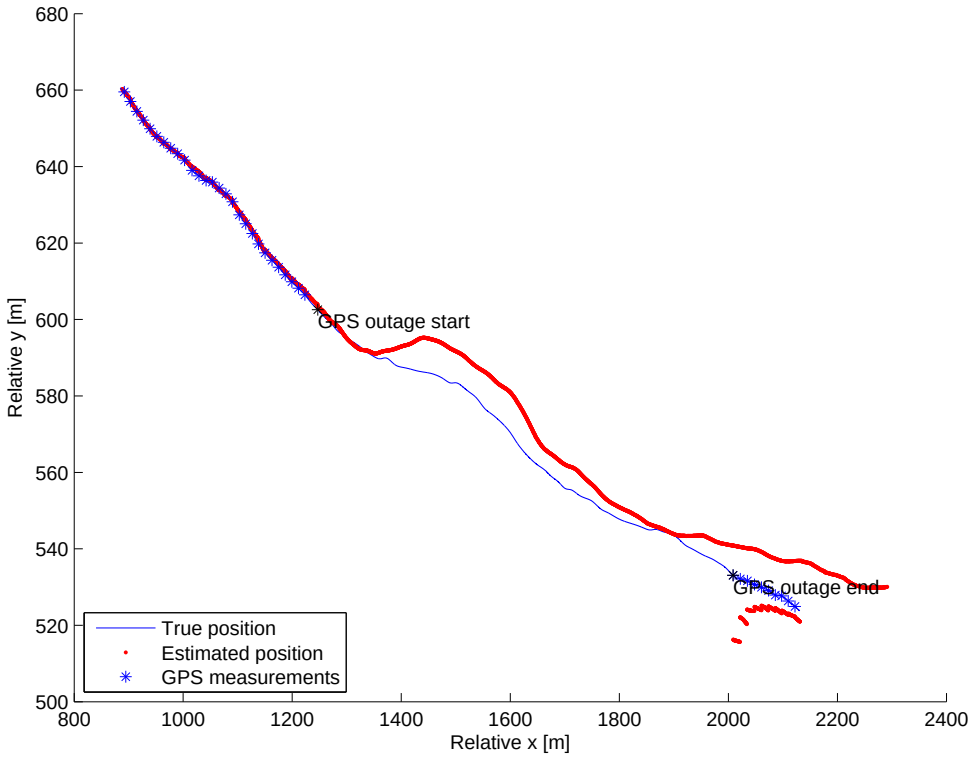

Figure 11.2: Zoom of the first GPS outage

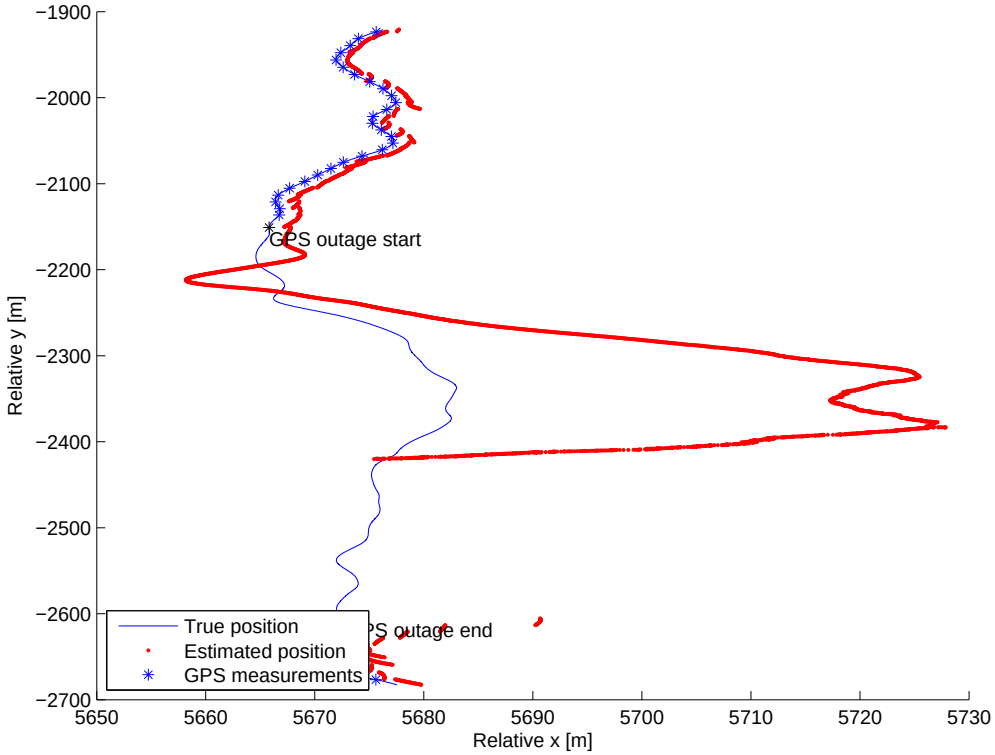

Figure 11.3: Zoom of the second GPS outage

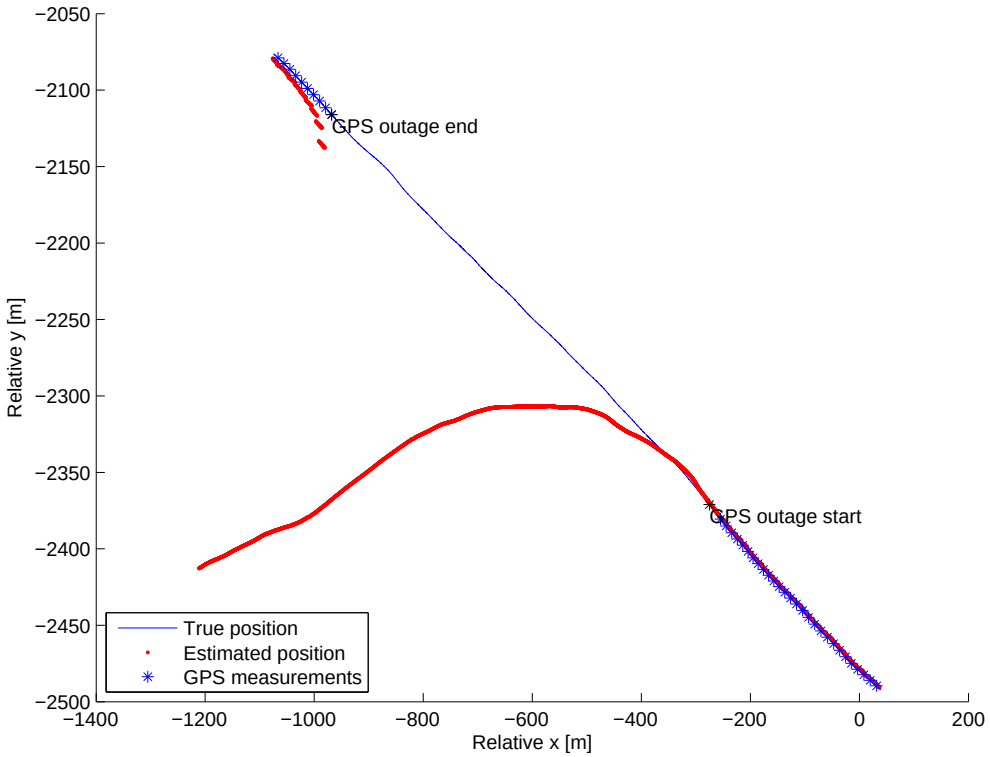

Figure 11.4: Zoom of the third GPS outage

11.1 Estimation Errors

In Fig. 11.5, the attitude estimation errors are shown. Is it noticed that the nature of the estimation errors varies substantial throughout the route. It seems as if the errors are either negative or positive biases. It could to be related to the direction of travel as the error changes occur at these points.

In Fig. 11.6, a plot of the measured horizontal speed has been included in which it can been seen that the speed of the boat is also changed at some of the points of changed travel direction. The changes in the attitude estimation errors might also be related to the changes of speed and the impact this has on the oscillations of the boat.

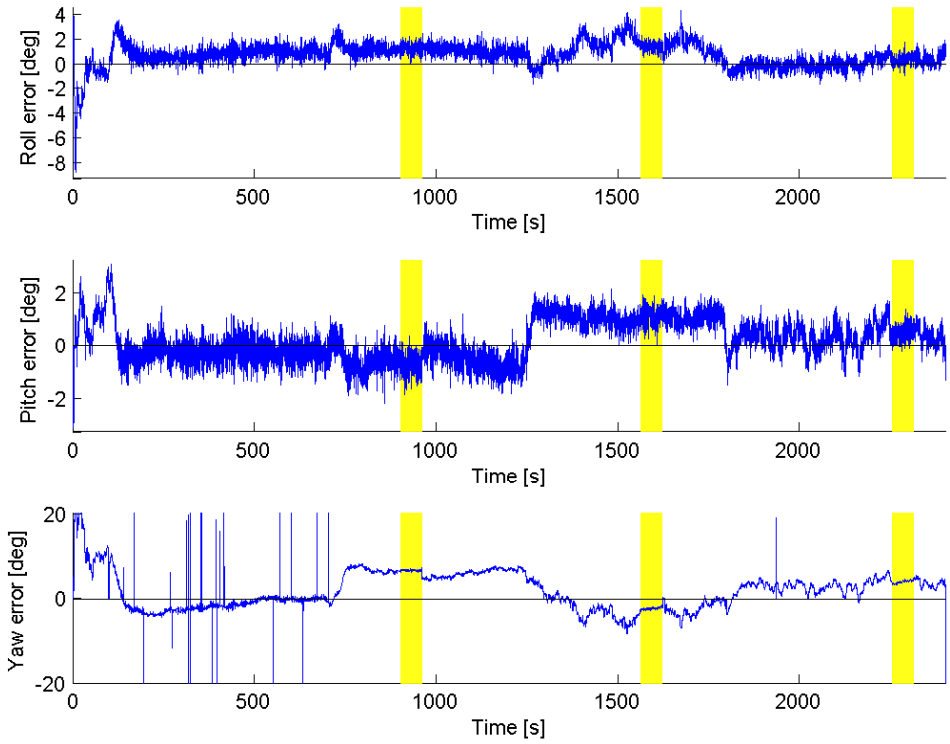

Figure 11.5: Attitude errors. The highlighted areas are the GPS outage periods.

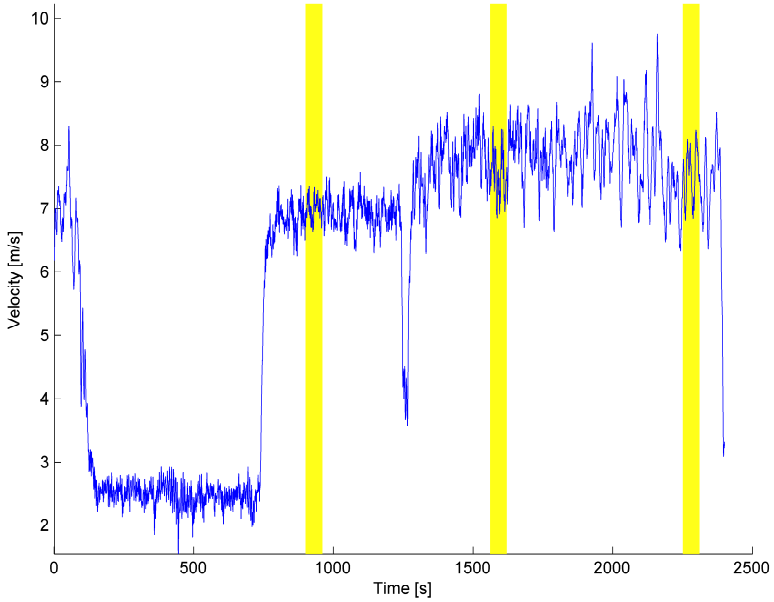

Figure 11.6: The norm of the horizontal velocity (horizontal speed) of the GPS measurements

The velocity estimation errors are shown in Fig. 11.7 in which it is seen that the estimation errors in the horizontal axis are at much larger magnitude than the vertical.

As in the simulation test, it is assessed that the velocity error is caused by erroneous gravity compensation and unestimated accelerometer biases.

The error of the position estimate is plotted and shown in Fig. 10.7 in which it is seen that the magnitude of the error reaches several 100 m within the duration of the GPS outages. The magnitude of the position errors during the GPS outages are not considered to be acceptable.

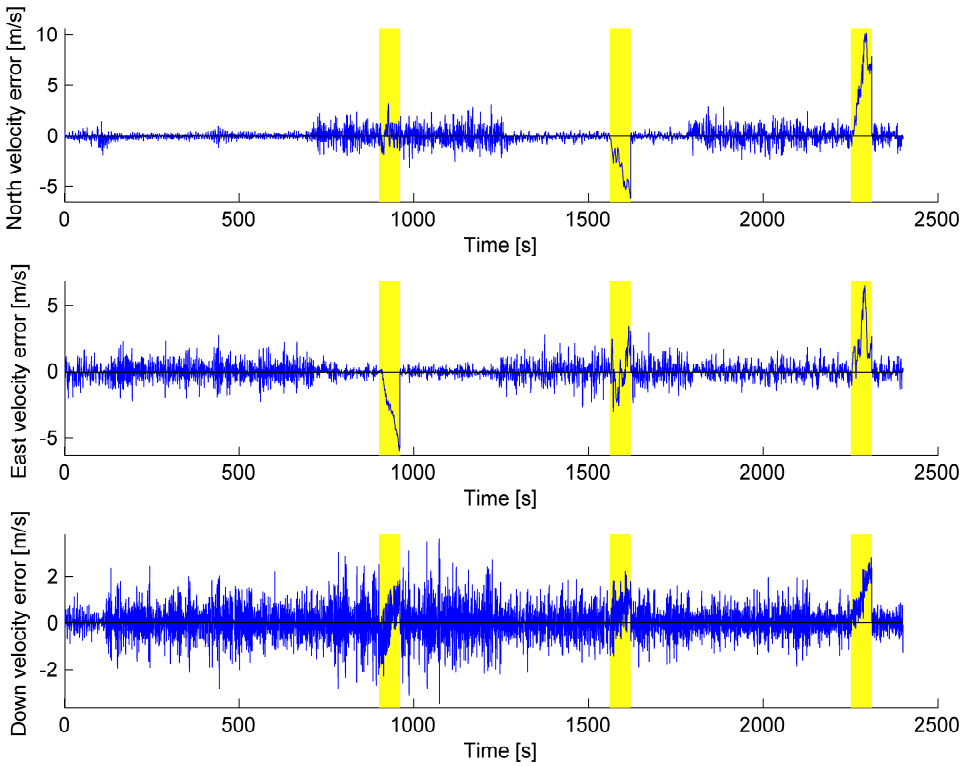

Figure 11.7: The velocity error of the two horizontal NRF axises. The highlighted areas are the GPS outage periods.

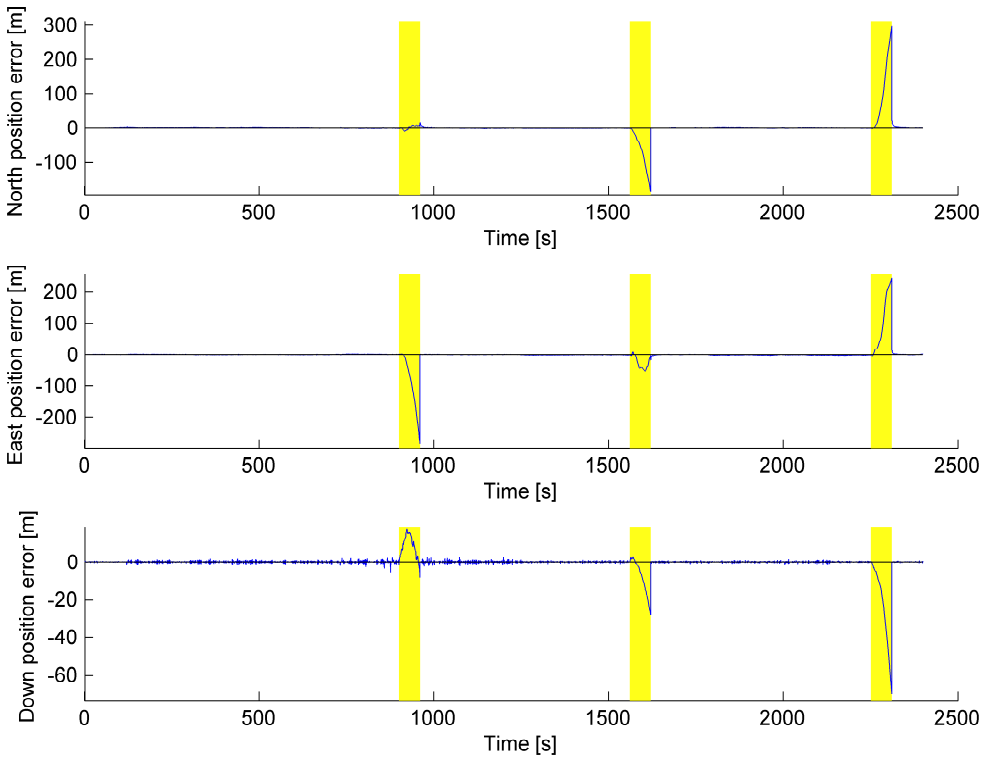

Figure 11.8: The position error of the different NRF axises. The highlighted areas are the GPS outage periods.

11.2 Bias Estimation

The estimated values of the gyroscopes biases are shown in Fig. 11.9. It is here seen that the gyroscope bias estimates very quickly converge and stays at these values throughout the rest of the test period. The biases in the all the axises converge in less than 1 *min*.

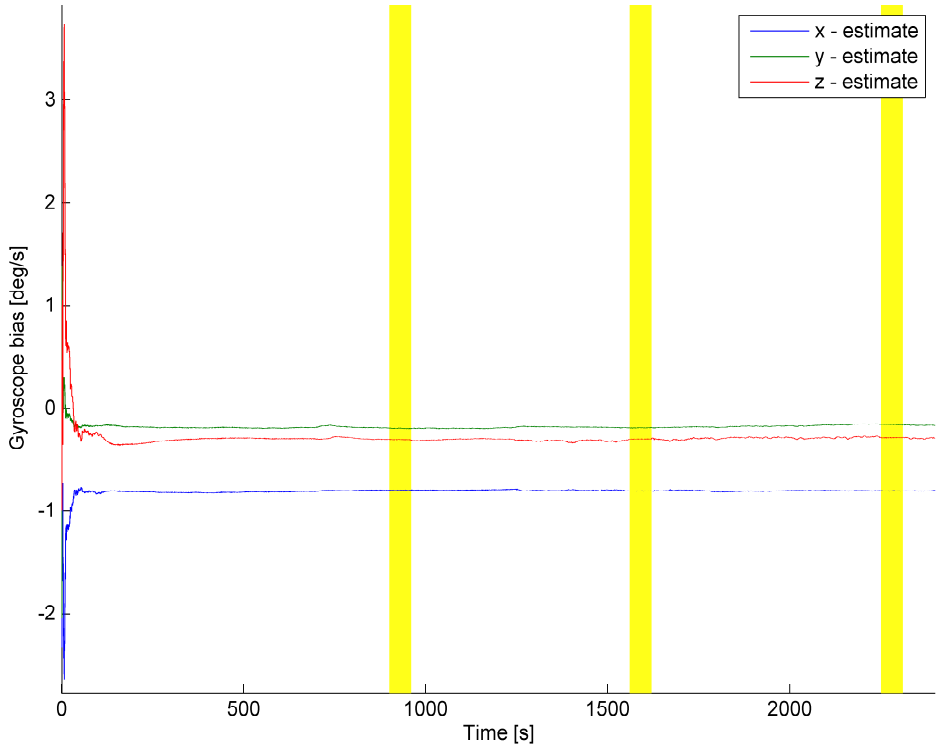

Figure 11.9: The estimated gyroscope bias.

The estimated values of the magnetometers biases are shown in Fig. 11.10. At first, it seems as if the bias converges, but each time the boat changes heading, the magnetometer bias seems to start converging towards new values. This could indicate a non-included effect having impact on the magnetometer. This is discussed further in the test conclusion.

The estimated values of the accelerometers bias are shown in Fig. 11.11. Some of the same tendencies, with correlation between the heading as seen in magnetometer bias estimates, is seen in the estimations of the accelerometer biases. When working with the estimation filter, it has been noticed that the estimation of the accelerometer biases are very sensitive. It is assessed that the change in the accelerometer bias estimates are a direct consequence of the changing magnetometer bias estimates.

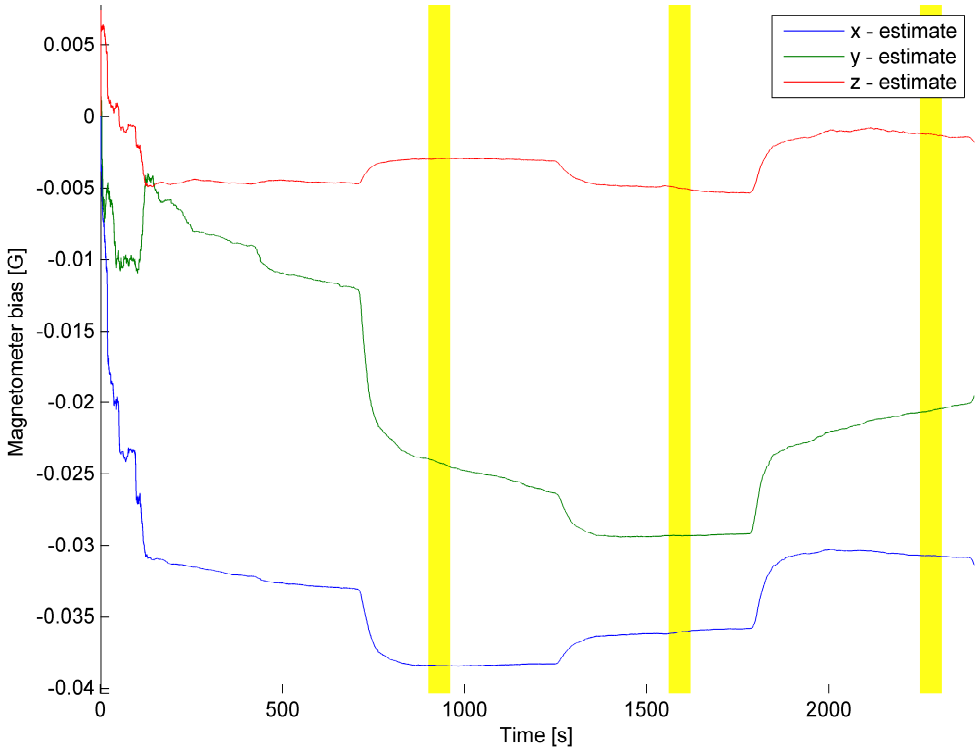

Figure 11.10: The estimated magnetometer bias.

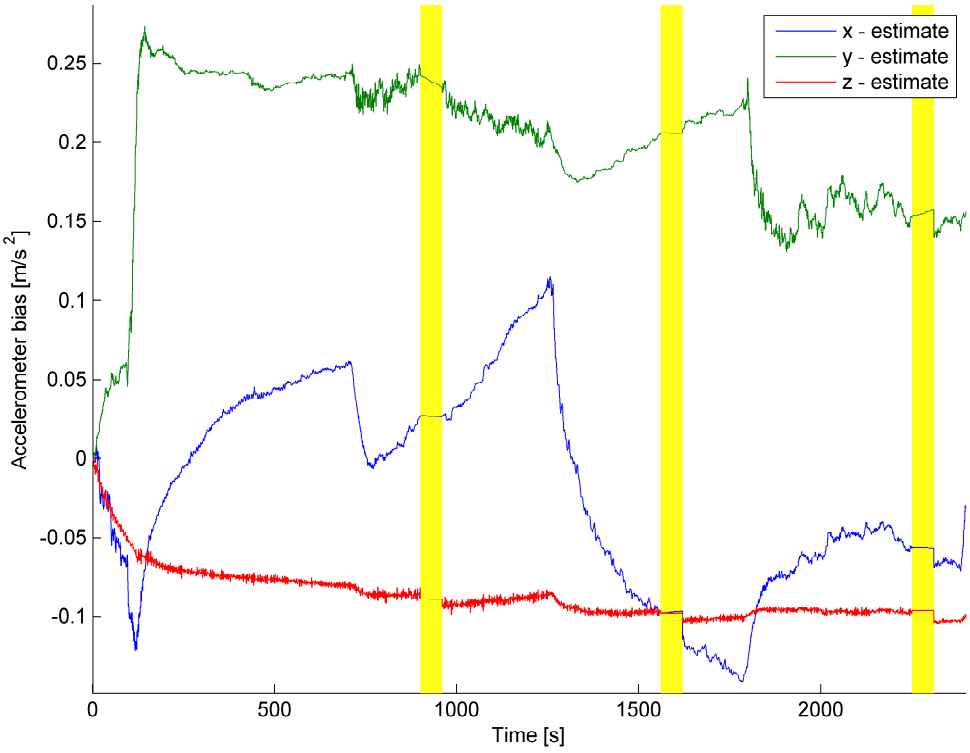

Figure 11.11: The estimated accelerometer bias.

11.3 Test Conclusion

The performance of the estimation filer does not seems to be acceptable.

The performance seems to be so bad that better position and velocity estimates probably could be achieved by simply designing a Kalman filter based on an assumption of the vessel having constant velocity and only aiding the filter with the GPS measurements.

The gyroscope bias estimate was able to converge to the presumptive correct bias values.

If the GPS antenna and the MS2 have not been located at the same position on the boat (known as a lever) this can cause an undesired effect. This effect is because that during changes in attitude, the GPS and MS2 will not be experiencing the same velocity. This is a considerable error source in the real world data when compared to the simulated data.

As mentioned, the spline interpolated GPS velocity measurements have been used as reference. An uncompensated lever could constitute an uncertainty in the correctness of this reference.

A change in the estimated magnetometer biases, which seemed to have correlation to the direction of travel, was observed. This could indicate a presence of an uncompensated effect in the magnetometers.

In Section 4.3, it was assessed that the magnetometers could be modeled as measuring the true magnetic field only corrupted by an additive bias and white noise. It seems as if this assumption was not justifiable.

The included additive bias in the model is also known as the "hard iron" effect. But an other commonly effect is the "soft iron" which can be modeled as a multiplicative scale/skew matrix ($\underline{\boldsymbol{\kappa}}$). If including this soft iron effect, the magnetometer model of (4.8) can be restated as:

$$ {}^{s}\widetilde{\boldsymbol{m}} = \underline{\boldsymbol{\kappa}}\, {}^{s}\underline{\boldsymbol{C}}_{n}\, {}^{n}\breve{\boldsymbol{m}} + {}^{s}\boldsymbol{b}_{mag} + \boldsymbol{v}_{mag} \tag{11.1} $$

It is assessed that the presence of an uncompensated $\underline{\boldsymbol{\kappa}}$ could lead to the behavior of the magnetometer bias estimate seen in the test on the real world data.

In an email from Rolf Christensen (Inertial Development Manager at CDL) [Christensen 14], late in the thesis progress, it has been confirmed that there indeed is a lever between the GPS antenna and the MS2. It is believed that the lever (l) from the MS2 to the GPS, given in the SRF, is roughly given as:

$$ {}^{s}\boldsymbol{l} \approx \begin{bmatrix} -4 & 0 & -0.7 \end{bmatrix}^{T} \; [m] \tag{11.2} $$

That is, the GPS antenna is placed roughly 4 m further back in the boat and approximately 0.7 m above the MS2.

Rolf Christensen also stated that the magnetometer had not been calibrated - neither for hard iron nor soft iron effects.

Unfortunately, due to insufficient remaining project time, there has not been conducted work regarding the compensation of the GPS lever and magnetometer soft iron effects.

Chapter 12

Conclusion

Early in the thesis, it was established that the focus should be to design a navigation solution based on a loosely coupling between the GPS and MS2. The designed estimation filter should be based on the structure of the extended Kalman filter and the filter should include the estimation of sensor biases of the MS2 sensors in order to compensate for these.

After introducing the relevant reference frames and small angle approximations, the differential equation of motion for travel on the earth was derived. The equation of motion translates measured accelerations into a velocity with respect to the surface of Earth. An expression for the relation between the measured angular velocity and the change in attitude with respect to the local navigation frame was also derived.

The sensor noise and bias parameters of the sensors of the MS2 was studied using the data sheets, Allan variance plot and processing of stationary measurement data. Both models for the sensors of the MS2 and the GPS was described, which involved the introduction of the IGRF magnetic field model.

As the extended Kalman filter structure had been chosen, a linear small perturbation model was derived for both the equations of motion and the sensor models.

For being able to test the basic concept of the designed filter, a simulation environment has been developed with the scope of generating oscillations comparable to the ones of a ship at sea.

A procedure for setting the initial state value estimate were described, including the determination of the initial attitude using the magnetometers and accelerometers. The different steps of a iteration of the designed extended Kalman filter were described and a pseudo code of the filter implementation was illustrated.

In the acceptance tests it was concluded that the performance, when evaluated on simulated data, was acceptable. Furthermore, the filter was able to correctly estimate all the sensor biases.

When the designed filter was applied to real world data, the resulting performance was not acceptable even though the filter was able to detect constant gyroscope biases.
The estimates of the magnetometer bias indicated that a non-included effect were present in the magnetometer measurements. This indicated that the previous assumption, regarding the magnetometers measuring the true magnetic field only corrupted by an additive bias and white noise was not justifiable.

Furthermore, it was suggested that the presence of an uncompensated lever between the GPS and MS2 could have a considerable impact on the results.

It was confirmed by Rolf Christensen at CDL, that the used magnetometer were uncalibrated and suffered from both hard iron (additive bias) and soft iron (scale/skew) effects. Furthermore, he confirmed the presence of a lever between the GPS and MS2 with a magnitude of several m.

12.1 Future Work

For continued work on the work of this thesis, the following subjects should be considered:

Include GPS lever in filter As mentioned, an uncompensated lever between the GPS antenna and MS2 were present in the real world data. This lever should be included in the filter design. If possible, the estimation of the lever should be included in the filter design.

Compensate for magnetometer soft iron effects A way to compensate for the presence of soft iron effects in the magnetometer should be studied.

Further development of the simulation environment The simulation environment should be further developed to include such phenomenons as GPS lever and soft iron effects. Favorably, a actual boat simulator could be used as basic instead of a point mass to realm more realistic movement and oscillations.

Optimize Implementation In the current MATLAB implementation, all variables are calculated in each step. A lot of the variables, such as the magnetic field and gravity changes very slowly, and hence there is no need to calculate these in each filter iteration.

Use ${}^s\boldsymbol{\omega}_{is}$ and ${}^s\boldsymbol{a}$ as inputs In the designed filter, ${}^s\boldsymbol{\omega}_{is}$ and ${}^s\boldsymbol{a}$ have been added as states. The reason for this choice was based on improved results seen in the work of [J. Wendel]. That article was based on data from a car on ground which does not experience the same fast sinus like oscillations as a boat at sea. It should be investigated if these extra states realms any performance improvement or, on the contrary, causes a decrease in performance. Instead, the gyroscope and accelerometer measurements could be fed to the filter as inputs. This is a method seen utilized in various articles.

Part IV

Appendix

Appendix A

General Rotational Equations

To be able to describe a rigid body with respect to an inertial frame a general description of rotational equations are described.

The rotation of frame (B) seen from the inertial frame (A) is denoted by:

$$ {}^{B}\underline{\mathbf{C}}_{A} \; : \quad A \rightarrow B \tag{A.1} $$

For short ${}^{B}\underline{\mathbf{C}}_{A} = \underline{\mathbf{C}}$. Frame A is spanned by a set of orthogonal unit vectors $[\, \boldsymbol{a_1}\ \boldsymbol{a_2}\ \boldsymbol{a_3} \,]^T$, likewise frame B is spanned by a set of orthogonal unit vectors $[\, \boldsymbol{b_1}\ \boldsymbol{b_2}\ \boldsymbol{b_3} \,]^T$. The matrix $\underline{\mathbf{C}}$ maps the set of vectors spanning frame A to the set of vectors spanning frame B by:

$$ \begin{bmatrix} \boldsymbol{b_1} \\ \boldsymbol{b_2} \\ \boldsymbol{b_3} \end{bmatrix} = \underline{\boldsymbol{C}} \begin{bmatrix} \boldsymbol{a_1} \\ \boldsymbol{a_2} \\ \boldsymbol{a_3} \end{bmatrix} \tag{A.2} $$

$$ \Updownarrow \tag{A.3} $$

$$ \underline{\boldsymbol{C}} = \begin{bmatrix} \boldsymbol{b_1} \\ \boldsymbol{b_2} \\ \boldsymbol{b_3} \end{bmatrix} \begin{bmatrix} \boldsymbol{a_1} & \boldsymbol{a_2} & \boldsymbol{a_3} \end{bmatrix} \tag{A.4} $$

$$ = \begin{bmatrix} \boldsymbol{b_1} \cdot \boldsymbol{a_1} & \boldsymbol{b_1} \cdot \boldsymbol{a_2} & \boldsymbol{b_1} \cdot \boldsymbol{a_3} \\ \boldsymbol{b_2} \cdot \boldsymbol{a_1} & \boldsymbol{b_2} \cdot \boldsymbol{a_2} & \boldsymbol{b_2} \cdot \boldsymbol{a_3} \\ \boldsymbol{b_3} \cdot \boldsymbol{a_1} & \boldsymbol{b_3} \cdot \boldsymbol{a_2} & \boldsymbol{b_3} \cdot \boldsymbol{a_3} \end{bmatrix} \tag{A.5} $$

From (A.4) it is seen that each entities in $\underline{\mathbf{C}}$ is described by an inner product of $\boldsymbol{b_i}$ and $\boldsymbol{a_j}$ vectors, which is the cosine of the angle between the two vectors. For this reason each entities is referred to as "direct cosines" and the matrix as the "direction cosine matrix". As $\underline{\mathbf{C}}$ maps between orthogonal unit vectors $\underline{\mathbf{C}}$ is an orthonormal matrix thus $\underline{\mathbf{C}}^T = \underline{\mathbf{C}}^{-1}$.

A.1 Euler Angles

The rotation performed by $\underline{\mathbf{C}}$ can be described by Euler angles, which rotates a coordinate system by three rotations over one body-axis at a time. Eulers rotation theorem states:

A rigid body can be moved from any orientation to an other by three successive rotations around the coordinate body axis or by three successive rotations around the coordinate initial axis, as long as the same two rotations are not successive.

In matrix form these rotations are referred to as (when using a 3-2-1 set of Euler rotation):

$$\underline{\mathbf{C}}_3(\theta_3) \; : \quad A \rightarrow A' \tag{A.6}$$
$$\underline{\mathbf{C}}_2(\theta_2) \; : \quad A' \rightarrow A'' \tag{A.7}$$
$$\underline{\mathbf{C}}_1(\theta_1) \; : \quad A'' \rightarrow B \tag{A.8}$$

and given by

$$\underline{\mathbf{C}}_1(\theta_1) = \begin{bmatrix} 1 & 0 & 0 \\ 0 & \cos\theta_1 & \sin\theta_1 \\ 0 & -\sin\theta_2 & \cos\theta_1 \end{bmatrix} \tag{A.9}$$

$$\underline{\mathbf{C}}_2(\theta_2) = \begin{bmatrix} \cos\theta_2 & 0 & -\sin\theta_2 \\ 0 & 1 & 0 \\ \sin\theta_2 & 0 & \cos\theta_2 \end{bmatrix} \tag{A.10}$$

$$\underline{\mathbf{C}}_3(\theta_3) = \begin{bmatrix} \cos\theta_3 & \sin\theta_3 & 0 \\ -\sin\theta_3 & \cos\theta_3 & 0 \\ 0 & 0 & 1 \end{bmatrix} \tag{A.11}$$

Successive rotation from any attitude to any other attitude in three-dimentional space can be described by 12 different sets of Euler rotation sequences. Using a 3-2-1 set of Euler angles creates the following direction cosine matrix:

$$\underline{\mathbf{C}}(\theta_1, \theta_2, \theta_3) = \underline{\mathbf{C}}_1(\theta_1)\underline{\mathbf{C}}_2(\theta_2)\underline{\mathbf{C}}_3(\theta_3) \tag{A.12}$$

$$\underline{\mathbf{C}}(\theta_1, \theta_2, \theta_3) = \begin{bmatrix} \cos\theta_2\cos\theta_3 & \cos\theta_2\sin\theta_3 & -\sin\theta_2 \\ \sin\theta_1\sin\theta_2\cos\theta_3 - \cos\theta_1\sin\theta_3 & \sin\theta_1\sin\theta_2\sin\theta_3 + \cos\theta_1\cos\theta_3 & \sin\theta_1\cos\theta_2 \\ \cos\theta_1\sin\theta_2\cos\theta_3 + \sin\theta_1\sin\theta_3 & \cos\theta_1\sin\theta_2\sin\theta_3 - \sin\theta_1\cos\theta_3 & \cos\theta_1\cos\theta_2 \end{bmatrix} \tag{A.13}$$

An example of three successive rotation is illustrated in Fig. A.1. Fig. A.1 shows a (3-1-3) rotation sequence (easier to draw in perspective than a 3-2-1 sequence). The initial coordinate system A (black) is rotated around the third body-axis into $A^{'}$ (cyan), then tilted around the first body-axis into $A^{''}$ (red) and then rotated around the third body-axis again into B (blue).

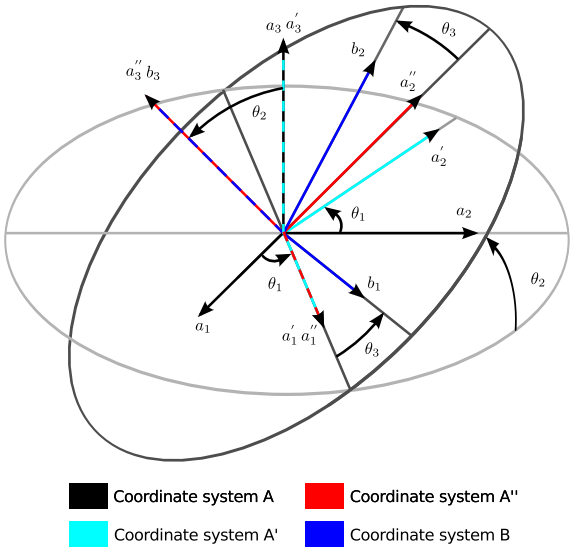

Figure A.1: Example of 3-1-3 Euler rotation sequence. $A \rightarrow A^{'} \rightarrow A^{''} \rightarrow B$

A.2 The Angular Velocity

In this report the angular velocity is described as a 3-dimensional vector, relative to three reference frames. Two reference frames are applied to describe the angular velocity of the object in the first frame with respect to the second frame, while the third describes in which coordinate system the velocity is expressed. This is written as

$$^{\boldsymbol{a}}\boldsymbol{\omega_{bc}} \tag{A.14}$$

and is interpreted as the angular velocity of b wrt. c, expressed in the coordinates of a. Often it will only be necessary to apply two different reference frames to describe an angular velocity of an object, for instance $^{\boldsymbol{c}}\boldsymbol{\omega_{ci}}$ (The angular velocity in c wrt. i expressed in c).

A.2.1 Addition of Angular Velocities

The angular velocity from frame a wrt. frame c is given by the angular velocity from a to b and that from b to c. This will of course need to be expressed in the same reference frame and the addition of angular velocities is thus given by

$$^{\boldsymbol{a}}\boldsymbol{\omega_{ac}} = {}^{\boldsymbol{a}}\boldsymbol{\omega_{ab}} + {}^{\boldsymbol{a}}\boldsymbol{\omega_{bc}} \tag{A.15}$$

A.3 The Skew Symmetric Representation

The angular velocity is often represented in the skew symmetric representation, but any 3-dimensional vector can be described using this representation.

The skew symmetric representation for a vector $\boldsymbol{a} = \begin{bmatrix} a_1 & a_2 & a_3 \end{bmatrix}^T$ is defined as:

$$\begin{bmatrix} 0 & -a_1 & a_2 \\ a_1 & 0 & -a_3 \\ -a_2 & a_3 & 0 \end{bmatrix} = \underline{\boldsymbol{A}} \tag{A.16}$$

One of the properties of the representation is the fact that:

$$\underline{\boldsymbol{A}}^T = -\underline{\boldsymbol{A}} \tag{A.17}$$

Now introducing the skew symmetric representation of the vector $\boldsymbol{b}$ as $\underline{\boldsymbol{B}}$.
Another very useful property is that:

$$\boldsymbol{a} \times \boldsymbol{b} = \underline{\boldsymbol{A}}\boldsymbol{b} = -\underline{\boldsymbol{B}}\boldsymbol{a} \tag{A.18}$$

If ${}^a\underline{\boldsymbol{V}}$ is a vector in the skew symmetric form in the reference frame A, given the DCM between A and B (${}^b\underline{\boldsymbol{C}}_a$), the corresponding skew symmetric form of the vector in reference frame B (${}^b\underline{\boldsymbol{V}}$) is given as:

$${}^b\underline{\boldsymbol{V}} = {}^b\,\underline{\boldsymbol{C}}_a\;{}^a\underline{\boldsymbol{V}}\;{}^a\underline{\boldsymbol{C}}_b = {}^b\,\underline{\boldsymbol{C}}_a\;{}^a\underline{\boldsymbol{V}}\left({}^b\underline{\boldsymbol{C}}_a\right)^T \tag{A.19}$$

A.4 DCM Equations

Throughout this thesis, severely equations regarding the DCM are utilized. This includes the equation regarding DCM kinematics, integration of DCM and reorthogonalityzation of DCMs which are all described in this section.

A.4.1 DCM Kinematics

In [Titterton 04, p. 40], it is stated that the derivative of a DCM ${}^b\dot{\underline{\boldsymbol{C}}}_a$, which denotes the rotation between frame a and frame b, is given as a function of the DCM and the angular velocity between the two frames as:

$${}^b\dot{\underline{\boldsymbol{C}}}_a = {}^b\,\underline{\boldsymbol{C}}_a\;{}^a\underline{\boldsymbol{\Omega}}_{ba} \tag{A.20}$$

A.4.2 Integration of DCMs

In [Titterton 04, p. 311-312], a method for integrating DCMs is stated.

The objective is to predict the next value of the DCM in the next discrete sample given the current DCM and the angular velocity between the two frames of interest.

This problem can be stated as the objective to find $\underline{\boldsymbol{\Pi}}[k]$ such that:

$${}^b\underline{\boldsymbol{C}}_a[k+1] = {}^b\,\underline{\boldsymbol{C}}_a[k]\underline{\boldsymbol{\Pi}}[k] \tag{A.21}$$

$\underline{\boldsymbol{\Pi}}[k]$ is here the DCM which rotates ${}^b\underline{\boldsymbol{C}}_a[k]$ into ${}^b\underline{\boldsymbol{C}}_a[k+1]$.

To describe $\underline{\boldsymbol{\Pi}}[k]$, it is first necessary to introduce $\boldsymbol{\sigma}[k]$, which is the angle change of the axis.

$$\begin{aligned}\boldsymbol{\sigma}[k] &= \int_{t_k}^{t_{k+1}} {}^a\underline{\boldsymbol{\omega}}_{ba} \\ &\approx TS^a\underline{\boldsymbol{\omega}}_{ba}[k]\end{aligned} \tag{A.22}$$

$\underline{\boldsymbol{\Pi}}[k]$ can then be calculated as:

$$\underline{\boldsymbol{\Pi}}[k] = exp\left(\boldsymbol{\sigma}[k]\right) \tag{A.23}$$

A.4.3 Reorthogonalityzation of DCMs

As numerical uncertainties and approximation in applied equation can slowly cause the orthogonality of the DCM to be voided, a procedure for correcting this has been studied.

The procedure here is based on the one of [Titterton 04, p. 323].

First introducing an arbitrary DCM as $\underline{\boldsymbol{C}}$ which is in slight error due to the causes mentioned above and denoting the rows i and j of this DCM as $\underline{\boldsymbol{C}}_i$ and $\underline{\boldsymbol{C}}_j$.

As the row of $\underline{\boldsymbol{C}}$ should be orthogonal, the dot product of $\underline{\boldsymbol{C}}_i$ and $\underline{\boldsymbol{C}}_j$ should equal zero.

The orthogonality error (Δ_{ij}) between $\underline{\boldsymbol{C}}_i$ and $\underline{\boldsymbol{C}}_j$ can thus be described as:

$$\Delta_{ij} \equiv \underline{\boldsymbol{C}}_i \underline{\boldsymbol{C}}_j^T \tag{A.24}$$

Since either row is equally likely to be in error, the correction is apportioned equally between them using [Titterton 04, p. 323]:

$$\begin{aligned} \underline{\boldsymbol{C}}_{ci} &= \underline{\boldsymbol{C}}_i - \frac{1}{2}\Delta_{ij}\underline{\boldsymbol{C}}_j \\ \underline{\boldsymbol{C}}_{cj} &= \underline{\boldsymbol{C}}_j - \frac{1}{2}\Delta_{ij}\underline{\boldsymbol{C}}_i \end{aligned} \tag{A.25}$$

In which $\underline{\boldsymbol{C}}_{ci}$ and $\underline{\boldsymbol{C}}_{cj}$ are the orthogonality corrected rows.

$\underline{\boldsymbol{C}}$ may also be subject to normalization errors. As each row should have a norm of one, the normalization error of each row (Δ_{ii}) can be found by comparing the dot product of the row with unity:

$$\Delta_{ii} \equiv 1 - \underline{\boldsymbol{C}}_i \underline{\boldsymbol{C}}_i^T \tag{A.26}$$

This can be corrected using [Titterton 04, p. 323]:

$$\underline{\boldsymbol{C}}_{ci} = \underline{\boldsymbol{C}}_i - \frac{1}{2}\Delta_{ii}\underline{\boldsymbol{C}}_i \tag{A.27}$$

In which $\underline{\boldsymbol{C}}_{ci}$ is the normalization corrected row.

Appendix B

The Kalman Filter

In the following, the deviation of the Kalman Filter will be conducted. The Kalman filter consist of the two steps: **predict** and **update**.

B.1 Underlaying Model

For later reference, it should be recalled that the linear Kalman filter is the Minimum Mean Square Error (MMSE) estimator, regarded the system can be described by the underlaying model:

$$\boldsymbol{x}[k+1] = \underline{\boldsymbol{A}}\boldsymbol{x}[k] + \underline{\boldsymbol{B}}\boldsymbol{u}[k] + \boldsymbol{w}[k] \tag{B.1}$$

$$\widetilde{\boldsymbol{y}}[k] = \underline{\boldsymbol{H}}\boldsymbol{x}[k] + \boldsymbol{v}[k] \tag{B.2}$$

In which $\boldsymbol{w}[\boldsymbol{k}]$ and $\boldsymbol{v}[\boldsymbol{k}]$ is assumed to be uncorrelated zero-mean Gaussian processes with:

$$E[\boldsymbol{w}[\boldsymbol{k}]\boldsymbol{w}[\boldsymbol{k}]^T] = \underline{\boldsymbol{\Sigma}}$$

$$E[\boldsymbol{v}[\boldsymbol{k}]\boldsymbol{v}[\boldsymbol{k}]^T] = \underline{\boldsymbol{\Lambda}} \tag{B.3}$$

B.2 The Prediction Step

The first step of the Kalman filter is the prediction step. In this step, the *a prior* estimate of the next state of the system is predicted ($\boldsymbol{x}_-[k]$). Furthermore, the covariance of the state estimation error ($\underline{\boldsymbol{P}}_-[k]$) is predicted.

The prediction of the state is straight forward when observing (B.1) and recalling that $\boldsymbol{w}[k]$ is zero-mean The prediction of the state is given as (B.4).

$$\boldsymbol{x}_-[k+1] = \underline{\boldsymbol{A}}\boldsymbol{x}_+[k] + \underline{\boldsymbol{B}}\boldsymbol{u}[k] \tag{B.4}$$

For later reference, the state prediction estimation error ($\delta\boldsymbol{x}_-[k]$) is expanded as:

$$\begin{aligned}\delta\boldsymbol{x}_-[k] &\equiv \boldsymbol{x}[k] - \boldsymbol{x}_-[k] \\ &= \boldsymbol{x}[k] - (\underline{\boldsymbol{A}}\boldsymbol{x}_+[k-1] + \underline{\boldsymbol{B}}\boldsymbol{u}[k-1])\end{aligned}$$

Insertion of (B.1) gives:

$$\begin{aligned}&= \underline{\boldsymbol{A}}\boldsymbol{x}[k-1] + \underline{\boldsymbol{B}}\boldsymbol{u}[k-1] + \boldsymbol{w}[k-1] - (\underline{\boldsymbol{A}}\boldsymbol{x}_+[k-1] + \underline{\boldsymbol{B}}\boldsymbol{u}[k-1]) \\ &= \underline{\boldsymbol{A}}\left(\boldsymbol{x}[k-1] - \boldsymbol{x}_+[k-1]\right) + \boldsymbol{w}[k-1] \\ &= \underline{\boldsymbol{A}}\left(\delta\boldsymbol{x}_+[k-1]\right) + \boldsymbol{w}[k-1]\end{aligned} \tag{B.5}$$

Taking the definition of $\underline{\boldsymbol{P}}_-[k]$ and inserting (B.5):

$$\begin{aligned}\underline{\boldsymbol{P}}_-[k] &\equiv E[\delta\boldsymbol{x}_-[k]\cdot\delta\boldsymbol{x}_-[k]^T]\\ &= E[(\underline{\boldsymbol{A}}\delta\boldsymbol{x}_+[k-1]+\boldsymbol{w}[k-1])\cdot(\underline{\boldsymbol{A}}\delta\boldsymbol{x}_+[k-1]+\boldsymbol{w}[k-1])^T]\end{aligned}$$

As $\boldsymbol{x}$[k] and $\boldsymbol{w}$[k] are independent, $\boldsymbol{u}$ is deterministic and E[$\boldsymbol{w}$[k]] = 0:

$$\begin{aligned}&= E[(\underline{\boldsymbol{A}}\delta\boldsymbol{x}_+[k-1])\cdot(\underline{\boldsymbol{A}}\delta\boldsymbol{x}_+[k-1])^T]+E[(\boldsymbol{w}[k-1])\cdot(\boldsymbol{w}[k-1])^T]\\ &= \underline{\boldsymbol{A}}E[\delta\boldsymbol{x}_+[k-1]\cdot\delta\boldsymbol{x}_+[k-1]^T]\underline{\boldsymbol{A}}^T+\underline{\boldsymbol{\Sigma}}\\ &= \underline{\boldsymbol{A}}\underline{\boldsymbol{P}}_+[k-1]\underline{\boldsymbol{A}}^T+\underline{\boldsymbol{\Sigma}}\end{aligned}\tag{B.6}$$

Where $\underline{\boldsymbol{P}}_+[k-1]$ is the *posterior* covariance of the state estimation error from the update step from the last iteration of the filter.

B.3 The Update Step

The update step is where the measurement ($\widetilde{\boldsymbol{y}}[k]$) with its appertaining covariance ($\underline{\boldsymbol{\Lambda}}$) are applied to create a *posterior* estimate of the state ($\boldsymbol{x}_+[k]$) and the covariance of the state estimation error ($\underline{\boldsymbol{P}}_+[k]$).

To derive this step, the orthogonal principle is applied, which can be seen in Subsection B.5. Furthermore, given the property that $\boldsymbol{x}$ and $\widetilde{\boldsymbol{y}}$ are jointly Gaussian, it is sufficient to seek a *posterior* state estimate that is a linear function of the *a prior* estimate and the measurement [Grewal 08, p. 115]. This is shown in (B.7).

$$\boldsymbol{x}_+[k] = \acute{\underline{\boldsymbol{K}}}[k]\boldsymbol{x}_-[k]+\bar{\underline{\boldsymbol{K}}}[k]\widetilde{\boldsymbol{y}}[k]\tag{B.7}$$

Where the objective is to determine the unknown $\acute{\underline{\boldsymbol{K}}}[k]$ and $\bar{\underline{\boldsymbol{K}}}[k]$.

It it desired to minimize the MMSE:

$$\begin{aligned}\min E\left[(\boldsymbol{x}[k]-\boldsymbol{x}_+[k])^2\right] &= \min E\left[\left(\boldsymbol{x}[k]-\left(\acute{\underline{\boldsymbol{K}}}[k]\boldsymbol{x}_-[k]+\bar{\underline{\boldsymbol{K}}}[k]\widetilde{\boldsymbol{y}}[k]\right)\right)^2\right]\\ &= \min E\left[\left(\left(\boldsymbol{x}[k]-\acute{\underline{\boldsymbol{K}}}[k]\boldsymbol{x}_-[k]\right)-\bar{\underline{\boldsymbol{K}}}[k]\widetilde{\boldsymbol{y}}[k]\right)^2\right]\end{aligned}\tag{B.8}$$

As it is shown in B.5, this can be minimized using the orthogonal principle, which gives:

$$\begin{aligned}0 &= E\left[\left(\left(\boldsymbol{x}[k]-\acute{\underline{\boldsymbol{K}}}[k]\boldsymbol{x}_-[k]\right)-\bar{\underline{\boldsymbol{K}}}[k]\widetilde{\boldsymbol{y}}[k]\right)\cdot\widetilde{\boldsymbol{y}}[k]^T\right]\\ &= E\left[\left(\boldsymbol{x}[k]-\acute{\underline{\boldsymbol{K}}}[k]\boldsymbol{x}_-[k]-\bar{\underline{\boldsymbol{K}}}[k]\underline{\boldsymbol{H}}\boldsymbol{x}[k]+\acute{\underline{\boldsymbol{K}}}[k]\boldsymbol{x}[k]-\acute{\underline{\boldsymbol{K}}}[k]\boldsymbol{x}[k]\right)\cdot\widetilde{\boldsymbol{y}}[k]^T\right]\\ &= E\left[\left(\boldsymbol{x}[k]-\bar{\underline{\boldsymbol{K}}}[k]\underline{\boldsymbol{H}}\boldsymbol{x}[k]-\acute{\underline{\boldsymbol{K}}}[k]\boldsymbol{x}[k]-\acute{\underline{\boldsymbol{K}}}[k]\left(\boldsymbol{x}_-[k]-\boldsymbol{x}[k]\right)\right)\cdot\widetilde{\boldsymbol{y}}[k]^T\right]\\ &= \left(\underline{\boldsymbol{I}}-\bar{\underline{\boldsymbol{K}}}[k]\underline{\boldsymbol{H}}-\acute{\underline{\boldsymbol{K}}}[k]\right)E\left[\boldsymbol{x}[k]\widetilde{\boldsymbol{y}}[k]^T\right]-\acute{\underline{\boldsymbol{K}}}[k]E\left[\delta\boldsymbol{x}_-[k]\widetilde{\boldsymbol{y}}[k]^T\right]\end{aligned}\tag{B.9}$$

As $\delta\boldsymbol{x}_-[k]$ has an expected value of 0 and is uncorrelated with $\widetilde{\boldsymbol{y}}[k]^T$, it is seen that (B.9) is satisfied if:

$$\acute{\underline{\boldsymbol{K}}} = \underline{\boldsymbol{I}}-\bar{\underline{\boldsymbol{K}}}[k]\underline{\boldsymbol{H}}\tag{B.10}$$

For use in the next equation, the error between the actual measurement and the predicted measurement is introduced as $\delta\widetilde{\boldsymbol{y}}[k]$, defined as:

$$\delta\widetilde{\boldsymbol{y}}[k] = \widetilde{\boldsymbol{y}}-\underline{\boldsymbol{H}}\boldsymbol{x}_-[k]\tag{B.11}$$

If the result from (B.10) is inserted into (B.7) a new expression for the *posterior* state estimate can be found:

$$\begin{aligned}\boldsymbol{x}_+[k] &= \acute{\underline{\boldsymbol{K}}}[k]\boldsymbol{x}_-[k] + \bar{\underline{\boldsymbol{K}}}[k]\widetilde{\boldsymbol{y}}[k] \\ &= \left(\underline{\boldsymbol{I}} - \bar{\underline{\boldsymbol{K}}}[k]\underline{\boldsymbol{H}}\right)\boldsymbol{x}_-[k] + \bar{\underline{\boldsymbol{K}}}[k]\widetilde{\boldsymbol{y}}[k] \\ &= \boldsymbol{x}_-[k] + \bar{\underline{\boldsymbol{K}}}[k]\left(\widetilde{\boldsymbol{y}}[k] - \underline{\boldsymbol{H}}\boldsymbol{x}_-[k]\right) \\ &= \boldsymbol{x}_-[k] + \bar{\underline{\boldsymbol{K}}}[k]\delta\widetilde{\boldsymbol{y}}[k] \end{aligned} \tag{B.12}$$

The next step is to determine $\bar{\underline{\boldsymbol{K}}}[k]$. This is obtained by first revisiting the original minimization problem in (B.8) and inserting (B.12):

$$\min E\left[\left(\boldsymbol{x}[k] - \boldsymbol{x}_+[k]\right)^2\right] = \min E\left[\left(\boldsymbol{x}[k] - \boldsymbol{x}_-[k] - \bar{\underline{\boldsymbol{K}}}[k]\delta\widetilde{\boldsymbol{y}}[k]\right)^2\right] \tag{B.13}$$

Again, using the orthogonal principle, it is know that this can be minimized by solving for $\bar{\underline{\boldsymbol{K}}}[k]$ such that:

$$\begin{aligned} 0 &= E\left[\left(\boldsymbol{x}[k] - \boldsymbol{x}_-[k] - \bar{\underline{\boldsymbol{K}}}[k]\delta\widetilde{\boldsymbol{y}}[k]\right)\cdot\delta\widetilde{\boldsymbol{y}}[k]^T\right] \\ &= E\left[\delta\boldsymbol{x}_-[k]\delta\widetilde{\boldsymbol{y}}[k]^T - \bar{\underline{\boldsymbol{K}}}[k]\delta\widetilde{\boldsymbol{y}}[k]\delta\widetilde{\boldsymbol{y}}[k]^T\right] \\ &= E\left[\delta\boldsymbol{x}_-[k]\delta\boldsymbol{x}_-[k]^T\underline{\boldsymbol{H}}^T - \bar{\underline{\boldsymbol{K}}}[k]\left((H\delta\boldsymbol{x}_-[k] + \boldsymbol{v}[k])(H\delta\boldsymbol{x}_-[k] + \boldsymbol{v}[k])^T\right)\right] \\ &= \underline{\boldsymbol{P}}_-[k]\underline{\boldsymbol{H}}^T - \bar{\underline{\boldsymbol{K}}}[k]E\left[\underline{\boldsymbol{H}}\delta\boldsymbol{x}_-[k]\delta\boldsymbol{x}_-[k]^T\underline{\boldsymbol{H}}^T\right] - \bar{\underline{\boldsymbol{K}}}[k]E\left[\boldsymbol{v}[k]\boldsymbol{v}[k]^T\right] \\ &= \underline{\boldsymbol{P}}_-[k]\underline{\boldsymbol{H}}^T - \bar{\underline{\boldsymbol{K}}}[k]\underline{\boldsymbol{H}}\underline{\boldsymbol{P}}_-[k]\underline{\boldsymbol{H}}^T - \bar{\underline{\boldsymbol{K}}}[k]\underline{\boldsymbol{\Lambda}} \\ &\Updownarrow \\ \underline{\boldsymbol{P}}_-[k]\underline{\boldsymbol{H}}^T &= \bar{\underline{\boldsymbol{K}}}[k]\left(\underline{\boldsymbol{H}}\underline{\boldsymbol{P}}_-[k]\underline{\boldsymbol{H}}^T + \underline{\boldsymbol{\Lambda}}\right) \end{aligned} \tag{B.14}$$

$$\Updownarrow$$

$$\bar{\underline{\boldsymbol{K}}}[k] = \underline{\boldsymbol{P}}_-[k]\underline{\boldsymbol{H}}^T\left[\underline{\boldsymbol{H}}\underline{\boldsymbol{P}}_-[k]\underline{\boldsymbol{H}}^T + \underline{\boldsymbol{\Lambda}}\right]^{-1} \tag{B.15}$$

To derive the covariance matrix of the *posterior* state estimate error ($\underline{\boldsymbol{P}}_+[k]$), it is first necessary to expand the *posterior* state estimate error expression:

$$\begin{aligned}\delta\boldsymbol{x}_+[k] &= \boldsymbol{x}[k] - \boldsymbol{x}_+[k] \\ &= \boldsymbol{x}[k] - \boldsymbol{x}_-[k] - \bar{\underline{\boldsymbol{K}}}[k]\left(\widetilde{\boldsymbol{y}}[k] - \underline{\boldsymbol{H}}\boldsymbol{x}_-[k]\right) \\ &= \delta\boldsymbol{x}_-[k] - \bar{\underline{\boldsymbol{K}}}[k]\underline{\boldsymbol{H}}\boldsymbol{x}[k] - \bar{\underline{\boldsymbol{K}}}[k]\boldsymbol{v}[k] + \bar{\underline{\boldsymbol{K}}}[k]\underline{\boldsymbol{H}}\boldsymbol{x}_-[k] \\ &= \delta\boldsymbol{x}_-[k] - \bar{\underline{\boldsymbol{K}}}[k]\underline{\boldsymbol{H}}\delta\boldsymbol{x}_-[k] - \bar{\underline{\boldsymbol{K}}}[k]\boldsymbol{v}[k] \\ &= \left(\underline{\boldsymbol{I}} - \bar{\underline{\boldsymbol{K}}}[k]\underline{\boldsymbol{H}}\right)\delta\boldsymbol{x}_-[k] - \bar{\underline{\boldsymbol{K}}}[k]\boldsymbol{v}[k] \end{aligned} \tag{B.16}$$

(B.16) is then inserted into the definition of ($\underline{\boldsymbol{P}}_+[k]$):

$$\begin{aligned}\underline{\boldsymbol{P}}_+[k] &\equiv E\left[\delta\boldsymbol{x}_+[k]\cdot\delta\boldsymbol{x}_+[k]^T\right] \\ &= E\left[\left(\left(\underline{\boldsymbol{I}} - \bar{\underline{\boldsymbol{K}}}[k]\underline{\boldsymbol{H}}\right)\delta\boldsymbol{x}_-[k] - \bar{\underline{\boldsymbol{K}}}[k]\boldsymbol{v}[k]\right)\left(\left(\underline{\boldsymbol{I}} - \bar{\underline{\boldsymbol{K}}}[k]\underline{\boldsymbol{H}}\right)\delta\boldsymbol{x}_-[k] - \bar{\underline{\boldsymbol{K}}}[k]\boldsymbol{v}[k]\right)^T\right] \\ &= \left(\underline{\boldsymbol{I}} - \bar{\underline{\boldsymbol{K}}}[k]\underline{\boldsymbol{H}}\right)E\left[\delta\boldsymbol{x}_-[k]\delta\boldsymbol{x}_-[k]^T\right]\left(\underline{\boldsymbol{I}} - \bar{\underline{\boldsymbol{K}}}[k]\underline{\boldsymbol{H}}\right)^T + \bar{\underline{\boldsymbol{K}}}[k]E\left[\boldsymbol{v}[k]\boldsymbol{v}[k]^T\right]\bar{\underline{\boldsymbol{K}}}[k]^T \\ &= \left(\underline{\boldsymbol{I}} - \bar{\underline{\boldsymbol{K}}}[k]\underline{\boldsymbol{H}}\right)\underline{\boldsymbol{P}}_-[k]\left(\underline{\boldsymbol{I}} - \bar{\underline{\boldsymbol{K}}}[k]\underline{\boldsymbol{H}}\right)^T + \bar{\underline{\boldsymbol{K}}}[k]\underline{\boldsymbol{\Lambda}}\bar{\underline{\boldsymbol{K}}}[k]^T \\ &= \left(\underline{\boldsymbol{I}} - \bar{\underline{\boldsymbol{K}}}[k]\underline{\boldsymbol{H}}\right)\left(\underline{\boldsymbol{P}}_-[k] - \underline{\boldsymbol{P}}_-[k]\underline{\boldsymbol{H}}^T\bar{\underline{\boldsymbol{K}}}[k]^T\right) + \bar{\underline{\boldsymbol{K}}}[k]\underline{\boldsymbol{\Lambda}}\bar{\underline{\boldsymbol{K}}}[k]^T \\ &= \underline{\boldsymbol{P}}_-[k] - \underline{\boldsymbol{P}}_-[k]\underline{\boldsymbol{H}}^T\bar{\underline{\boldsymbol{K}}}[k]^T - \bar{\underline{\boldsymbol{K}}}[k]\underline{\boldsymbol{H}}\underline{\boldsymbol{P}}_-[k] + \bar{\underline{\boldsymbol{K}}}[k]\underline{\boldsymbol{H}}\underline{\boldsymbol{P}}_-[k]\underline{\boldsymbol{H}}^T\bar{\underline{\boldsymbol{K}}}[k]^T + \bar{\underline{\boldsymbol{K}}}[k]\underline{\boldsymbol{\Lambda}}\bar{\underline{\boldsymbol{K}}}[k]^T \\ &= \left(\underline{\boldsymbol{I}} - \bar{\underline{\boldsymbol{K}}}[k]\underline{\boldsymbol{H}}\right)\underline{\boldsymbol{P}}_-[k] - \underline{\boldsymbol{P}}_-[k]\underline{\boldsymbol{H}}^T\bar{\underline{\boldsymbol{K}}}[k]^T + \bar{\underline{\boldsymbol{K}}}[k]\left(\underline{\boldsymbol{H}}\underline{\boldsymbol{P}}_-[k]\underline{\boldsymbol{H}}^T + \underline{\boldsymbol{\Lambda}}\right)\bar{\underline{\boldsymbol{K}}}[k]^T \end{aligned}$$

If (B.14) is inserted, this can be further simplified to:

$$\begin{aligned} &= \left(\underline{\boldsymbol{I}} - \bar{\underline{\boldsymbol{K}}}[k]\underline{\boldsymbol{H}}\right)\underline{\boldsymbol{P}}_{-}[k] - \underline{\boldsymbol{P}}_{-}[k]\underline{\boldsymbol{H}}^T\bar{\underline{\boldsymbol{K}}}[k]^T + \underline{\boldsymbol{P}}_{-}[k]\underline{\boldsymbol{H}}^T\bar{\underline{\boldsymbol{K}}}[k]^T \\ &= \left(\underline{\boldsymbol{I}} - \bar{\underline{\boldsymbol{K}}}[k]\underline{\boldsymbol{H}}\right)\underline{\boldsymbol{P}}_{-}[k] \end{aligned} \tag{B.17}$$

B.4 Sum up of the procedure of a Kalman filter step

To sum up, the following equations is used in the two steps of the Kalman filter:
Predict:
First (B.4) is applied to predict the state and afterwards (B.6) is used to predict the covariance matrix of the state estimation error.
Update:
To obtain the optimal gain, (B.15) is used. Then the estimation of the state is updated using (B.12). As the last part of the Kalman filter step, the covariance matrix of the state estimation error is updated using (B.17).

B.5 The Orthogonal Principle

The object of the Kalman filter is to minimize the mean squared error e, given in (B.18).

$$e = E[(\boldsymbol{x} - \underline{\boldsymbol{k}}\boldsymbol{y})^2] \tag{B.18}$$

The k that minimizes this equation, is such that $x - kyis$ orthogonal on y. This is referred to as the orthogonal principle, and is illustrated in the scalar case in Fig. B.1.

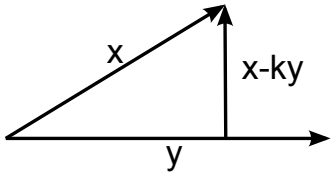

Figure B.1: The orthogonal principle

This means that the k should be found such that:

$$E[(\boldsymbol{x} - \underline{\boldsymbol{k}}\boldsymbol{y}) \cdot \boldsymbol{y}] = 0 \tag{B.19}$$

Bibliography

[Ana 11] Analog Devices. *ADIS16362 - rev D*, February 2011. IMU data sheet.

[B. Hoffmann-Wellenhof 01] H. Lichtenegger B. Hoffmann-Wellenhof & J. Collins. Gps - theory and practice, 5th edition. Springer, 2001.

[CDL 10] CDL. *CDL MiniSense2 Technical Manual - rev D*, 2010. MiniSense2.

[Christensen 14] Rolf Christensen & Bjørn Eskildsen. *Mail*, Feb 2014.

[Crassidis] John L. Crassidis. *Sigma-Point Kalman Filtering for Integrated GPS and Inertial Navigation.*

[Grewal 08] Mohinder S. Grewal & Angus P. Andrews. Kalman filtering - theory and practice using matlab - third edition. Wiley, 2008.

[Gyro 97] Gyro, Accelerometer Panel of the IEEE Aerospace & Electronic Systems Society. *IEEE Standard Specification Format Guide and Test Procedure for Single-Axis Interferometric Fiber Optic Gyros.* September 1997.

[Hon 11] Honeywell. *HMC5883L*, March 2011. Magnetometer data sheet.

[J. Wendel] C. Schlaile J. Wendel & Gert F. Trommer. *Direct Kalman Filtering of GPS/INS for Aerospace Applications.*

[of Electronic Systems 10] Group 823 Department of Electronic Systems. Attitude control and fault detection for aausat3. Aalborg University, 2010.

[of Geomagnetism 12] The International Association of Geomagnetism & Aeronomy. *International Geomagnetic Reference Field*, 2012. `http://www.ngdc.noaa.gov/IAGA/vmod/igrf.html`.

[Pifu Zhang 05] Evangelos E. Milios Pifu Zhang Jason Gu & Peter Huynh. *Navigation with IMU/GPS/Digital Compass with Unscented Kalman Filter.* July 2005.

[Prasad 05] Ramjee Prasad & Marina Ruggieri. Applied satellite navigation using gps, galileo and augmentation systems. Artech House, 2005.

[Rogers 03] Robert M. Rogers. Applied mathematics in integrated navigation systems, 2nd edition. AIAA Education Series, 2003.

[Simonsen 12] Torben R. Simonsen & Martina Zabic. *Ny afhandling: GPS-teknologi er klar til roadpricing.* Janary 2012.

[Titterton 04] D. H. Titterton & J. L. Weston. Strapdown inertial navigation technology - second edition. AIAA, 2004.

[Totu 02] Luminita-Cristiana Totu & Simon Konge Koldbaek. Improving mems gyroscope performance using homogeneous sensor fusion. 2002.

[Tri 98] Trimble. *RMS750 - Dual-Frequency RTK Receiver for Marine Applications*, 1998. GPS data sheet.

[Wikipedia 12a] Wikipedia. *Newton's laws of motion*, 2012. `http://en.wikipedia.org/wiki/Newton's_laws_of_motion`.

[Wikipedia 12b] Wikipedia. *Wiener process*, 2012. `http://en.wikipedia.org/wiki/Wiener_process`.